



Master thesis project

Design and implementation of a bi-directional 3 phase converter for a 30kW range extender application

Author : Ferdinand Visser
Student ID : 1525530
Date : September 12th, 2011

Thesis Committee : Prof. Dr. J.A. Ferreira
: Dr. H. Polinder
: Dr. A. Smets
: Ing. D.J. Toeters

ABSTRACT

Increasing fuel prices and political pressure to reduce the pollution in the mobile transport lead to new technologies for electric transport. PEEC-Power B.V. is developing a range extender for parallel hybrid vehicles and wants to contribute to the transition towards electric driving. The range extender consists of three subsystems: combustion engine, generator and the power electronic system. This thesis is about the design and implementation of this power electronic system.

First the specifications and operating conditions of the combustion engine, generator and battery-bus are investigated. The power electronic system has to operate with these systems and therefore, voltage and current ratings, expected frequencies and losses are investigated.

Based on the parameters of the connected systems, two converter topologies are discussed: a passive rectifier combined with a boost converter and an active full bridge converter. This includes the control flexibility, harmonic distortion, weight and price. Based on these aspects the active full bridge converter is chosen and discussed in more detail. The basic operation is presented and a complete hardware design is proposed to meet the functional requirements. Also a test setup is developed in order to investigate the operating behavior of the hardware components and different PWM methods.

Research is done to four PWM methods (Hysteresis modulation, carrier modulation, space vector modulation and harmonic elimination) and two control methods (direct torque control and field oriented control). This includes harmonic distortion, switching losses, robustness and DSP implementation. Based on these aspects and application specific simulations, a complete power electronic converter is proposed with space vector modulation combined with field oriented control.

At last, an open loop control with the chosen PWM method is implemented on the test setup. Measurements are performed on switching performance, starting the synchronous machine, harmonic distortion and efficiency. The results are compared to the expectations based on literature study and simulations.

TABLE OF CONTENTS

Chapter 1: Introduction	- 4 -
1.1. BACKGROUND	- 4 -
1.2. PROBLEM DEFINITION	- 5 -
1.3. THESIS LAYOUT	- 7 -
Chapter 2: System description	- 8 -
2.1. COMBUSTION ENGINE	- 8 -
2.2. GENERATOR.....	- 9 -
2.3. BATTERY-BUS.....	- 9 -
2.4. POWER ELECTRONIC SYSTEM	- 9 -
Chapter 3: Converter topologies	- 11 -
3.1. PASSIVE AC/DC CONVERTER.....	- 11 -
3.2. ACTIVE AC/DC CONVERTER.....	- 14 -
3.3. TOPOLOGY CHOICE POWER ELECTRONIC CONVERTER	- 16 -
Chapter 4: Hardware design	- 18 -
4.1. BASIC OPERATION FULL BRIDGE CONVERTER	- 18 -
4.2. HARDWARE LAYOUT	- 23 -
4.2.1. <i>Switches</i>	- 24 -
4.2.2. <i>Gate driver</i>	- 25 -
4.2.3. <i>DC Supply</i>	- 26 -
4.2.4. <i>Isolator</i>	- 27 -
4.2.5. <i>Sensors</i>	- 27 -
4.2.6. <i>Controller</i>	- 29 -
4.3. LOSSES.....	- 29 -
4.4. THERMAL DESIGN.....	- 32 -
4.5. TEST SETUP	- 33 -
4.5.1. <i>I/O board</i>	- 34 -
Chapter 5: PWM and control methods	- 37 -
5.1. HYSTERESIS MODULATION.....	- 37 -
5.2. CARRIER BASED MODULATION	- 40 -
5.2.1. <i>Carrier waveform</i>	- 40 -
5.2.2. <i>Reference waveform</i>	- 41 -
5.3. SPACE VECTOR MODULATION	- 46 -
5.4. SELECTIVE HARMONIC ELIMINATION (SHE)	- 48 -
5.5. CONTROL METHODS.....	- 49 -
5.5.1. <i>Direct Torque Control (DTC)</i>	- 49 -
5.5.2. <i>Field Oriented Control (FOC)</i>	- 50 -
5.6. CHOSEN PWM AND CONTROL METHOD	- 51 -
Chapter 6: Implementation and measurements	- 52 -
6.1. SWITCHING PERFORMANCE	- 52 -
6.2. SOFTWARE DSP	- 55 -
6.3. STARTING	- 59 -
6.4. THD AND EFFICIENCY.....	- 61 -
Chapter 7 : Conclusion and future work	- 63 -
7.1. CONTRIBUTIONS AND CONCLUSIONS	- 63 -

7.2. FUTURE WORK.....	- 64 -
References	65 -
Appendix A: Datasheet 48T SMPM generator set	67 -
Appendix B: Hardware cost price calculation of proposed designs	68 -
Appendix C: Datahseet Fuji 2MBI200U4B-120-50.....	69 -
Appendix D: Test setup.....	83 -

LIST WITH ABBREVIATIONS

PEEC:	Piston energized electro cell
PWM:	Pulse width modulation
AC:	Alternating current
DC:	Direct current
SVC:	Space vector
SIN:	Sinus
THD:	Total harmonic distortion
THI:	Third harmonic injection
PMSM:	Permanent magnet synchronous machine

Chapter 1: Introduction

1.1. Background

People have always looked for ways to travel longer distances in shorter times. With the introduction of the first steam driven vehicle (1769) a rapid development of mobile vehicles has begun. Because of the long startup time, high cooling demands and large weight of the steam engine, people start looking for other solutions and developed the combustion engine. Commercial drilling and production of petroleum in the mid-1850s resulted in a permanent transition from steam to combustion engine. In this period electrical vehicles were developed as well, but high costs, low top speed and short driving range led to a worldwide decline in their use [1]. In the beginning of the 20th century the combustion engine had the highest potential for mobile road transport so people started to improve the engine, with the modern combustion engine as result.

Not only the combustion engine encountered a big development in the past 100 years, also the world's welfare increased enormously. The quality of living is increasing in a lot of countries and people can afford more luxury and energy consuming goods. Over the years energy demand increased and the air quality deteriorated due to pollution as result of burning fossil fuels. Nowadays road transport is responsible for 10% of the worldwide pollution [2].

Because of increased fuel prices and political pressure to decrease pollution people start looking for cheaper and cleaner solutions to transport and so electric vehicles took the attention of the researching companies. The drawbacks of the electrical vehicles in the 19th century are partly overcome by the development of the electrical motor in the last 100 years. Compared to a combustion engine electrical driving is much cheaper and cleaner, but the energy storage problem still exists. The batteries are improved in the last decades, but the driving range is still too limited to replace the vehicles with an internal combustion engine.

A combination of electrical and a combustion engine, called hybrid vehicles can be a temporary solution towards a full electric powered vehicle. The hybrid vehicles can be divided in two categories: parallel and series hybrid vehicles. Parallel hybrid vehicles can directly be driven by a combustion engine or an electrical motor. Depending on speed and maximum efficiency one of the motors will be used to drive the car. Series hybrid vehicles are only driven by an electrical machine, which is supplied directly by the battery or indirectly by a combustion engine and generator. The utilization of the combustion engine and generator will depend on the charge level of the battery. PEEC-Power B.V. is doing research in such a combustion engine and generator combination and with this product they want to contribute to the transition from internal combustion to electric road transport.

1.2. Problem definition

Despite of a fast developing battery market the batteries are still a bottleneck in modern electric vehicles. Limited charge density causes heavy and expensive batteries packs and a small driving range. PEEC-Power B.V. has the intention to solve these shortcomings through the application of a simple, cost-effective, compact, silent, reliable and efficient range extender that includes the unique Piston Energized Electro Cell (PEEC). The combination of a battery pack and this range extender should be the best transition to full electric transport. Figure 1.1 (a) shows that 90% of the daily driving range is less than 40 kilometers [3]. The battery packs in vehicles with a range extender can be matched to these 40 kilometers which results in a cost and weight optimized solution. If the batteries are drained after 40 kilometers the range extender will be turned on and supply the electric energy to continue traveling by using the battery as buffer.

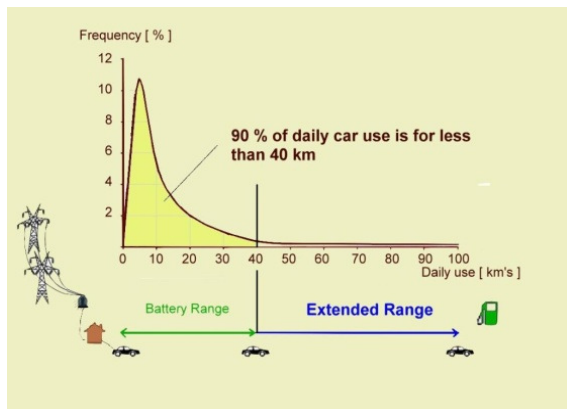
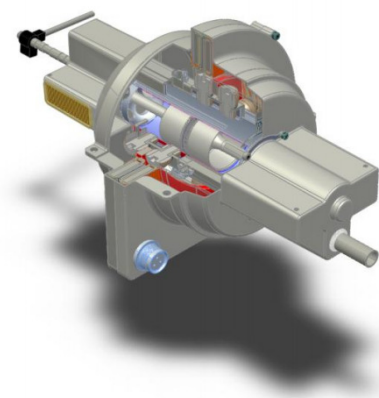


Figure 1.1: (a) Daily car use



(b) 3D model of range extender

The range extender consists of three main parts: a combustion engine, a generator and a power electronic system. The unique combustion engine developed by PEEC-Power B.V. has two horizontal opposed pistons which cause lower friction and results in a higher efficiency compared to other combustion engines. This horizontal movement is transformed to rotational movement by a sinusoidal ring which is directly connected to the shaft of the generator (Figure 1.1 (b)). The generator is used to transform kinetic energy into electrical energy. A power electronic system has to be developed which connects the electrical generator with the battery-bus of the electric vehicle to provide the vehicle with electricity. A systematic overview is presented in figure 1.2.

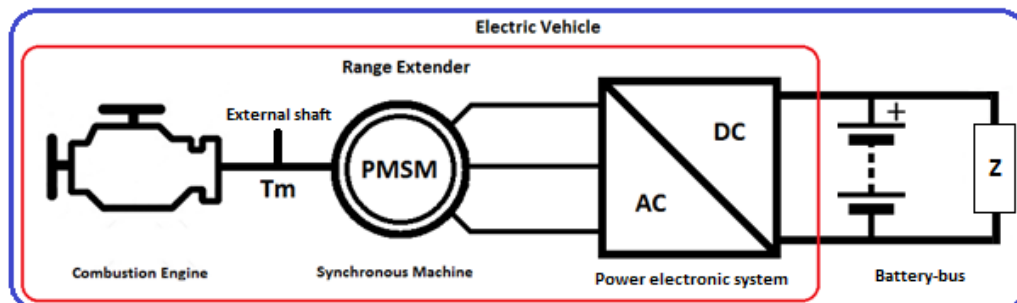


Figure 1.2: System layout range extender

Since the range extender is a commercial product, all the parts and systems are and must be optimized according the following criteria and priority:

- Low cost
- Small size
- High efficiency

The main objective of this thesis is to design a power electronic system which can transfer energy from the generator to a battery-bus and in the reverse way to start the combustion engine. In order to realize this design the next objectives have to be accomplished:

- Investigate the parameters and behavior of the combustion engine, generator and battery-bus
- Determine the best converter topology for the range extender
- Calculate the optimal components specifications for the hardware design
- Determine the best PWM and control strategies for the prototype of the range extender

The next paragraph describes the different steps to achieve an economic, low weight and high efficient power electronic system between the generator and the battery-bus.

1.3. Thesis layout

Designing a power electronic system is an application specific process. Because the power has to be transferred from a source to the load, the solution will depend on these connected systems. The first important step is to define the behavior and parameters of the connected systems and then start to design a specific solution:

- Define design criteria
- Topology choice
- Hardware layout
- Investigate and define PWM and control methods
- Optimal PWM and control method
- Measurements on test setup

Define design criteria

Before starting the design, a system overview and design criteria have to be defined. These criteria depend on the connected generator, battery-bus and functional requirements. The solution has to be designed according these criteria and optimized in cost, weight, efficiency and flexibility as mentioned in paragraph 1.2.

Topology choice

When the system overview and design criteria are known, different topologies need to be investigated and a choice has to be made according to these defined design criteria. A system overview and topology comparison is made in chapter 2 and chapter 3 respectively.

Hardware layout

In chapter 4 the chosen topology is investigated in more detail. Calculations on hardware components are made and driver and protection circuits of the test setup are designed.

Investigate and define PWM and control methods

Different PWM methods are discussed briefly in chapter 5. The impact of harmonics in the generator and switching losses in switches are investigated. Also, the practical requirements for PWM generation are taken into account, such as implementation and processor resources. Additionally, control methods are discussed with focus on practical implementation and robustness.

Optimal control and PWM method

A choice for the best control and PWM method is made in paragraph 5.6. The choice is based on implementation, switching losses, harmonic distortion and robustness.

Results

Chapter 6 shows results of the measurements on the test setup of the chosen control and PWM method. The switching behavior, starting the synchronous machine, harmonics and efficiency will be discussed and compared to the expectations based on literature study.

Chapter 2: System description

PEEC-Power B.V. is developing a range extender which converts liquid fuel to electric energy in order to supply electrical energy to an electric vehicle. Therefore the range extender consists of three main parts, the combustion engine, a generator and a power electronic system. The combustion engine is connected by a unique patented way to the generator, the design of these two subsystems are well advanced and some prototypes have been build. To connect these system parts to the electric vehicle a power electronic system is required. This system is the connection between the generator and the battery-bus of the electric vehicle. The power electronic system also needs to start the combustion engine; an external shaft is available to connect a possible external starting motor. Figure 2.1 shows a systematic overview of the range extender and its application.

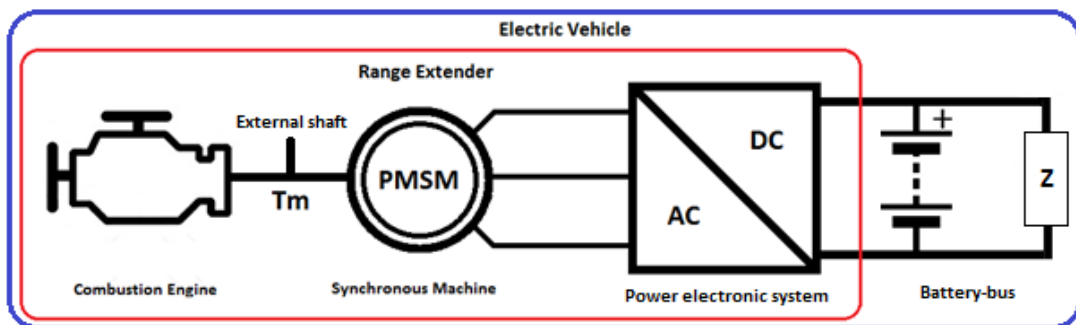


Figure 2.1: Global system layout

The combustion engine and generator are cooled by the water cooling system of the vehicle. This system is also available to cool the power electronic system. According PEEC-Power B.V. a water temperature of 65°C can be assumed. In the next subparagraphs specifications of all the main parts of the range extender will be discussed in more detail.

2.1. Combustion engine

The special developed two stroke combustion engine is the key component of the range extender. The horizontal movement of the two opposed pistons is transformed in a rotational movement by a unique patented sinusoidal ring. In this setup the crankshaft is eliminated and should provide a higher efficiency than engines with a crank shaft, because the friction of the pistons is reduced. The maximum power of the engine will be 35kW at a mechanical rotational speed of 3000 RPM. Starting the combustion engine will require 2.2 times the nominal torque which results in a starting torque of 220Nm. Because of the compression and combustion in the cylinder the torque and speed characteristic will show some fluctuation. Figure 2.2 shows the speed and torque characteristic at a constant load. It appears that the fluctuation will be between 733Hz and 800Hz.

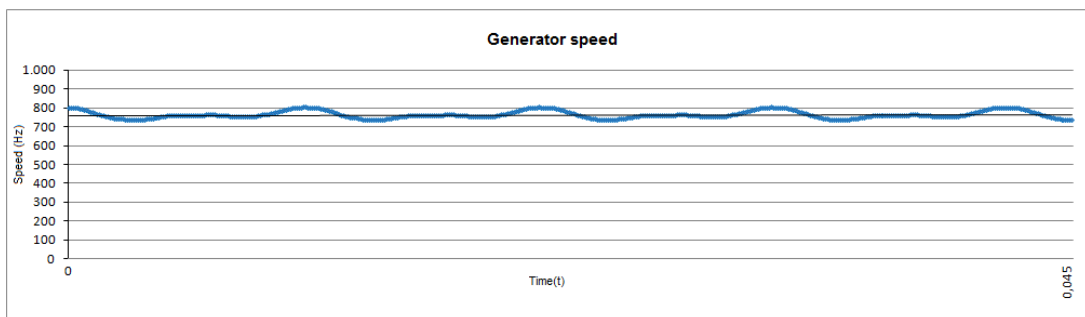


Figure 2.2: Speed fluctuations combustion engine

2.2. Generator

The next important part in the range extender is the generator. During normal operation the rotational movement is transformed to electrical energy by the permanent magnet synchronous machine. During starting operation the synchronous machine will operate as starting motor. It is developed with low weight and high efficiency as the most important design criteria. Due to the 32 poles the nominal electrical frequency will be 800Hz with an RMS voltage on the terminals of 251 volts. Nominal operation conditions are shown in table 2.1.

P	30.8	kW		U _t	251	V
n _m	3000	RPM		I _{ph}	45	A
f _e	800	Hz		Cosφ	0.91	
p	16			η	95.8	%

Table 2.1: Nominal operating conditions

- Generator parameters:

Induced voltage	: E _{ph}	= 241	V
	: C _T	= 0.1	%/°C
Phase resistance	: R _{ph}	= 63	mΩ
	: C _T	= 0.43	%/°C
Phase inductance	: L _{ph}	= 410	μH

A detailed datasheet of the synchronous machine can be found in appendix A.

2.3. Battery-bus

The power generated by the range extender should be delivered to the battery-bus. During normal operation the combustion engine will run at nominal speed and deliver about 30kW to the battery-bus. A high energy demand of the electronic motor of the car will result in a direct energy flow to this load. If the demand is lower than the range extender supplies, the energy will be stored in the battery pack of the car. Battery management is not taken into account in this thesis.

Since there is no specific standard for the battery-bus connection in electric vehicles, it is hard to define voltage and current ratings. In consultation to TNO, PEEC-Power B.V. decided to support a battery-bus voltage of 450V-600V in order to supply the largest amount of customers.

2.4. Power electronic system

All the previously discussed parts of the range extender will come together at the power electronic system. During generator operation the power electronic system have to convert and transfer the power from the generator to the battery-bus. During starting operation, energy from the battery-bus is used to start the combustion engine by using the synchronous machine or an external DC-machine.

Since the properties of the battery-bus connection depend on a third party, the range extender should be flexible to supply the maximum amount of customers. PEEC-Power B.V. decided to support a battery-bus voltage of 450 to 600 volts.

An important requirement is the possibility to start the combustion engine. An additional machine has to turn up the speed of the combustion engine until a point where the ignition can be started. Normally, the internal combustion engine of a car is started by using a DC-machine, but the synchronous machine in the range extender can also be used to start the combustion engine. Paragraph 3.3 will explain the optimal solution based on costs, weight, flexibility and efficiency.

Another important aspect is the frequency swing. The synchronous machine will not provide a constant frequency, due to the compression and combustion cycle of the engine (figure 2.2.). This swing causes vibrations in the range extender, the power electronic system should provide the possibility for future research to reduce these vibrations.

The power electronic system needs to meet the following requirements:

- Flexibility on output (support a battery-bus voltage of 450V-600V)
- Possibility to start the internal combustion engine
- Variable torque and frequency profile
- Future possibility to reduce vibrations in combustion engine would be a pre
- Nominal terminal phase voltage: 251V
- Nominal phase current: 45A

Chapter 3: Converter topologies

In a system with a variable AC source and a DC load only a few topologies can be applied. One option is a passive rectifier combined with a DC/DC converter and external starting motor to meet the variable output voltage and combustion engine starting requirement. Another way is to use an active rectifier to control and rectify the voltage with one converter. An additional starting motor is not needed, because the active rectifier can operate bi-directional. The passive rectifier solution is discussed in paragraph 3.1 and the active rectifier solution is discussed in paragraph 3.2.

3.1. Passive AC/DC converter

The range extender will mainly be operated in generator mode; the combustion engine provides energy to the battery-bus. This paragraph shows a solution with a passive AC/DC converter combined with an active DC/DC converter and external starting motor.

A passive rectifier can convert the AC to a DC voltage. Since this DC voltage is uncontrolled, an additional DC/DC converter is required to guarantee a flexible and controlled output to support different battery-bus configurations. A consequence of the passive diode rectifier is the need of an external starting motor for the combustion engine, because the diode rectifier cannot operate bi-directional. An overview of this setup is shown in figure 3.1.

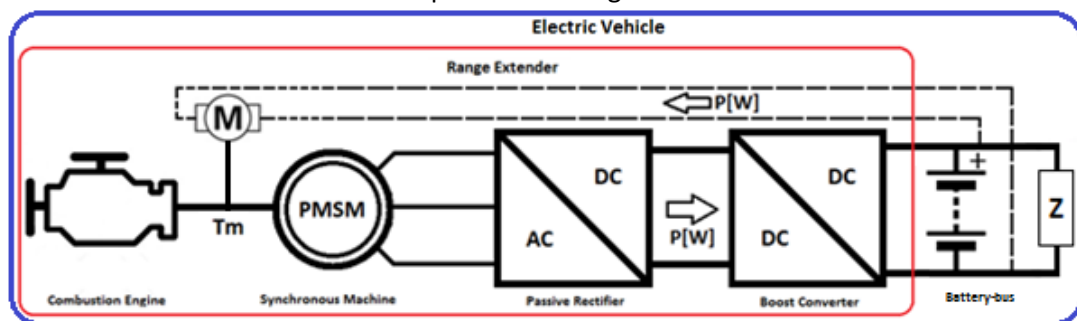


Figure 3.1: Passive rectifier with external starting motor

Figure 3.2 shows the synchronous machine and AC/DC block in more detail.

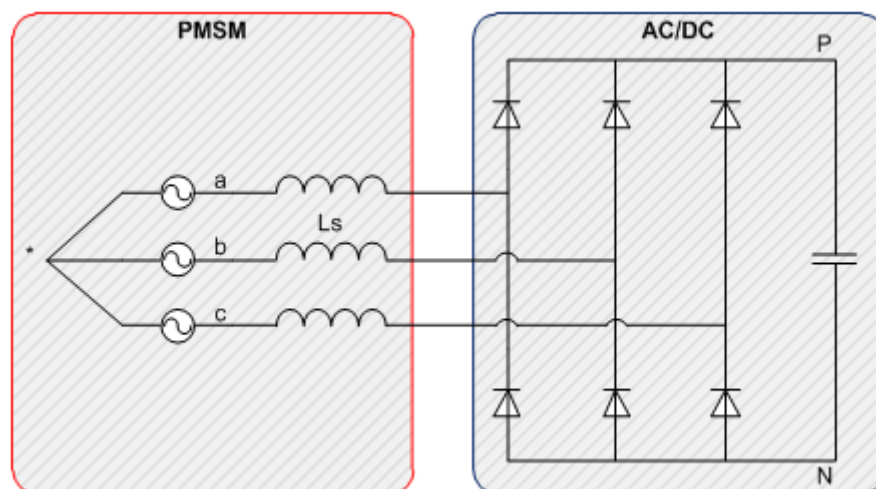


Figure 3.2: Detailed implementation passive rectifier

The full bridge rectifier is commonly used in industrial applications because it is a small and economic solution to rectify an alternating current. For the drawbacks we have to analyze the operation of the passive rectifier has in more detail.

Non sinusoidal current

Because of the passive diodes, current can only start flowing when the line to line voltage of the PMSM is higher than the uncontrolled DC voltage. Since the machine inductance is in between of the machine and uncontrolled DC voltage the current will increase according:

$$U_{Ls}(t) = L_s \frac{di_s(t)}{dt} \quad (3.1)$$

$$i_s(t) = \frac{1}{L_s} \int (U_{an} - U_{PN}) dt \quad (3.2)$$

After rectifying the three phase voltage from the synchronous machine, the six pulse voltage waveform results in a non smooth sinusoidal and pulsating phase current shown in figure 3.3.

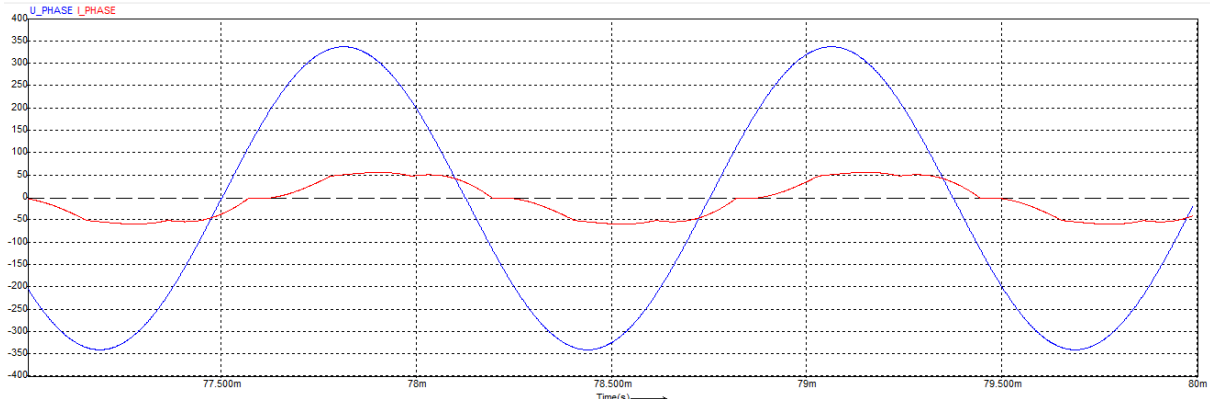


Figure 3.3: Current and voltage of passive rectifier

The pulsating current has several disadvantages; it causes a pulsating torque which can lead to vibrations in the combustion engine. Since the current is not sinusoidal, the harmonics will cause losses in the synchronous machine. Beside these drawbacks there is no flexibility to control the vibrations and to start the combustion engine, therefore an additional starting motor is needed which is heavy and costly.

To meet the output flexibility requirement from paragraph 2.4, an additional active DC/DC converter is required. The AC/DC and DC/DC design from figure 3.1 is explained below.

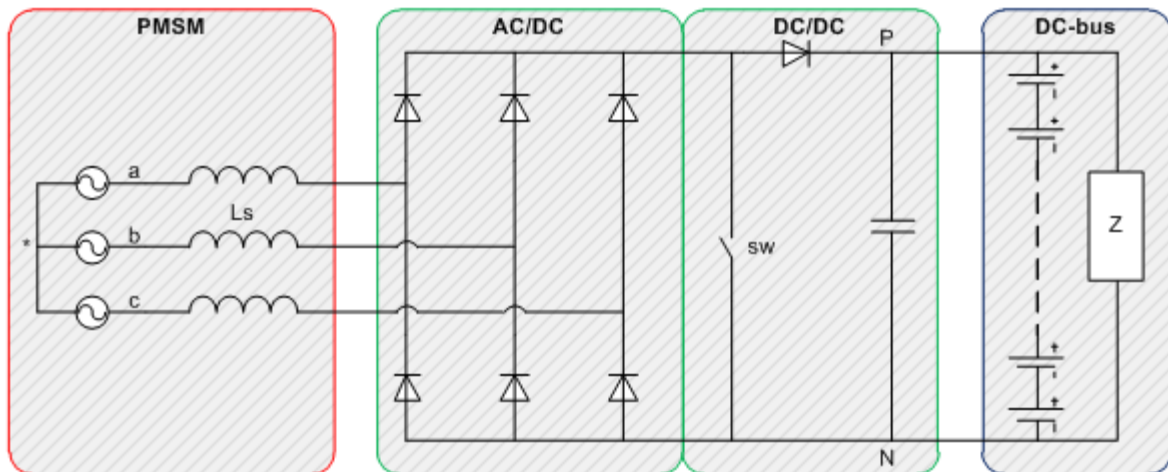


Figure 3.4: Passive ac/dc combined with active dc/dc

The figure above shows a passive diode rectifier combined with a boost converter. Because the boost converter is connected to a synchronous machine, the self inductance L_s is used and an additional inductance can be cut out of the boost design.

The switch in the boost converter adds some flexibility to the design. It is possible to control the output voltage and the harmonics in the machine can be reduced by using smart switching patterns [4].

The summarized specifications for described passive AC/DC solution are:

- Small and lightweight electronic components but unidirectional
- Harmonics control possible
- No possibility to control vibrations
- A pulsating torque will cause vibrations
- Additional heavy starting motor required
- The additional starting motor will increase costs

3.2. Active AC/DC converter

In the previous paragraph an economic but heavy solution was presented to meet the design requirements of paragraph 2.4. This paragraph presents an all-in-one solution to transfer power from the synchronous machine to the battery-bus and vice versa. Figure 3.5 shows a systematic overview with one active AC/DC converter.

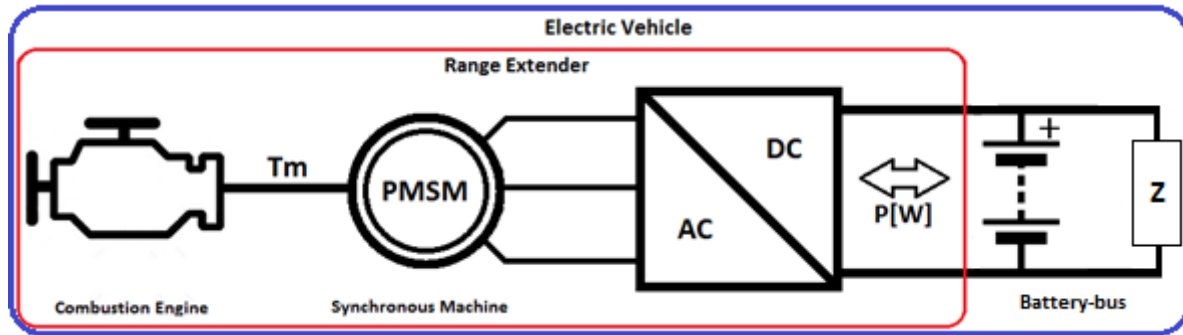


Figure 3.5: system overview active ac/dc converter

The bi-directional AC/DC converter eliminates the external starting motor because the combustion engine can be started by using the synchronous machine. A detailed implementation of the full bridge converter is shown in figure 3.6.

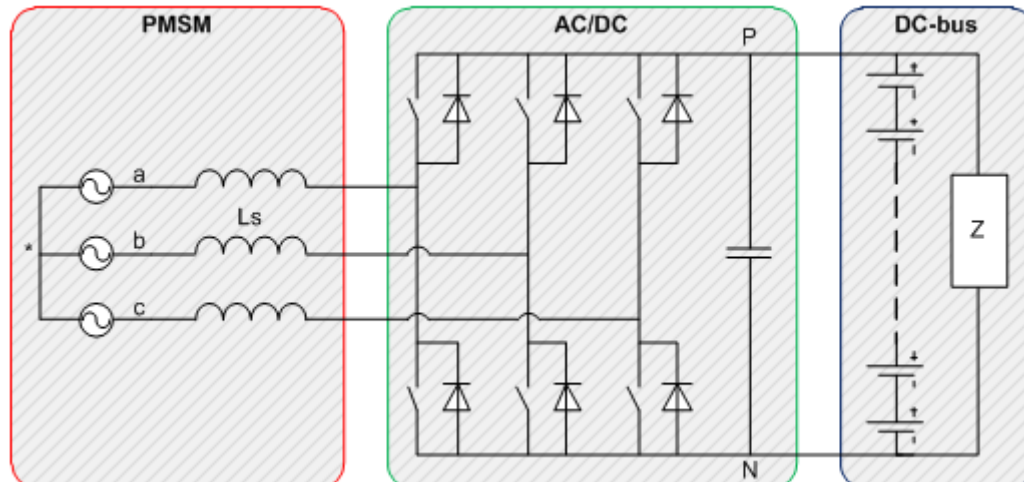


Figure 3.6: FullBridge Active AC/DC converter

The full bridge converter consists of three legs with two switches and two anti-parallel diodes. A lot of flexibility is offered via the six switches: all desirable current and voltage waveforms can be achieved by using different PWM methods.

Each phase can be switched to the positive or negative terminal of the battery-bus by using the six switches. The current waveform depends on the switching pattern; a high switching frequency will result in a smooth sinusoidal current waveform, but also in higher switching losses. A low switching frequency will result in a choppy current waveform with a high harmonic distortion but also in less switching losses. Figure 3.7 shows a switched current waveform with a switching frequency of 16 times the fundamental frequency.

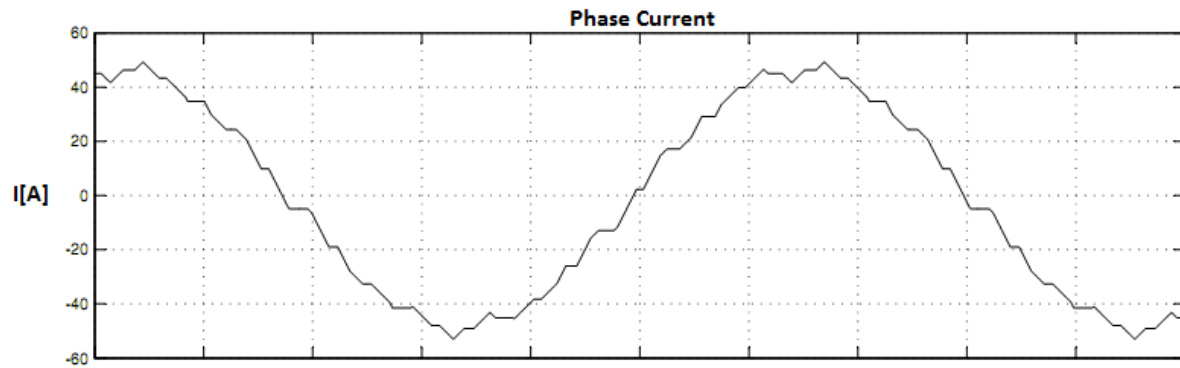


Figure 3.7: Switched current waveform

Another advantage of the proposed topology in figure 3.6 is the possibility to control the power factor. By changing the power factor the amount and the direction of the power flow can be controlled.

The summarized specifications for described active AC/DC solution are:

- Bi-directional converter, no additional starting motor required
- Possibility to control vibrations of the combustion engine
- Sinusoidal current results in less harmonics and vibrations
- Power factor is controllable
- The electronic components will be heavier and more expensive compared to a passive AC/DC converter

3.3. Topology choice power electronic converter

Paragraph 1.3 and 2.4 stated different requirements and design criteria for the power electronic converter. Combining the requirements and design criteria lead to the following four key aspects:

- Costs
- Weight
- Efficiency
- Controllability

Both presented solutions meet the requirements stated in paragraph 2.4, but each design has its own strong and weak characteristics. The proposed solutions in chapter 3 are weighted to the key aspects stated above.

Costs

The passive AC/DC design consists of a power electronics part and a starting motor. Since the power electronic design is build with seven passive diodes and a switch, the passive AC/DC solution will be half as economic as the active AC/DC solution which is build with six active switches with anti-parallel diodes. However, the external starting motor is a big cost driver in the passive AC/DC design which will double the cost price of the total solution. For a large number of components the cost price is expected to be equivalent for the passive and active AC/DC design [Appendix B].

Weight

Size and weight are the second most important aspects for the range extender, it must be as small and lightweight as possible. The power electronic components of the two proposed solutions are quite similar, the active switches of the active AC/DC solution may be a little heavier, but the required external starting motor of the passive AC/DC solution will make the design very bulky and heavy.

Controllability

Controllability is also an important aspect in the range extender. The harmonic distortion, output flexibility and vibration reduction contribute to a more silent, reliable and efficient product. Due to the active boost converter in the passive AC/DC design, the harmonics and output voltage can be controlled, but the solution cannot provide vibration reduction and bi-directional power flow. The active AC/DC solution excels in flexibility and is able to control current, power flow, harmonics and offers the possibility to reduce the vibrations of the combustion engine.

Efficiency

PEEC-Power B.V. aims to contribute to the sustainability of future transport and therefore it is important to design a high efficient converter to limit the energy loss caused by conversion. Another efficiency related topic is heat transfer. A small and compact sized converter can cause trouble with heat transfer. The smaller the losses, the lower the dissipation and the less heat has to be transferred. So it is important to make the total system as efficient as possible. This means that the losses in the generator and losses in the power electronics have to be optimized. The passive AC/DC solution has low switching losses because of the single switch, but the conduction losses in the diodes are significant [4]. The losses in the active AC/DC solution depends on the switching frequency, a high frequency will cause high switching losses, but less harmonic losses in the synchronous machine, so an optimum efficiency point has to be calculated here.

All the solutions can be weighted to the key aspects in a quadrangle representation shown in figure 3.8. The representation is based on the discussion on the previous page.

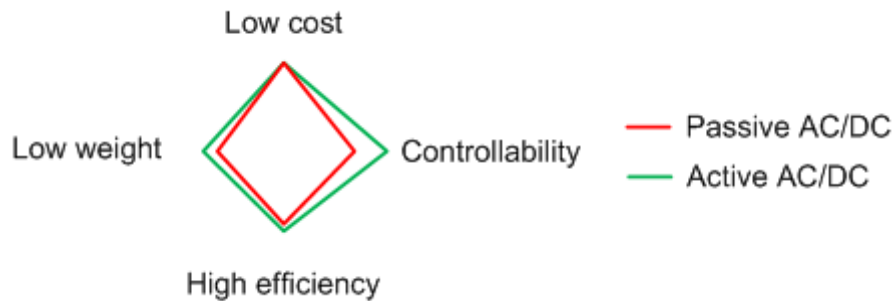


Figure 3.8: key aspects of proposed solutions

As stated in paragraph 1.2 costs are the most important key aspect in the power electronic solution of the range extender. The combustion engine and synchronous machine were designed to meet different design criteria with low costs as most important key factors. Figure 3.8 shows that the expected cost price will be equal of both presented solutions. Additionally, it also shows the benefits of the active AC/DC design in weight, controllability and efficiency. Therefore the active AC/DC topology with six switches and anti-parallel diodes will be proposed as the best solution for the range extender. Besides that, the active switches are widely used in the automotive industry and PEEC-Power B.V. expects that the price of these components will decrease in the near future. In the next chapter the full bridge converter will be discussed in more detail and calculations are made on components and operation.

Chapter 4: Hardware design

4.1. Basic operation full bridge converter

The full bridge converter proposed in the previous chapter is also called force-commutated converter. Those converters are built with semiconductors with gate-turn-off capability, which means that the switches can be switched ON and OFF whenever is required. This allows the commutation of the switches hundreds of times in one period with the following advantages: the current or voltage can be modulated, control of the harmonic distortion, power factor control and bidirectional power flow.

During rectifier operation, the basic operation principle of the converter consist on keeping the battery-bus voltage and/or current at a desired level by using a feedback control loop as shown in figure 4.1. During inverter operation, mechanical speed and phase currents are used as feedback to control the torque or speed of the synchronous machine.

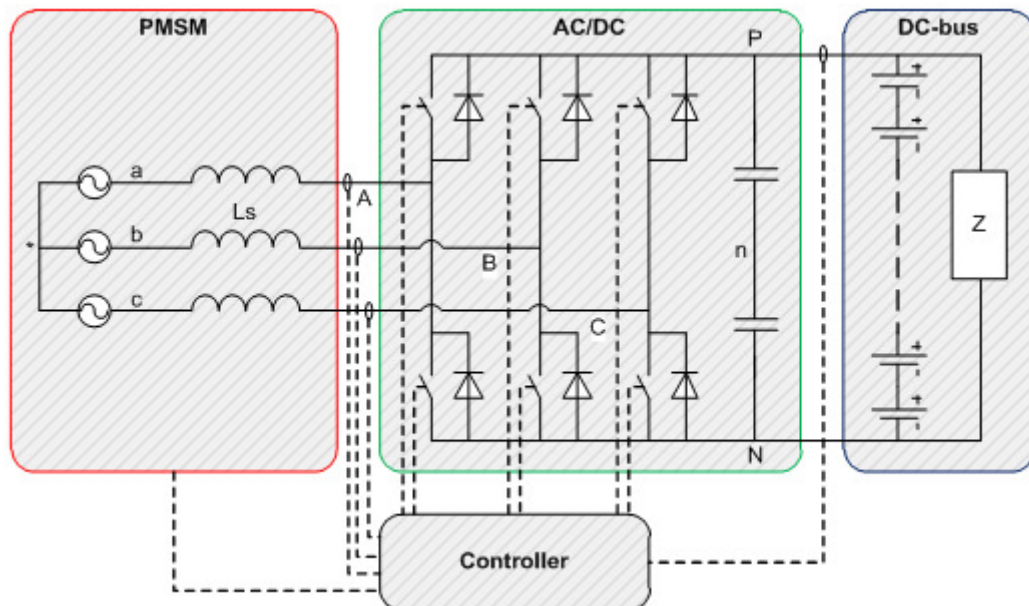


Figure 4.1: operation principle full bridge converter

In both operation modes, the feedback signals are compared to desired reference values and the error signal generated from this comparison is used to create a PWM waveform, which will switch ON and OFF the six switches of the full bridge converter. In this way power can flow to the battery or to the synchronous machine.

The PWM control not only can manage active power, but also reactive power, allowing this type of converter to correct the power factor. Additionally, the AC current waveforms can be maintained almost sinusoidal, which will reduce the harmonic contamination to the synchronous machine.

The Pulse-Width-Modulation consists of switching the switches ON and OFF, following a pre-defined template. Particularly, this template could be a sinusoidal or a modified sinusoidal waveform (see also the detailed PWM discussion in chapter 5). For example, the modulation of one phase could be like the one shown in figure 4.2. This PWM pattern is a periodical waveform whose fundamental is a voltage with the same frequency of the template. The amplitude of this fundamental, called U_{ref} in figure 4.2 is also proportional to the amplitude of the template.

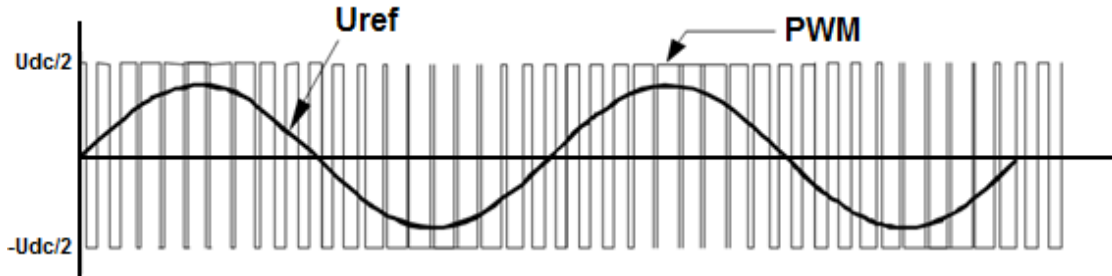


Figure 4.2: PWM Pattern and Fundamental [5]

To make the converter work properly, the PWM pattern must generate a fundamental U_{ref} with a desired frequency. Changing the amplitude of this fundamental, and its phase-shift with respect to the induced voltage of the synchronous machine, the converter can be controlled to operate in the four quadrants: leading power factor rectifier, lagging power factor rectifier, leading power factor inverter, and lagging power factor inverter. By changing the modulation pattern, as shown in figure 4.3, effective DC component and the amplitude of U_{ref} will increase. Displacing the PWM pattern changes the phase-shift.

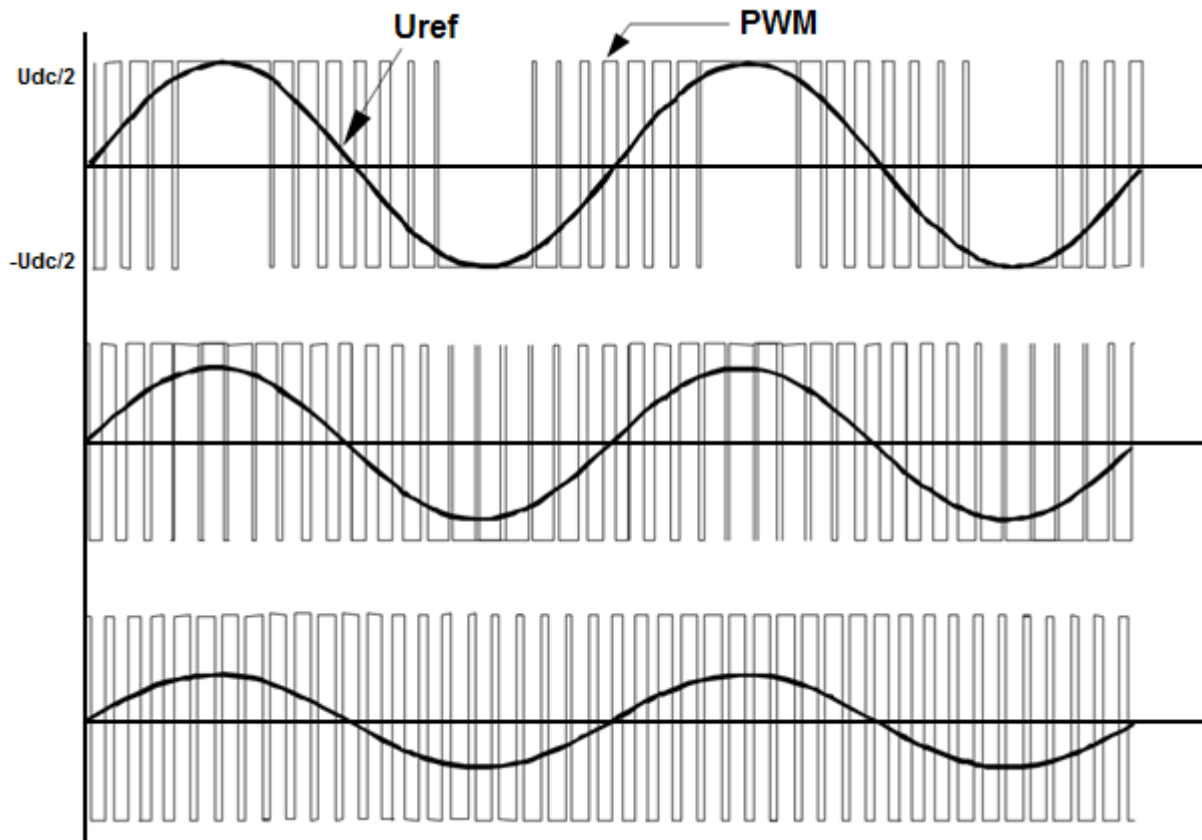


Figure 4.3: Different reference amplitudes [5]

The relation between U_{ref} and the induced voltage can be seen through a phasor diagram. This relation permits to understand the four-quadrant capability of the rectifier. In figure 4.4, the following operations are displayed: a) rectifier at unity power factor, b) inverter at unity power factor, c) capacitor (zero power factor), and d) inductor (zero power factor).

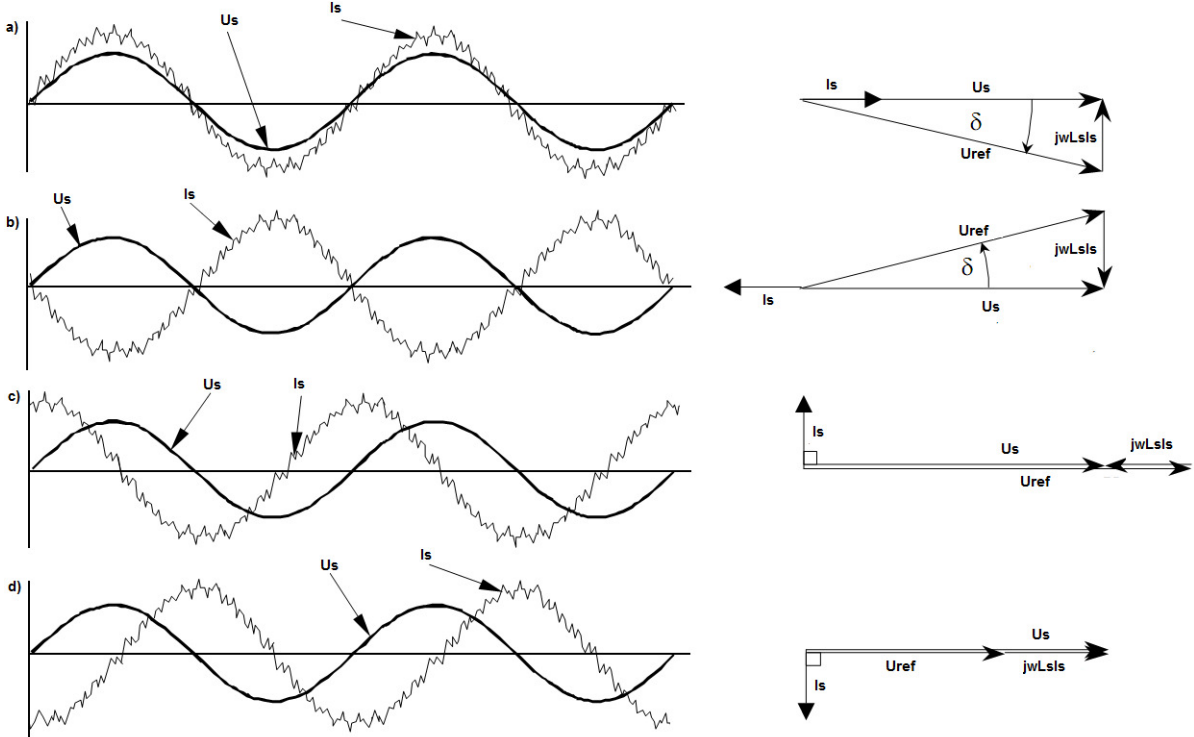


Figure 4.4: a) unity rectifier, b) unity inverter, c) Purely capacitive, d) Purely inductive [5]

The phase current I_s in figure 4.4 is the RMS value of the source current. To get better understanding the current flow through the semiconductors, the phase current is analyzed in more detail in figure 4.5.

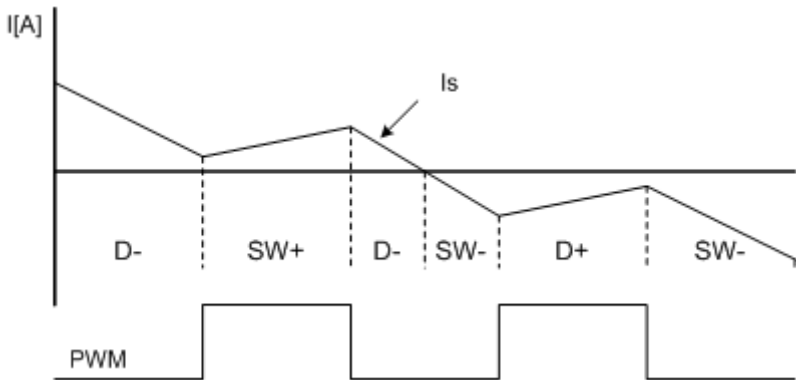


Figure 4.5: Current & PWM waveform and conducting semiconductors

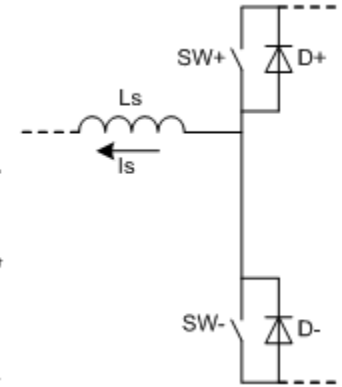


Figure 4.6: One switching leg

The waveform shown in figure 4.5 illustrates the behavior of the current during different switching actions in one switching leg. The example is given for inverter operation, but rectifier operation can be simply illustrated by alternating the current, diode and switch signs. During the positive half cycle, the switch $SW+$ connected to the positive terminal of the battery-bus is turned ON, and the current starts to increase. The current goes to the synchronous machine and comes back to the switches, closing a loop with another phase, and passing through a diode connected at the same positive terminal of the battery-bus. The current can also go to the synchronous machine and return through another transistor located at the negative terminal of the battery-bus. When the switch $SW+$ is turned OFF, the current path is interrupted, and the current begins to flow through the diode $D-$, connected at the negative terminal of the battery-bus. The inductances L_s are very important in this process, because they generate an induced voltage which allows the conduction of the diode $D-$. Similar operation occurs during the negative half cycle, but with $SW-$ and $D+$ (see figure 4.5).

To have full control of the operation of the converter, the six diodes must be polarized negatively at all values of instantaneous ac voltage supply. Otherwise diodes will conduct, and the PWM rectifier will behave like a common diode rectifier bridge. The way to keep the diodes blocked is by ensuring a battery-bus voltage higher than the peak voltage generated by the diodes alone, as shown in figure 4.7. In this way, the diodes remain polarized negatively, and they only will conduct when at least one valve is switched ON, and favorable instantaneous AC voltage conditions are given. In figure 4.7 Udc represents the battery-bus voltage, which is higher than the normal diode-bridge rectification value Ubridge. To maintain this condition, the rectifier must have a control loop like the one displayed in figure 4.1.

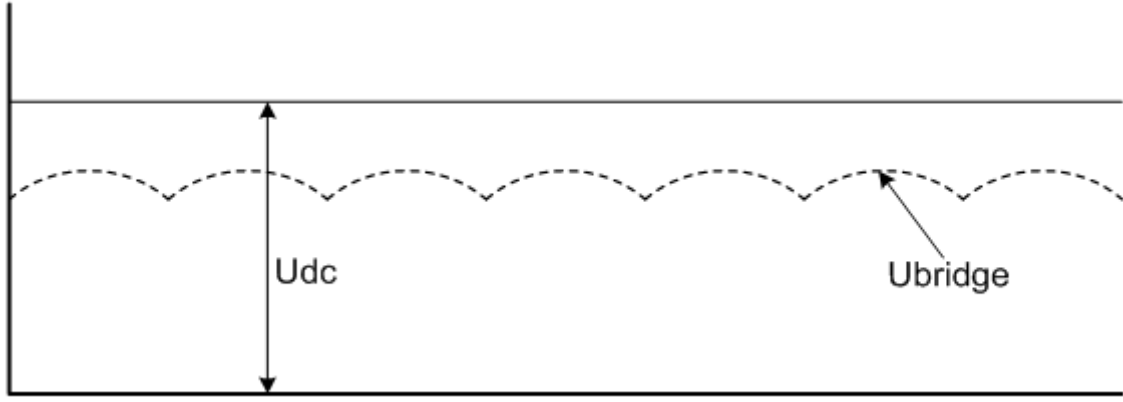


Figure 4.7: Rectified voltage and battery-bus voltage

The PWM waveforms showed in previous figures are voltages measured between the middle point of the battery-bus voltage (n) and the corresponding phase. The phase-to-phase PWM voltages can be obtained with the help of equation (4.1) where the phase_a-to-phase_b voltage U_{PWM}^{AB} is evaluated.

$$U_{PWM}^{AB} = U_{PWM}^A - U_{PWM}^B \quad (4.1)$$

U_{PWM}^{A*} and U_{PWM}^B are the voltages measured between the middle point of the battery-bus voltage, and the phases a and b respectively. With equation (4.2) the phase to neutral voltage can be evaluated.

$$U_{PWM}^{A*} = \frac{1}{3} (U_{PWM}^{AB} - U_{PWM}^{CA}) \quad (4.2)$$

U_{PWM}^{A*} represents the phase a to star point voltage and U_{PWM}^{jk} represents the phase-to-phase voltage between phase j and phase k. Figure 4.8 shows the PWM and ref. voltage, phase-to-phase voltage and the phase to neutral voltage.

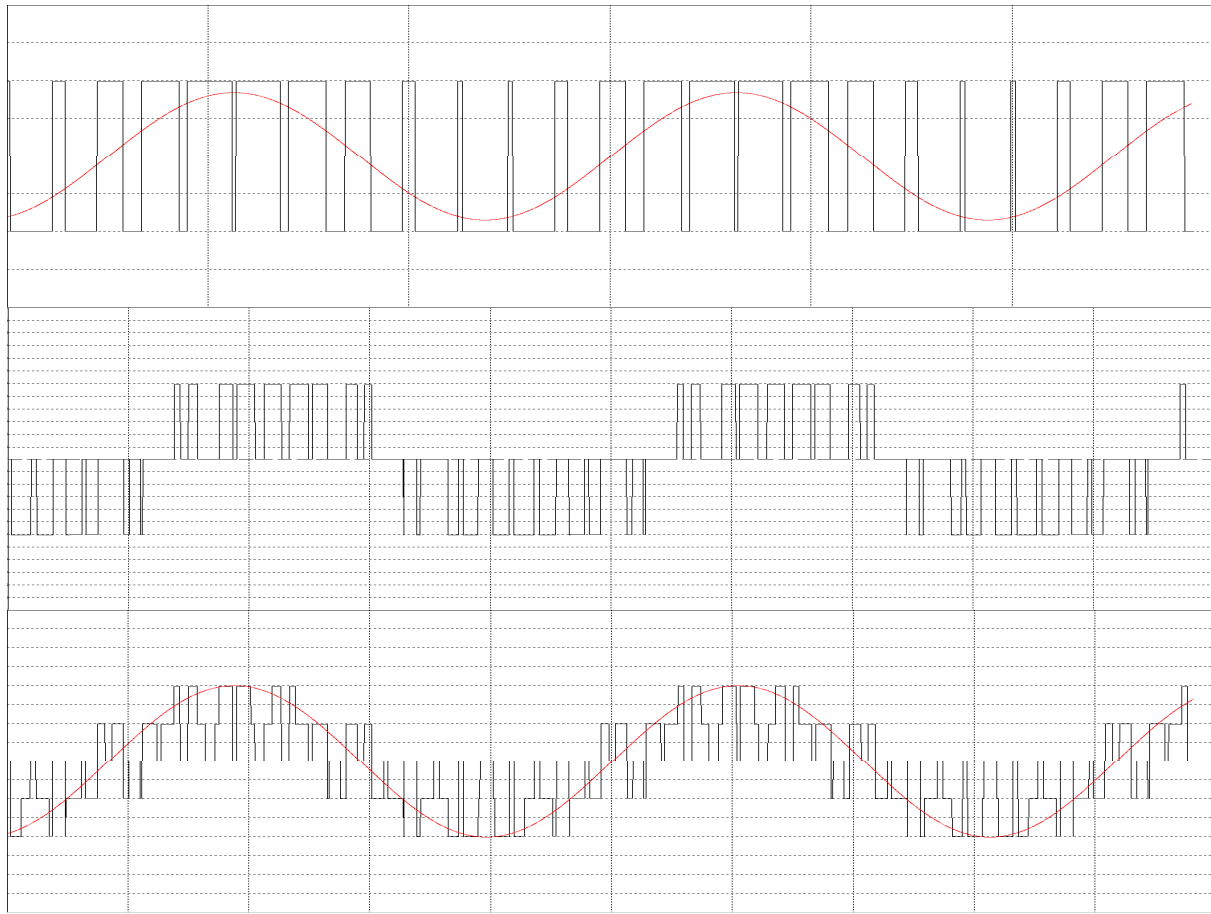


Figure 4.8: top) PWM phase, middle) phase-to-phase voltage, bottom) phase-to-neutral voltage

The PWM patterns can be generated in different ways, chapter 5 gives a detailed description about different PWM and control methods. The following paragraph will discuss the hardware layout of the converter.

4.2. Hardware layout

The proposed power electronic converter in the previous chapter is connected between the synchronous generator and the battery-bus. Therefore the semiconductors, gate drivers and cooling have to be designed according the specifications of these connected systems. Calculations have to be carried out on component ratings, gate drivers and thermal requirements, the outcomes have to be optimized in cost, weight and efficiency as stated in chapter 1.2.

By summarizing chapter 2, the following hardware requirements can be presented:

- Topology is full bridge three phase converter with six active switches
- Nominal phase current is $45 \text{ A}_{\text{rms}}$
- The system has to be able to operate at $2.2I_{\text{nom}}$ in order to start the combustion engine
- Nominal phase-to-neutral generator voltage is $251 \text{ U}_{\text{rms}}$
- The nominal operating frequency is 800 Hz
- The inverter has to provide starting torque of 220 Nm, which is equivalent to $99 \text{ A}_{\text{rms}}$
- The battery-bus voltage is 600 V and its minimal value is 450 V (75%)
- The inductance and resistance of the generator are equal to $410 \mu\text{H}$ and $63 \text{ m}\Omega$ per phase respectively
- Water cooling will be available, with the water temperature equal to 65°C

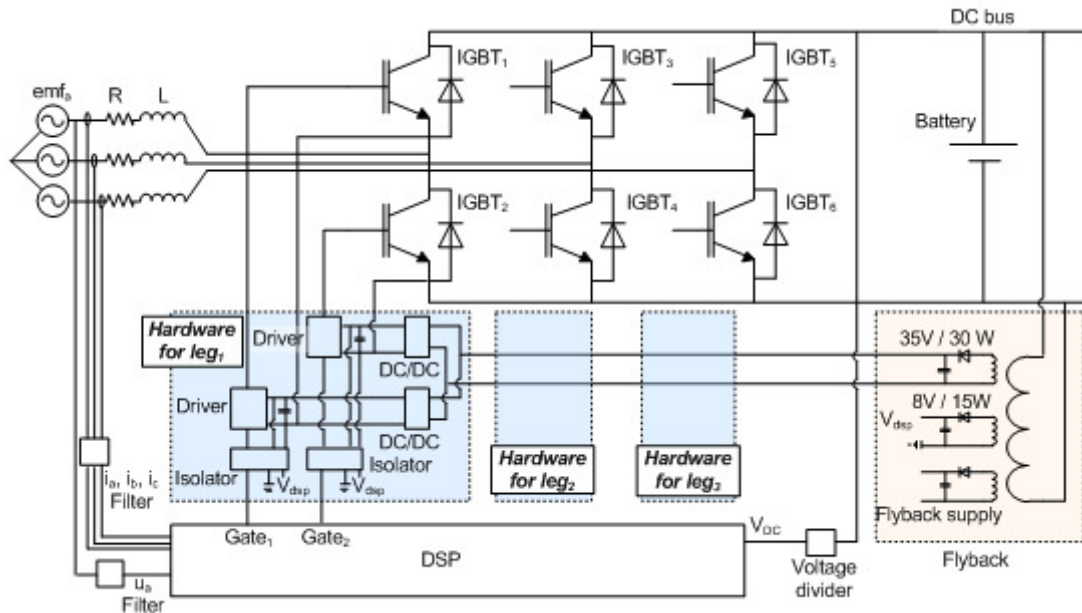


Figure 4.9: Detailed system design

Figure 4.9 shows a more detailed and complete implementation of the basic full bridge converter shown in Figure 4.1. The six IGBT's are driven by specific designed gate drivers which are powered by isolated DC/DC supplies. A DSP will generate the PWM patterns and control the converter by using feedback signals coming from the sensors. All the hardware parts are investigated in more detail in the next subchapters.

4.2.1. Switches

The six switches are the key components in the force commutated full bridge converter. Due to the high fundamental frequency of 800Hz, fast switching devices with short turn on and turn off times are required to obtain efficient switching. Additionally, the switches have to resist a DC voltage of at least 600 volts and 2.2 times the nominal current, 140A at high temperatures since the cooling water temperature is already 65°C.

The BJT, GTO and thyristors are not taken into account here, because of their frequency, voltage or current limitations [6].

MOSFET

MOSFET's have a strong switching performance and are used a lot in switched mode power supplies, motor drives and amplifiers. However, high on state resistance, limited power rating means that MOSFETs cannot meet the high current and voltage requirements and are therefore not suitable for the proposed full bridge converter [7].

SiC MOSFET

SiC MOSFET is a better power semiconductor than Si MOSFET, because of a 10-times higher electric-field breakdown capability, higher thermal conductivity and higher temperature operating capability due to a wide electronic bandgap. Compared to Si IGBT the SiC MOSFET has lower conduction losses and no tail current at turn-off which results in reduced turn-off losses [5][8]. However, the SiC semiconductors cannot operate at very high currents (>100A) and are still quite expensive, therefore the SiC semiconductor is not the best option at this moment, but based on expected future developments it could be the best choice in about a few years.

IGBT

The IGBT combines the simple gate-drive characteristics of the MOSFETs with the high-current and low-saturation-voltage capability of bipolar transistors by combining an isolated gate FET for the control input, and a bipolar power transistor as a switch, in a single device [9]. The IGBTs can handle switching frequencies up to 200Khz, currents up to 1kA and voltages up to 1.5kV [10][11]. Compared to MOSFETs the IGBTs are a bit slower, but have much higher power ratings.

The full bridge converter for the range extender will operate at high power rating (30kW) and a high fundamental frequency (800Hz). IGBTs will be used in the converter because of their high power rating and the ability to operate at relative high switching frequencies (<200kHz) [11].

The required specifications for the IGBTs are:

- Current rating at 85°C: $I_{peak} = I_{start} \cdot \sqrt{2} = 2.2 \cdot I_{nom} \cdot \sqrt{2} = 140A$
- Voltage rating: >600V
- Switching frequency: 7kHz - 20kHz

Manufacturers can offer IGBT modules with 2 IGBT's comprised with the anti-parallel diodes in one case with a voltage rating of 600V or 1200V. Since 600V is too critical with a battery-bus voltage of 600V, the chosen module will have a 1200V DC voltage rating. A current rating of 140A was calculated above, but with a safety margin and future flexibility a module with 200A (@85°C) rating is chosen for the first prototype. These requirements lead to a Fuji Electric module: 2MBI200U4B-120-50, the datasheet can be found in appendix C.

The switches will be operated by 15V gate drivers. It can be found from datasheet that 750 nC of charge is required to increase the voltage across the input capacitance from 0 to 15 V. From here, the effective value of input capacitance is calculated:

$$C_{eff} = \frac{Q}{\Delta V} = \frac{750 \text{ nC}}{15 \text{ V}} = 50 \text{ nF} \quad (4.3)$$

By checking the datasheet, it can be concluded that this capacitance is larger than the actual IGBT input capacitance C_{ies} (22nF). Which is expected because of the Miller effect.

4.2.2. Gate driver

The IGBT modules have capacitive gates with a input capacity as calculated in equation (4.3). The IGBT will start turning on or off when the gate-emitter threshold voltage of 6.5V is crossed. Therefore, the turn-on and turn-off times depends on the charging current on the gate. It is important to choose a gate driver which can source and sink high currents to guarantee fast switching and low switching losses.

The chosen high performance gate driver “Microchip TC4451” is efficient, fast and can source and sink a peak current of 12A [12]. Drivers with higher source and sink power are available, but they are much larger in size and significantly more expensive and are therefore not considered suitable for this converter [13].

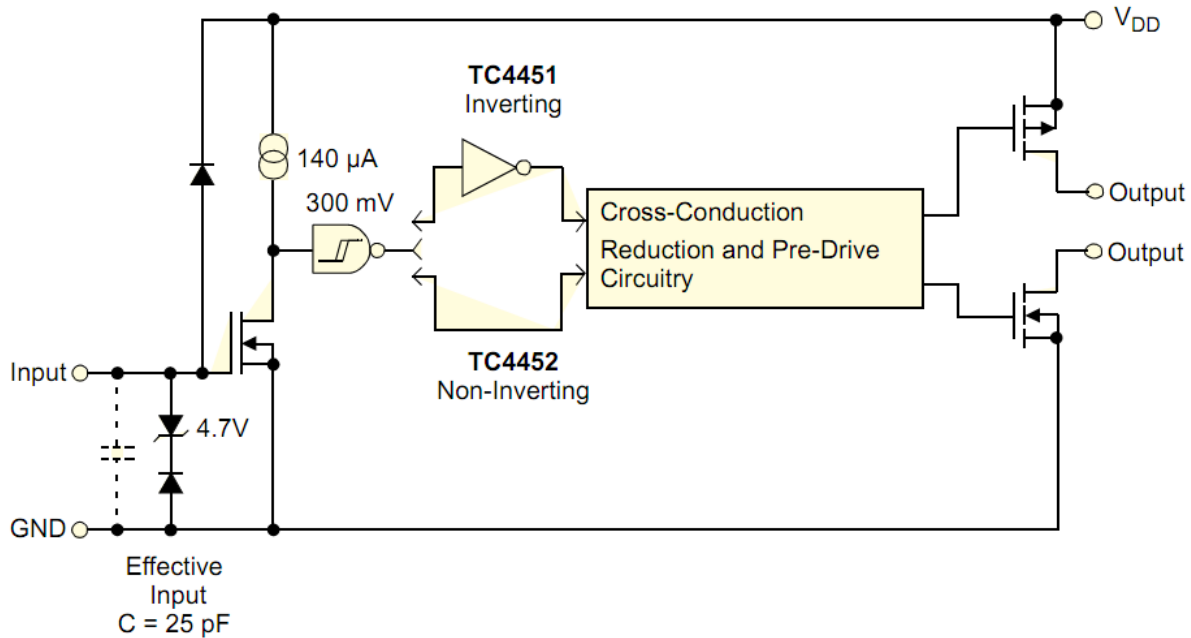


Figure 4.10: Block diagram gate driver

The TC4451 contains a push pull output to source and sink high currents. An input MOSFET with diode protection provides a low capacitive input with negative and positive pulse protection. The control logic ensures matched output rise and fall times, as well as matched leading and falling-edge propagation delay times. The device also has very low cross-conduction current, reducing the overall power dissipation of the device.

The power which is needed to operate one switch during one half cycle of the fundamental frequency is calculated as follows (assumed switching frequency of $21 \cdot f_{\text{fundamental}} = 16.8 \text{ kHz}$).

$$P = C_{eff} \cdot \Delta U^2 \cdot f_{carrier} = 50 \text{ nF} \cdot (15 \text{ V})^2 \cdot 16.8 \text{ kHz} = 0.2 \text{ W} \quad (4.4)$$

At lower frequencies, less power is required for the gates of the IGBTs. Therefore it is not expected that the switching frequency exceeds 16.8 kHz (21·f_{fundamental}, see also paragraph 5.2). Thus, equation (4.4) takes into account the worst case when the largest amount of power is supplied by the driver. This power is also needed to determine the power rating of the gate resistor which is used to limit the current supplied by the gate driver to gate capacitance.

The total dissipation of the driver is given in datasheet [12] and equals to 6mW. Taking into account the required gate power as well, the total power needed by the driver is:

$$P_{total} = 400 \mu\text{A} \cdot 15 + 0.2 \text{ W} = 0.206 \text{ W} \quad (4.5)$$

The safety factor of, for example 2.4 can be taken, so that the total power becomes 0.5 W. Therefore, the gate driver needs current supply of 0.5 W/15 V = 0.033 A, which can be rounded at 0.05A. The gate resistor has to be calculated in order to limit the gate current. The condition that has to be satisfied is that the peak current must not exceed the maximal rating of the gate driver. To limit the current at 10A a resistor of 1.5Ω can be applied with a source voltage of 15V. The turn-on and turn-off times of the IGBT are calculated as follows:

$$t_{off} = -\tau \cdot \ln \frac{U_{threshold}}{U_{driver}} = -1.5 \cdot 50n \cdot \ln \frac{0.5}{15} = 255 \text{ ns} \quad (4.6)$$

$$t_{on} = -\tau \cdot \ln \left(1 - \frac{U_{threshold}}{U_{driver}} \right) = -1.5 \cdot 50n \cdot \ln \left(1 - \frac{14.5}{15} \right) = 255 \text{ ns} \quad (4.7)$$

One capacitor has to be placed next to each driver. Its value is determined based on the acceptable voltage drop due to the single charge of the IGBT input capacitance. For the minimal voltage of 14.5V (3.3% ripple), the required capacitance is found according equation (4.8).

$$C = \frac{Q}{\Delta U} = \frac{750 \text{ nC}}{0.5 \text{ V}} = 1.5 \mu\text{F} \quad (4.8)$$

With a safety margin a capacitor of 2.2μF with a voltage rating of 25V will be chosen for the test setup.

4.2.3. DC Supply

The DC/DC converters ensure that supply of each gate driver is galvanically isolated from the input. More important, they provide floating supply voltage for three upper IGBT switches. Figure 4.9 illustrates that six DC/DC converters will be used. However, only four converters are required: each upper gate driver has one DC/DC converter and all three lower gate drivers are connected to only one converter. The reason for such a connection is that all three lower gate drivers have common ground while three upper drivers are connected to separate floating grounds.

The DC/DC converter has to supply the total power required by the gate drivers. As already mentioned above, four converters are needed, where each upper switch has one converter and all three lower switches are supplied from only one. The converter for the upper switch has to supply power of 0.5W and power output of the converter used for three lower switches is 3 · 0.5W = 1.5W.

An economic and robust solution would be a fly-back converter which can convert the battery-bus voltage to several isolated output voltages by using a transformer with multiple output windings. Figure 4.11 shows such a design. The DC/DC converter on the output of each winding is required to provide a high quality and stable voltage for the connected loads.

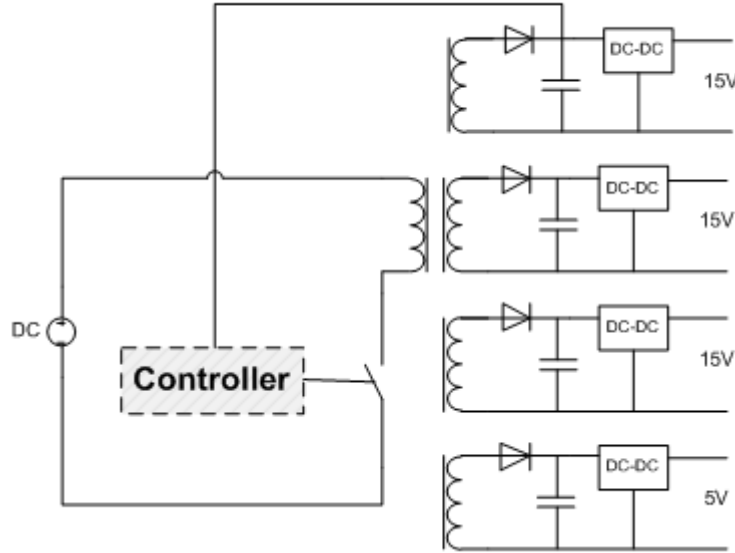


Figure 4.11: Fly-back converter

Although a fly-back converter is the best solution for the production version of the range extender, the test setup will be designed with standard DC/DC converters to save time and guarantee directly the required robustness. The Emerson ASA00C18-L DC/DC converter is chosen for the supply of the six gate drivers. It can deliver 15V/0.4A with ca. 80% efficiency at an input voltage range of 9 – 36V. The maximum power demand from the PSU for the gate drivers will be around $6 \cdot 0.5\text{W} \cdot (100/80) = 3.75\text{W}$ including safety margin.

4.2.4. Isolator

The isolator is needed to galvanically decouple lower power output of the DSP from high power system stage, comprising gate drivers and IGBTs. Isolation can be provided by opto-couplers or optical links with fiber cables. Opto-couplers are more compact, economic and are the best solution for the range extender, but the optical cables are chosen for the test setup because of the long distance between the emitter and receiver, the low power stage of the DSP will be less interfered by the switching actions of the high power stage. Therefore the fibre optical link “Avago HFBR-1521Z” is chosen to send the gate signals from the DSP to the gate drivers and the “Avago HFBR-2521Z” is chosen to receive the gate signals from the DSP.

The optical transceivers are supplied with the same voltage as DSP (5V) and can withstand $1\mu\text{s}$ pulses of 1A [14]. The isolator provides a very high isolation depending on the distance between the transmitter and receiver (in test setup 1m) and can send data with a speed of 5megabaud, which is fast enough for the gate signals. One isolator is used for one gate driver, thus, six in total are needed.

4.2.5. Sensors

Sensors are important components in a test setup. By using sensors, the current, voltage and speed can be measured and this information can be used in the control loop in order to control the power electronic switches. Disadvantages of sensors are the fact that they increase the failure rate of the control loop. For the production version of the range extender a sensorless control strategy has to be

investigated, but for the test setup, a speed sensor and three voltage and current sensors will be placed to have all the possibilities for closed loop control.

Current measurement

The phase currents can be measured in three different ways:

- Current transformer
- Resistor
- Hall sensor

A current transformer transforms the primary current to a smaller secondary current by using a high winding ratio. The limited frequency and the lack of DC current measurement are reasons not to apply this technique.

Another way to measure the current is by putting a resistor in series with the connected load. The high dissipation and losses are undesirable and therefore the series resistor is not used to measure the currents.

The hall sensor is measuring the current by using the magnetic field around the conductor where the current is flowing through. The sensors are mostly internal compensated and support frequencies up to 500kHz with almost no losses. Therefore the hall sensor “LEM LA 125-P” will be used to measure the current in the test setup. This current transducer is able to measure currents up to $\pm 200A$ and 100kHz with an accuracy of 0.8% [15].

Voltage measurement

The voltage will be measured with a “LEM LV 25-P” voltage transducer. The transducer acts like a current transformer with a winding ratio of 2500:1000 and a primary maximum of 10mA. The primary winding of the transducer is connected with a series resistance to the phase voltage. The secondary winding will induce a voltage in an external connected resistor. The transducer provides 1600V isolation between the primary and secondary voltage and has 0.8% accuracy with a response time of $25\mu s$ [16].

Speed measurement

The speed will be measured by the Bourns EMS22D51-B28-LS5 rotary encoder. This encoder will be mounted on the axis of the synchronous machine and provide the DSP with speed and position information. The encoder generates a pulse signal with 512 pulses in one turn and a direction signal [17]. These two pulses will be processed by the DSP to measure speed and position.

Each of measured signals might have to be filtered (except for the speed signal). This is particularly important for the voltage and current, whose waveform will be highly distorted due to high switching frequency of the rectifier. The voltage and current can be filtered using a RC filter. The cut-off frequency of the filter is equal to $1/(2\pi RC)$ and should be higher than the fundamental frequency and high enough so that it does not slow down the response of the control system. A resistor of 1800Ω and capacitor of $100nF$ will result in:

$$fc = \frac{1}{2 \cdot \pi \cdot R \cdot C} = \frac{1}{2 \cdot \pi \cdot 1800\Omega \cdot 100nF} = 884Hz \quad (4.9)$$

The influence of the filter on the control loop has to be analyzed experimentally

4.2.6. Controller

The controller is probably the most important part of the design. The gate and sensor signals come together at the controller in order to control the behavior of the hardware. The electrical engineering department of the TU-Delft recommended the “Spectrum Digital eZdsp TMS320 F2808” evaluation board to control the hardware, because of their positive experience with this DSP and the application of it. This DSP is programmable from MATLAB Simulink and is supplied with a Simulink library with motor control blocks. The F2808 chip offers different PWM outputs and ADC input for sensor signal processing [18]. The evaluation board will be used for the test setup and a specific design will be made for the production version of the range extender.

4.3. Losses

Losses in the full bridge converter can be divided in two different types: conduction losses and switching losses. Conduction losses occur in the IGBT itself or in the anti-parallel diode and depend on the amount of current flowing through the IGBT or diode. The relationship between the diode voltage drop and current can be found in the appendix C. The Uce curve for 15V and 125°C can be approximated by a linear equation:

$$U_{ce}(i) = i(t) \cdot 0.0055 + 1 \quad (4.10)$$

Assuming the same equation for the forward on voltage of the diode (appendix C), the expected conduction losses for one switching leg can be approximated according equation (4.11).

$$P_{con}(i(t)) = (i(t) \cdot 0.0055 + 1) \cdot i(t) \quad (4.11)$$

By applying a sinusoidal current with nominal values (45A, 800Hz), a RMS value of the losses in one switching leg is obtained:

$$i(t) = 45 \cdot \sqrt{2} \cdot \sin(800 \cdot 2\pi \cdot t) \quad (4.12)$$

$$P_{diss} = \sqrt{800 \int_0^{\frac{1}{800}} ((i(t) \cdot 0.0055 + 1) \cdot i(t))^2 dt} = 47W \quad (4.13)$$

The total expected conduction losses of the three phase full bridge converter during nominal operation will become then 141W.

Estimation of switching losses is more difficult because it depends on many variables, such as turn-on time, turn-off time, current, switching frequency, DC-voltage and PWM method. A turn off and turn on waveform of a circuit with inductive load is presented in figure 4.12.

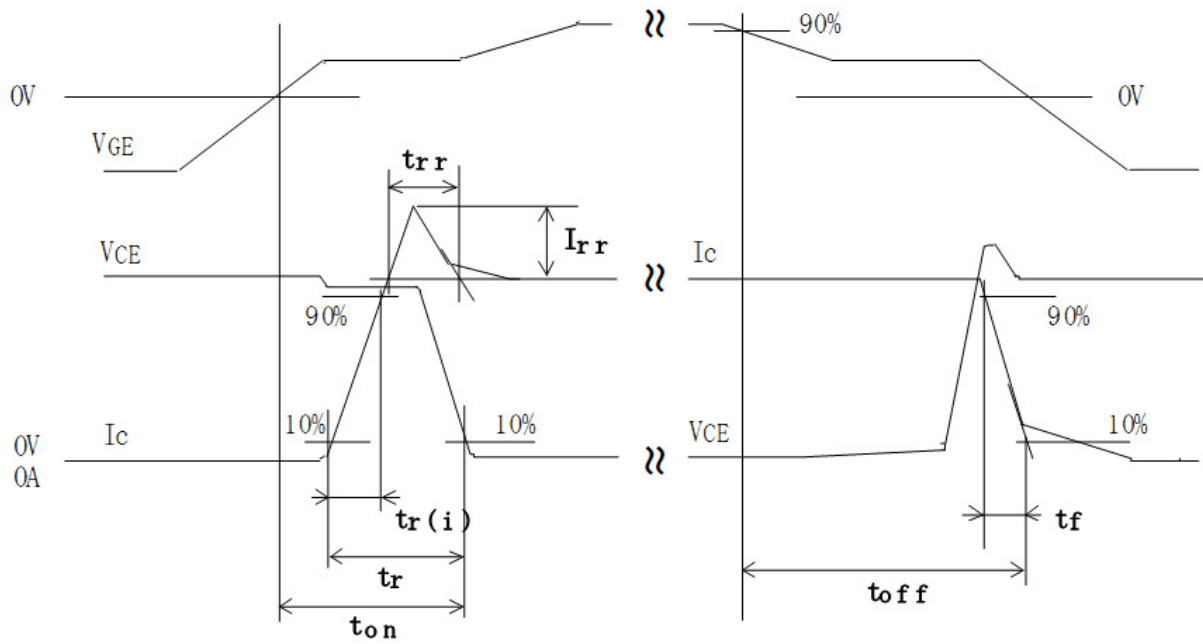


Figure 4.12: Switching waveforms [appendix c]

At turn on, the current through the IGBT is increasing, but the voltage across the IGBT is still at a high level and starts decreasing when the anti-parallel diode is fully recovered. Therefore there will be a dissipation peak during t_r . At turn off, the voltage across the IGBT is increasing, but the current through the IGBT is still at the same level and starts decreasing when the anti-parallel diode of the opposite IGBT starts conducting. Therefore there will be a dissipation peak during t_f . During turn off, the waveform shows a “tail current”. The holes in the IGBT structure are left with some electrons and therefore a small current can still flow until all holes are swept out or recombined [19].

The datasheet of the IGBT show some dissipation figures of the switching actions (appendix C). By using linearization on these figures, the following dissipation equations can be presented at 125°C:

$$\begin{aligned} E_{on}(I) &= I \cdot 80 \cdot 10^{-6} \\ E_{off}(I) &= I \cdot 127 \cdot 10^{-6} \\ Err(I) &= I \cdot 159 \cdot 10^{-6} \end{aligned} \quad (4.14)$$

Since the current on the switching action depends on the PWM method, it is difficult to calculate the expected switching losses. However, by assuming the switching frequency is equally distributed over the period of the fundamental, a rough estimation can be made.

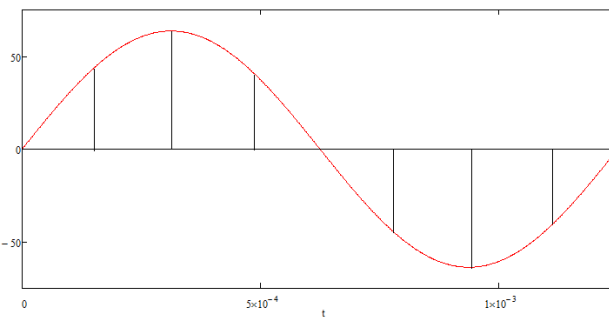


Figure 4.13: equal divided switching actions, $ts=8*t1$

By combining the equations of (4.14) with a summation of the currents at the switching intervals, the following equations can be found for the on, off and reverse recovery dissipation during nominal operation and 125°C:

$$P_{on}(ts) = \sum_{n=1}^{t/ts} (45\sqrt{2} \cdot |\sin(2\pi \cdot 800 \cdot n \cdot ts)| \cdot 80 \cdot 10^{-6} \cdot 800) \quad (4.15)$$

$$P_{off}(ts) = \sum_{n=1}^{t/ts} (45\sqrt{2} \cdot |\sin(2\pi \cdot 800 \cdot n \cdot ts)| \cdot 127 \cdot 10^{-6} \cdot 800) \quad (4.16)$$

$$P_{rr}(ts) = \sum_{n=1}^{t/ts} (45\sqrt{2} \cdot |\sin(2\pi \cdot 800 \cdot n \cdot ts)| \cdot 159 \cdot 10^{-6} \cdot 800) \quad (4.17)$$

Where t is the period of the fundamental and ts is the period of the switching frequency. These equations can be plot with an increasing switching frequency:

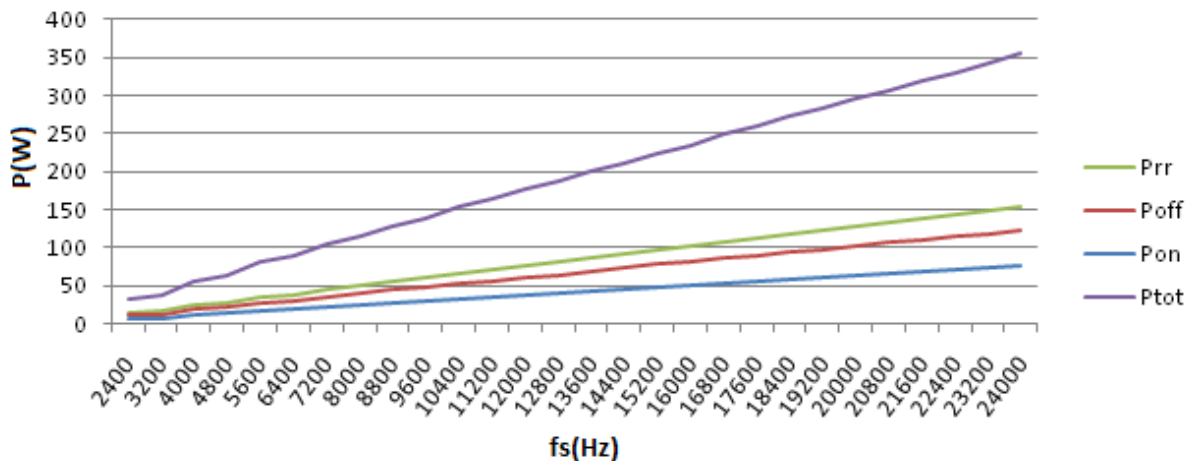


Figure 4.14: Estimated switching losses

Figure 4.14 shows the switching losses of one switching leg during nominal operation. To obtain the total losses of the converter, the losses in figure 4.14 have to be multiplied by three and the conduction losses of 141W have to be added. Chapter 5 shows a more specific approach to determine the switching losses, depending on the chosen PWM method.

4.4. Thermal design

The switching losses in the converter will result in heat increase in de switches. This heat has to be transferred to a colder ambient to keep the junction temperature below 150°C and guarantee proper operation [appendix c]. As stated in chapter 2, the water cooling channel of the electric vehicle is available for cooling the electronics. The losses created in the junction of the switches have to go through some barriers before the heat can be absorbed by the cooling water. These barriers are: junction to case, case to heat sink, and heat sink to cooling water, this configuration is shown in figure 4.15.

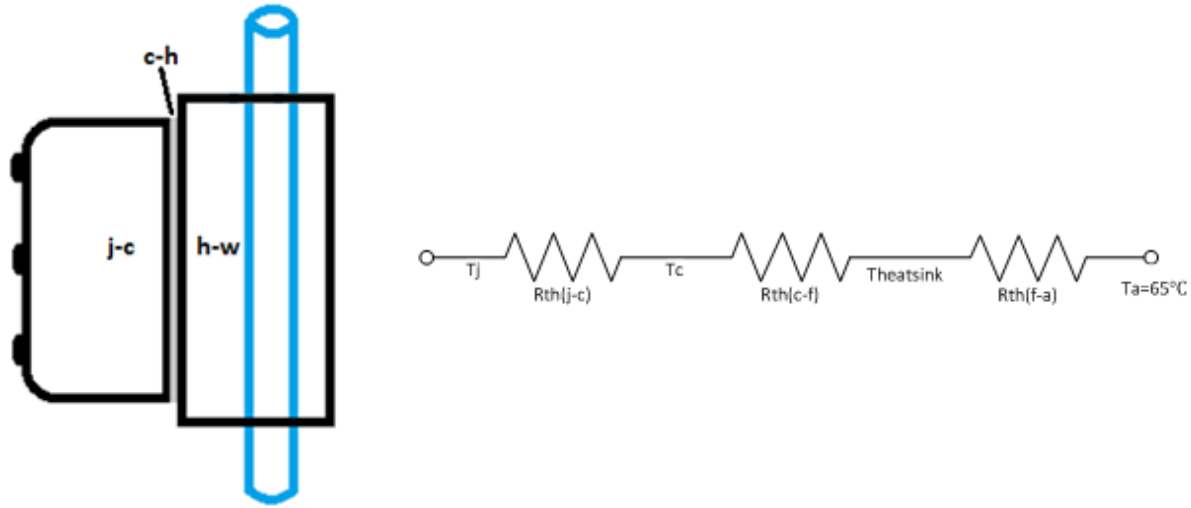


Figure 4.15: (a) Hardware configuration with thermal barriers, (b) Equivalent circuit

Figure 4.15 (b) shows an equivalent circuit representation of the hardware configuration shown in figure 4.15 (a). With this circuit is it easy to calculate the maximum power dissipation and heat sink requirements. The values for $R_{th(jc)}$, $R_{th(cf)}$ can be found in the datasheet of the IGBT (appendix c):

$R_{th(j-c)}$ (IGBT):	0.12°C/W
$R_{th(j-c)}$ (Diode):	0.20°C/W
$R_{th(c-f)}$:	0.025°C/W

The minimum temperature difference between the junction and cooling water is 85°C. In the worst case scenario and an ideal heat sink the maximum dissipation will be:

$$P_{\max} = \frac{150 - 65}{R_{th(j-c)} + R_{th(c-f)}} = \frac{85}{0.225} = 377W \quad (4.18)$$

However, the heat sink will never be ideal and the heat sink requirements depend on the dissipation, which depends on the PWM method. The test setup will be cooled by a heat sink with a thermal resistance of 0.06°C/W. Therefore the worst case maximum dissipation per switching leg will be:

$$P_{\max} = \frac{150 - 65}{R_{th(j-c)} + R_{th(c-f)} + R_{th(f-a)}} = \frac{85}{0.285} = 298W \quad (4.19)$$

4.5. Test setup

Before a prototype of the power electronic system can be made many aspects have to be investigated in practice. Therefore a test setup is developed to analyze the following things in more detail:

- Hardware component operating performance
- Sensors output signals
- IGBT operation
- PWM methods

By doing these measurements, the final design can be improved and the best PWM solution can be applied. Figure 4.16 shows the test setup of the power electronic converter which is connected to the synchronous machine.

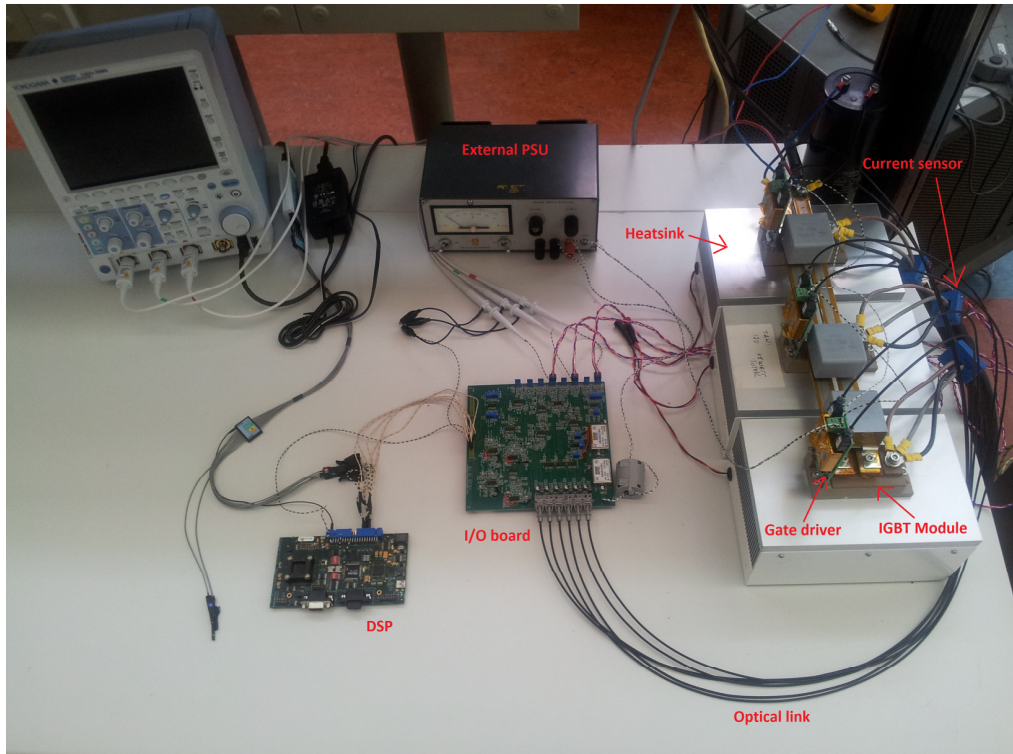


Figure 4.16: Test setup

A schematic diagram of the test setup is presented in Figure 4.17.

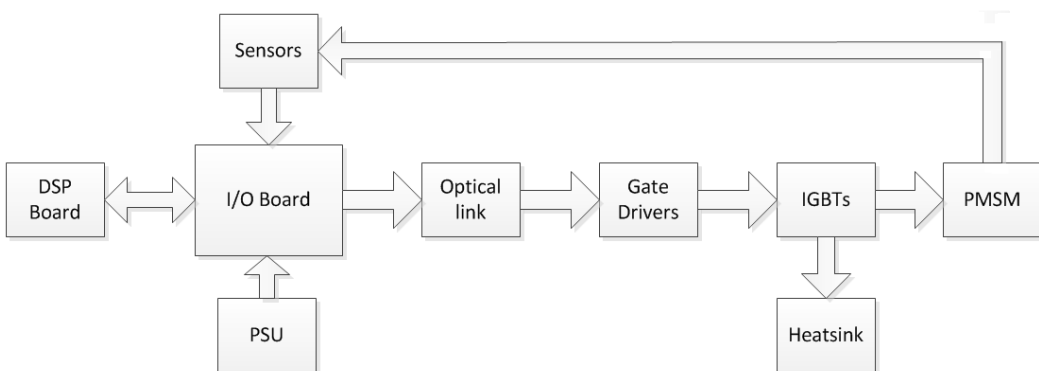


Figure 4.17: Schematic diagram test setup

Most of the hardware is already mentioned in the previous paragraphs and will not be discussed any further. However, the I/O board is only designed for the test setup and will be discussed in the next subparagraph.

4.5.1. I/O board

The I/O board manages all the signals of the test setup and provides overvoltage, overcurrent and gate signal protection. Signals from the sensors are level shifted to make them compatible with the inputs of the DSP. A systematic overview of the I/O board is given below in figure 4.18.

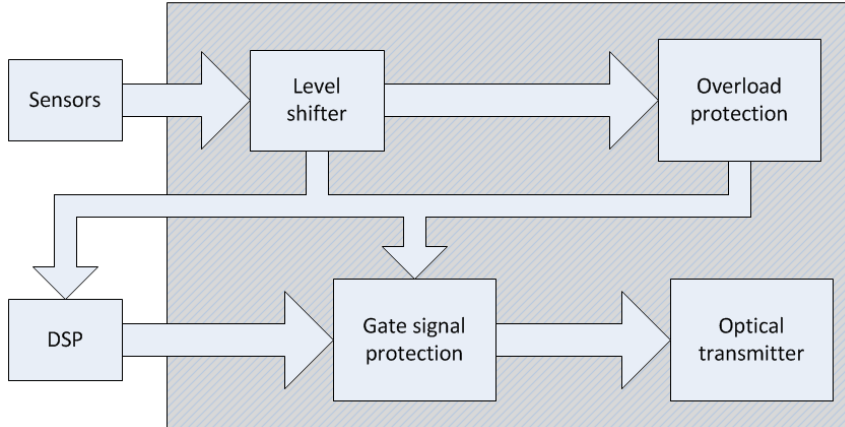


Figure 4.18: I/O board

The $\pm 8V$ from the current and voltage sensors are not compatible with the 0-3.3V input of the DSP. Therefore they are level shifted by a comparator with an external offset voltage (figure 4.19a)

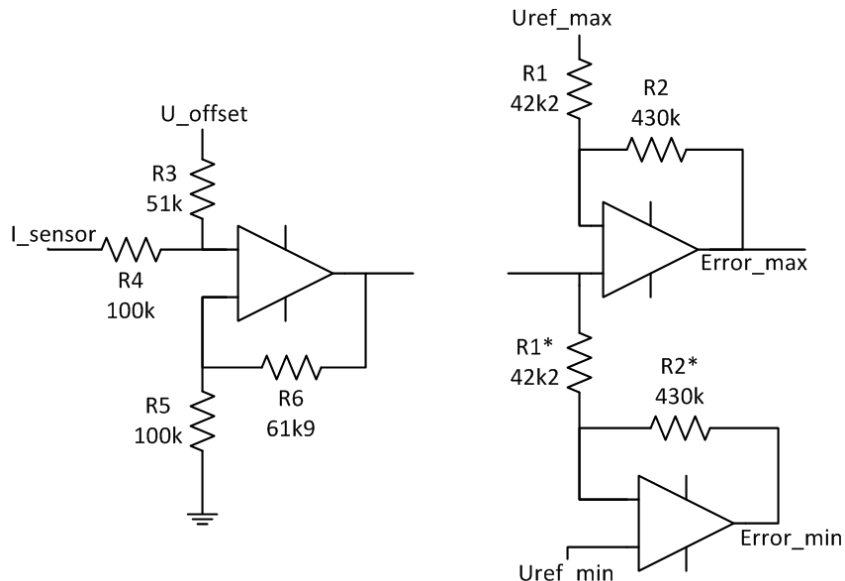


Figure 4.19: (a)Level shifter

(b) Current protection

The non inverting opamp is biased by 7.5V and has a gain of 2.6 in order to shift the $\pm 8V$ to a 3.5V to 11.5V output voltage which represents a current of 160A and -160A. The 0 to 3.3V range of the DSP is achieved by adding a resistor divider with a ratio of 0.22.

After the voltage is level shifted, the voltage is compared by two comparators with hysteresis in order to provide overcurrent or overvoltage protection (figure 4.19b). In case of an error, the outputs of the comparators will go to zero and the gate signals will be disabled. The hysteresis will prevent oscillation and is determined with the following equations, assuming a U_{ref_max} of 11.1V:

$$U_{ref_H} = U_o \text{ max} - (U_o \text{ max} - U_{ref_max}) \cdot \frac{R2}{R1 + R2} \quad (4.20)$$

$$U_{ref_H} = 15 - (15 - 11.1) \cdot \frac{430K}{42K2 + 430K} = 11.5V$$

$$U_{ref_L} = \frac{R2}{R1 + R2} \cdot U_{ref_max} \quad (4.21)$$

$$U_{ref_L} = \frac{430K}{42K2 + 430K} \cdot 11.1 = 10.1V$$

The same calculations can be done for the lower side of the sinus, a reference voltage of 2.4V results in thresholds of 3.5V and 2.1V. A waveform with protection and the resulting error signal (active low) is shown in figure 4.20.

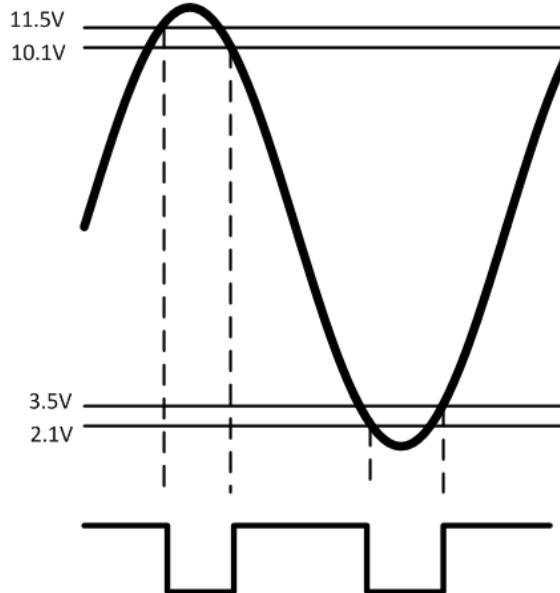


Figure 4.20: Overload protection

Another protection offered by the I/O board is the gate signal protection. A software error can cause two active gate signals of the same leg which results in a short circuit. Therefore a logic schematic is placed between the DSP and the optical transmitters. The third input (enable) is pulled to zero when there is an overvoltage or overcurrent error (figure 4.21).

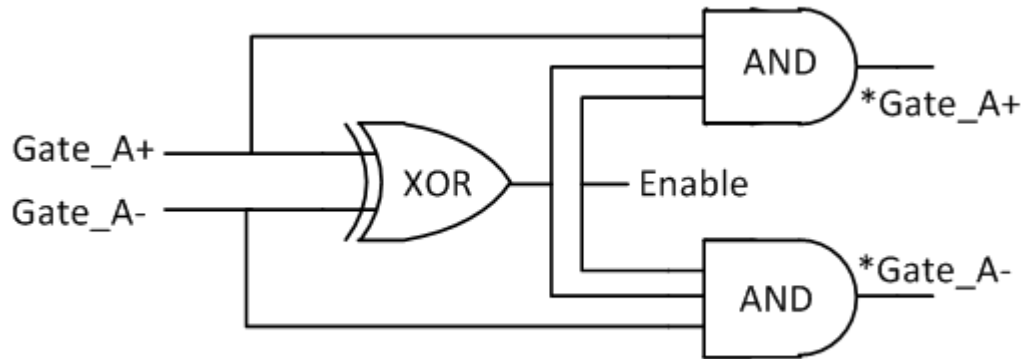


Figure 4.21: Gate signal protection

The truth table of the protection circuit shows that it is impossible to have two active signals on the output of the AND gates. Therefore it is impossible to create a short circuit between the positive and negative terminal of the battery-bus by sending corrupt signals from the DSP.

Gate_A+	Gate_A-	Enable	*Gate_A+	*Gate_A-
0	0	1	0	0
0	1	1	0	1
1	0	1	1	0
1	1	1	0	0

Table 4.1: Truth table gate signal protection

Chapter 5: PWM and control methods

The full bridge topology chosen in chapter 4 is based on price, weight, efficiency and controllability. The high controllability factor shown in figure 3.8 can be realized because of the six active switches in the full bridge hardware design (figure 4.1). These two state switches are controlled by a PWM signal, already mentioned in paragraph 4.1. The goal of each PWM method is to achieve a sinusoidal phase current in the machine with a controllable magnitude and frequency. PWM is actually a signal between 2 levels and can be generated in different ways with harmonic distortion, switching losses, calculation power, complexity, robustness, and EMC as differentiators. The PWM signal is generated based on the error signal of the control loop and is therefore closely related to the control method. Some PWM methods are based on a voltage error signal; voltage controlled, other PWM methods are based on a current error signal; current controlled. This chapter presents the operation and characteristics of four PWM methods: Hysteresis modulation, carrier based modulation, space vector modulation and harmonic elimination. A literature study of these PWM methods is presented and simulations are done with the range extender as application. Beside the PWM methods, also two related control methods are discussed: Direct torque control and field oriented control. Finally the PWM methods are weighted to the requirements stated in chapter 1.2 and the best PWM and control method is chosen.

5.1. Hysteresis modulation

Hysteresis modulation is a current control method where the phase current tracks a reference waveform within a hysteresis band. The controller generates the sinusoidal reference waveform of required magnitude and frequency which is compared to the actual phase current. If the phase current exceeds the upper limit of the desired hysteresis band, the upper switch of the inverter leg is turned off and the lower switch is turned on, which results in a decreasing current. If the current crosses the lower limit of the hysteresis band, the lower switch of the inverter leg is turned off and the upper switch is turned on. As a result, the current gets back into the hysteresis band and the actual current is forced to track the reference current within the hysteresis band. In a three phase system, three reference waveforms with a phase shift of 120 degrees between each other are generated and every phase is controlled separately by switching the corresponding inverter leg.

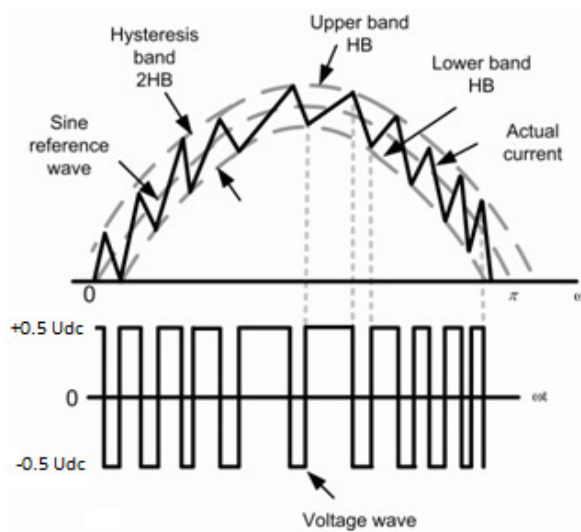


Figure 5.1: Hysteresis modulation

Figure 5.1 shows how the PWM signal is generated. The maximum switching frequency in the hysteresis modulator depends on the hysteresis band and the rate of change of the current, thus the value of L_s and the voltage across L_s as shown in equation (5.1) [20].

$$f^{\max} = \frac{Udc}{4 \cdot h \cdot L_s} \quad (5.1)$$

A small hysteresis band results in a smooth sinusoidal phase current with low harmonic distortion. However, according to equation (5.1), it will also result in a high switching frequency which will result in high switching losses. Additionally, there is no defined switching frequency since the current response depends on the connected load. An equation for the THD can be found in reference [20]:

$$THD(\%) = \frac{100}{I_{rms}} \sqrt{\frac{1}{T} \int_T (i_{phase} - i_{ref})^2 dt} \quad (5.2)$$

To investigate the harmonic distortion at different hysteresis bands and switching frequencies, simulations are done in CASPOC [28]. The simulations are done with the generator parameters shown in paragraph 2.2 and during nominal operation:

- RMS phase voltage: 241V
- frequency: 800Hz
- Udc: 600V
- Irms: 45A

The simulations are carried out with different hysteresis bands: 1, 5, 10, 15 and 20A, the results are shown in figure 5.2.

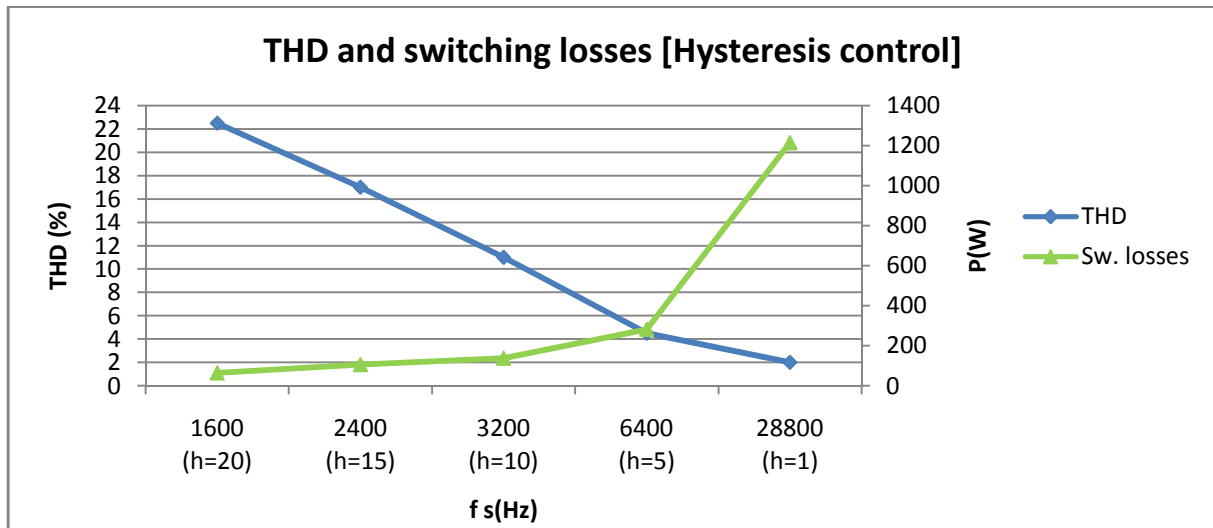


Figure 5.2: Simulation results for hysteresis control with different hysteresis bands

As expected, the harmonic distortion is decreasing when the switching frequency increases. However, a high switching frequency results in very high losses. Therefore an optimum has to be found; from figure 5.2 can be concluded that a switching frequency around 6400Hz looks optimal.

The hysteresis controller can be implemented analog and digitally as well. An analog amplifier with hysteresis band is a simple and low cost solution. However, it is also sensitive for noise and requires a very accurate and robust current measurement. An incorrect current measurement can cause a DC offset in the phase current or an undesirable high switching frequency. The power factor and amount of power can be controlled by changing the current reference waveform depending on the output power.

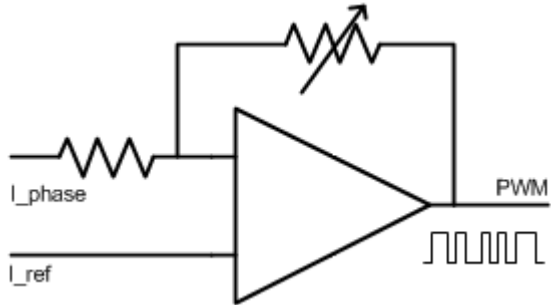


Figure 5.3: Analog hysteresis comparator

The characteristics of hysteresis modulation can be summarized as follows:

- Simple implementation
- Switching frequency depends on load and hysteresis margin
- No defined switching frequency, but can be limited by hysteresis band
- High quality current measurement required, high sampling rate
- Noise or EMI can disturb measurements and can cause incorrect gate signals.

5.2. Carrier based modulation

Carrier based modulation is a voltage control method where a phase-to-phase voltage is generated based on a comparison between a carrier and a reference waveform. The carrier can be triangular or saw-tooth shaped, while the reference voltage is purely or edited sinusoidal. These two waveforms are generated and compared by a digital or an analog circuit and results in a PWM waveform. The choice between analog and digital depends on the application, but nowadays a digital controller is preferred because it is also able to handle other tasks (logging, control, communication) in its application.

5.2.1. Carrier waveform

As mentioned above, the carrier can be saw-tooth or triangular shaped. During operation the reference voltage is compared to the carrier voltage, when the reference is higher than the carrier a positive pulse is generated and otherwise a zero pulse is the result.

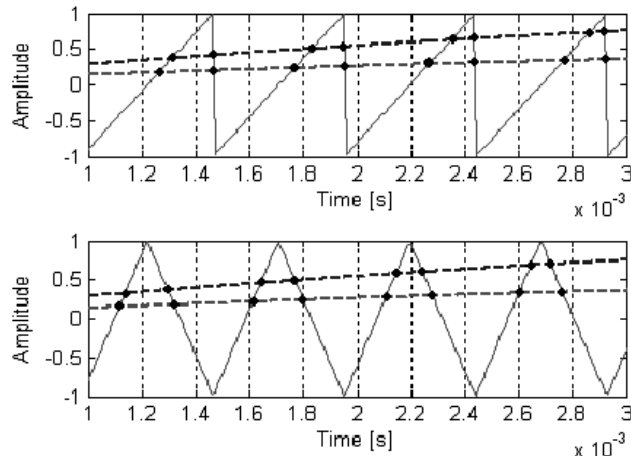


Figure 5.4: PWM with saw-tooth and triangular carrier [23]

For the saw-tooth carrier only the trailing edge of the pulse varies when the value of the modulation index changes, in contrast to the triangular carrier, both sides of the switched output pulse from the phase leg are modulated which results in a symmetrical waveform (figure 5.4.). The advantage of the symmetrical waveform is that the odd harmonic sideband components around odd multiples of the carrier fundamental and even harmonic sideband components around even multiples of the carrier fundamental are eliminated [23]. Due to the bad harmonic performance of the saw-tooth carrier, only the triangle carrier will be used in this chapter.

Looking at one period of the reference voltage, the phase voltage with respect to the neutral (n) looks like in figure 5.5(a):

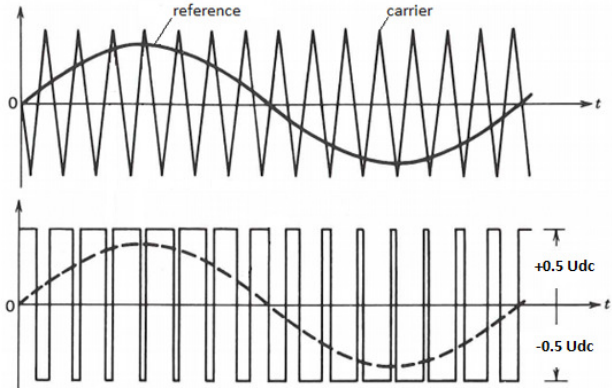
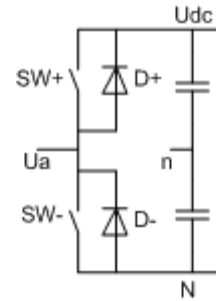


Figure 5.5: (a) Carrier based PWM generation



(b): Switching leg with neutral reference

The relationship between the reference and carrier frequency is called “frequency modulation ratio” and is defined as:

$$mf = \frac{f_s}{f_1} \quad (5.3)$$

Where f_s is the triangular carrier frequency and f_1 is the fundamental frequency. The mf should be an odd integer in order to achieve an odd symmetry waveform and half-wave symmetry with the time origin. Therefore only odd harmonics are present and the even harmonics disappear from the phase to star point voltage (U_{a0}). This means that only the coefficients of the sine series in the Fourier analysis are finite; those for the cosine series are zero [29].

When looking to a three phase system, only the harmonics in the line-to-line voltages are of concern, since the impedance is between the line-to-line voltages. The harmonics in the output voltage of the switching legs (U_{an} , U_{bn} , U_{cn}) are identical to the harmonics in the phase to star point voltages (U_{a0} , U_{b0} , U_{c0}): $(\hat{U}_{an})_h = (\hat{U}_{a0})_h$ [29]. In the phase to start point voltages only the odd harmonics exists as sidebands, centered around mf and its multiples. Considering the harmonic mf and its odd multiples, the phase difference between the mf harmonic in U_{an} and U_{bn} is $(120 mf)$ degrees. This phase difference will be equivalent to zero if mf is odd and a multiple of 3 (e.g.: 3, 9, 15, 21) As a consequence, the harmonic at mf is suppressed in the line-to-line voltage U_{ab} .

5.2.2. Reference waveform

The output of the carrier based modulator can be controlled by changing the reference waveform which is compared with the carrier waveform. A sinusoidal fundamental output voltage can be achieved by using a sinusoidal reference. Output frequency can be determined and the effective phase-to-phase voltage amplitude can be controlled by changing the amplitude of the reference voltage, also called the modulation index (ma):

$$ma = \frac{\hat{U}_{ref}}{\hat{U}_{tri}} \quad (5.4)$$

Where \hat{U}_{ref} is the amplitude of the reference voltage, and \hat{U}_{tri} is the amplitude of the triangular voltage. Since the amplitude of the triangular carrier is 1, ma should be kept lower or equal than 1 to avoid over modulation and undesirable harmonics in the system [21] [30].

The averaged output voltage over one switching time period in a three phase converter is given by the following equations [29]:

$$(\hat{U}a0)_1 = ma \frac{Udc}{2} \quad (5.5)$$

$$U_{LL1} = \frac{\sqrt{3}}{\sqrt{2}} \cdot (\hat{U}a0)_1 \quad (5.6)$$

$$U_{LL1} = \frac{\sqrt{3}}{\sqrt{2}} \cdot ma \frac{Udc}{2} \quad (5.7)$$

Performance of a carrier based pulse with modulator can be increased by including a zero sequence voltage in the modulation reference signal. In the beginning (80's) only sinusoidal reference waveforms were used to generate the PWM patterns. Since there will be undesirable harmonics when the modulation index is pushed above 1, the linear modulation range is limited when using sinusoidal reference waveforms. Research showed the possibility to extend this linear modulation range by using different modulation signals [21][22][24].

A universal representation of the carrier PWM modulator reference voltage is as follows:

$$u_i(t) = u_i^*(t) + e_i(t) \quad (5.8)$$

Where e_i represents the injected waveform and u_i^* represents the regular sinusoidal reference voltage:

$$\begin{aligned} u_a^*(t) &= ma \cdot \sin(wt) \\ u_b^*(t) &= ma \cdot \sin(wt + \frac{2\pi}{3}) \\ u_c^*(t) &= ma \cdot \sin(wt + \frac{4\pi}{3}) \end{aligned} \quad (5.9)$$

By combining eq. (5.5)(5.8) and (5.9) the next expressions for the line-to-neutral voltages can be presented:

$$\begin{aligned} U_{a-N} &= \frac{Udc}{2} [ma \cdot \sin(wt) + e_i(t)] \\ U_{b-N} &= \frac{Udc}{2} [ma \cdot \sin(wt + \frac{2\pi}{3}) + e_i(t)] \\ U_{c-N} &= \frac{Udc}{2} [ma \cdot \sin(wt + \frac{4\pi}{3}) + e_i(t)] \end{aligned} \quad (5.10)$$

The output line-to-line voltages U_{ab} , U_{bc} , U_{ca} are then [21]:

$$\begin{aligned}
U_{a-b}(t) &= \frac{U_{dc}}{2} \sqrt{3} \cdot ma \cdot \sin\left(wt + \frac{\pi}{6}\right) \\
U_{b-c}(t) &= \frac{U_{dc}}{2} \sqrt{3} \cdot ma \cdot \sin\left(wt + \frac{5\pi}{6}\right) \\
U_{c-a}(t) &= \frac{U_{dc}}{2} \sqrt{3} \cdot ma \cdot \sin\left(wt + \frac{3\pi}{2}\right)
\end{aligned} \tag{5.11}$$

These expressions show that the zero sequence signal $ei(t)$ does not appear in the phase-to-phase voltage and that the peak line-to-line voltage amplitude for a three phase inverter is limited to 0.866 times U_{dc} (known that $0 < ma < 1$), which is significantly lower.

In order to improve the utilization ratio of the battery-bus voltage and reduce the harmonic distortion the zero sequence voltage is used to change the reference voltage. In reference [24], the harmonic distortion of six different reference waveforms are tested by using the “Harmonic distortion determining factor”. Only the 3rd harmonic injection (THI) is discussed here this section in more detail since it is most discussed in literature and provides substantial improvements.

The original sinusoidal reference can be modified by superposing the third harmonic of the reference on to it as shown in figure 5.6. The amplitude of the third harmonic should be 16,6% of the sinusoidal reference [24], therefore the modified reference voltage becomes:

$$u_i(t) = ma \cdot \sin(wt) + \frac{1}{6} ma \cdot \sin(3wt) \tag{5.12}$$

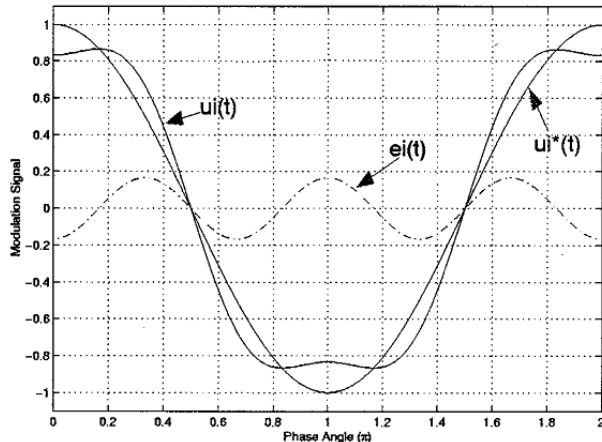


Figure 5.6: Third harmonic injection [21]

The new reference waveform ($ui(t)$) is wider and more flat on the top, which makes it possible to operate with a modulation index up to 1.16. Therefore the utilization ratio of the battery-bus voltage is increased. Also the harmonics are decreased compared to a classical sinusoidal reference. Figure 5.7 shows the total harmonic power for different modulation indexes and modulation methods mentioned above.

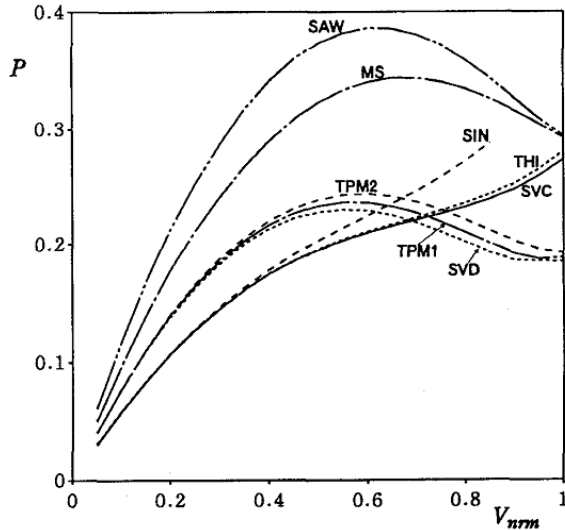


Figure 5.7: Total harmonic distortion power [24]

Knowing that the nominal RMS voltage of the machine is 251V and the battery-bus voltage can be 450V to 600V, the expected modulation index can be calculated by using equation (5.7):

$$\hat{U}_{LL} = \frac{Udc \cdot \sqrt{3}}{2} \cdot ma = 251 \cdot \sqrt{2} \rightarrow ma = 0.68...0.91 \quad (5.13)$$

Looking in figure 5.7 at SIN and THI in this modulation range, the third harmonic injection method produces less harmonics compared to the original sinus reference. However, TPM2, TPM1 and SVD are more efficient than THI. Since the converter will operate with a synchronous machine, not only the total harmonic power is important, but also the vibrations caused by these harmonics. Therefore reference [24] presents also a graph with the harmonic power in the q-axis compared to different modulation indexes. The power in the q-axis will directly cause torque and vibrations in the machine.

Figure 5.8 shows the total harmonic power in de q-axis of different modulation methods.

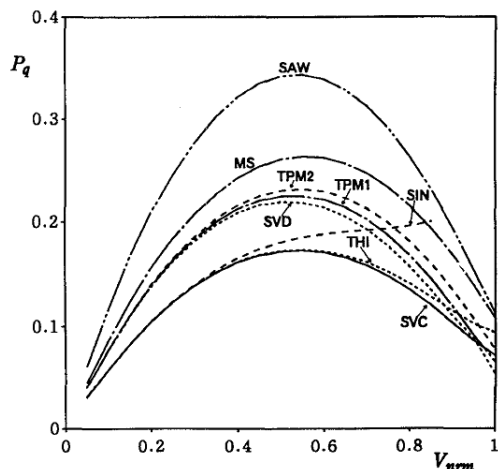


Figure 5.8: Harmonic distortion in q-axis [24]

Not only the total harmonic power is much higher with a classic sinusoidal reference, the harmonic power in de q-axis is much higher as well, especially at higher modulation indexes. Besides that, the THI is more efficient compared to TPM1, TPM2 and SVD which are more efficient looking at the total harmonic power.

To verify the results of THI and SIN shown in figure 5.7, a simulation with these two PWM methods for the range extender application are carried out. The total harmonic distortion and switching losses are calculated at different switching frequencies, the results are shown in figure 5.9.

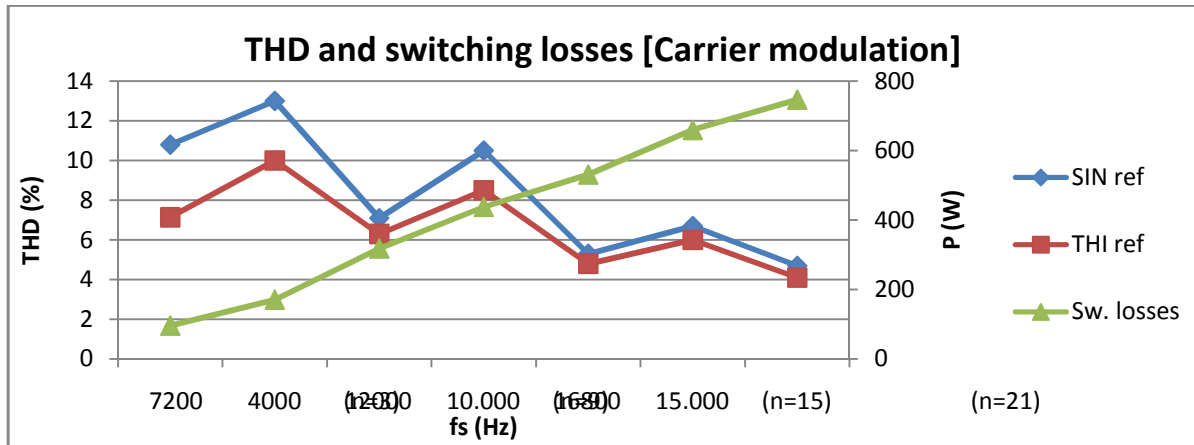


Figure 5.9: Simulation results for SIN and THI carrier modulation

As already stated at the end of 5.2.1, the harmonic distortion is minimized when the modulation factor is odd and a multiple of 3. Therefore, the THD is lower at 2400, 7200, 12000 and 16800Hz as shown in figure 5.9. The best switching frequency seems to be 7200Hz, where the losses and THD are at an appropriate level.

The choice of modulation reference depends on its application. Looking at carrier based methods and a synchronous machine as application; the third harmonic injection operating at 7200Hz is the best option.

The characteristics of carrier modulation can be summarized as follows:

- Simple implementation (digital or analog)
- Fixed switching frequency
- Losses and THD are directly related to the switching frequency
- Starting the machine may cause problems since mf has to be odd and a multiple of 3

The space vector modulation methods (SVD, SVC) shown in figure 5.7 and figure 5.8 are discussed in the next subchapter.

5.3. Space vector modulation

Space vector modulation is a voltage control method based on the space vector representation of the reference and inverter/rectifier voltages in the $\alpha\beta$ domain shown in figure 5.10. The space vector technique averages three switching state vectors over an interval of one switching cycle T_s . The reference switching phasor V_{ref} is realized by computing the duty ratios (fraction of switching period) of the two nearest switching vectors.

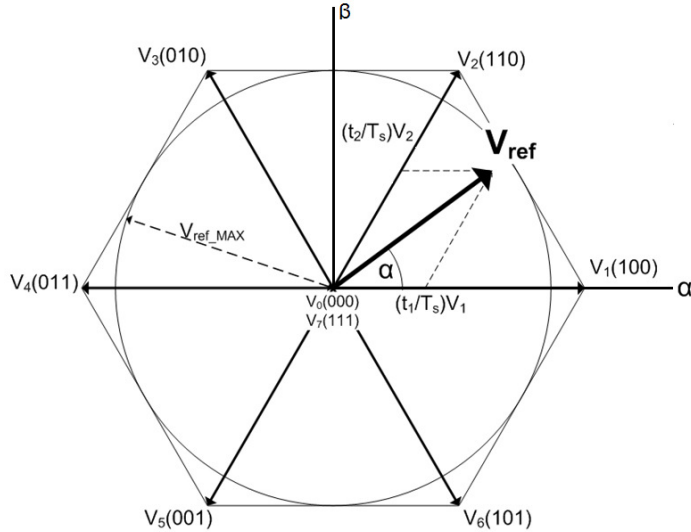


Figure 5.10: Space vector representation [25]

The space vector representation shown above consists of two zero vectors (U_0 and U_7) and six switching vectors (U_1-U_6) representing the six switching states of the converter:

Vector	A ⁺	B ⁺	C ⁺	A ⁻	B ⁻	C ⁻
$U_0=000$	OFF	OFF	OFF	ON	ON	ON
$U_1=100$	ON	OFF	OFF	OFF	ON	ON
$U_2=110$	ON	ON	OFF	OFF	OFF	ON
$U_3=010$	OFF	ON	OFF	ON	OFF	ON
$U_4=011$	OFF	ON	ON	ON	OFF	OFF
$U_5=001$	OFF	OFF	ON	ON	ON	OFF
$U_6=101$	ON	OFF	ON	OFF	ON	OFF
$U_7=111$	ON	ON	ON	OFF	OFF	OFF

Table 5.1: Eight switching states and vectors

The reference vector created by the controller rotates through the reference frame with a desired frequency and amplitude and can always be decomposed in the two nearest switching vectors. Therefore the length of those two nearest vectors is calculated which also can be seen as the ON time of the switching state. This method allows one reference vector to be decomposed in a three state switching pattern:

$$\bar{s}_{ref} T_s = \bar{s}_k T_k + \bar{s}_{k+1} T_{k+1} + \bar{s}_0 T_0 \quad (5.14)$$

Where T_s is the switching period, T_k and T_{k+1} are the switching times of the corresponding vectors and T_0 is a zero vector time to keep the switching frequency constant. A graphical explanation is given in figure 5.10, where t_1 and t_2 represent the switching times of the corresponding switching states (V_1 and V_2).

The controller can create a locus and force the reference vector to follow this locus. This can be done in different ways: U_{ref} follows the locus from the inside at one sampling and from the outside at the next sampling, alternating (SVC) or from the inside and outside at every sampling (SVD) [24].

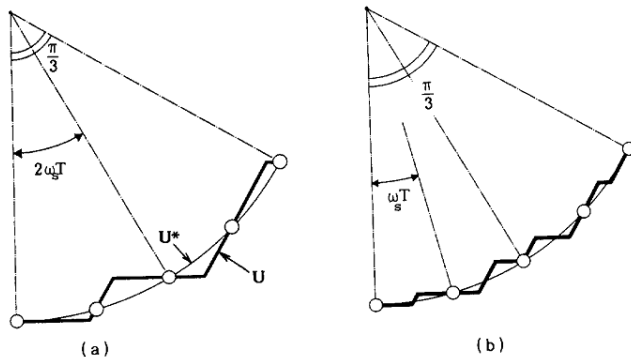


Figure 5.11: SVC (a) and SVD (b) locus method [33]

The harmonic distortion generated by the two presented space vector modulation methods is discussed in reference [23] [24] and the total harmonic power and harmonic torque power are plotted in figure 5.7 and figure 5.8 respectively. The SVC method has slightly higher harmonic losses, but performs better looking at the harmonic torque ripple. Therefore the SVC method is preferred for electrical machine application. The optimal solution will be a combination of these two, which can be realized because the control method can be changed during operation when it is digitally implemented.

As in the previous PWM methods, simulations carried out for SVC modulation with range extender application. THD and switching losses are simulated and presented in figure 5.12.

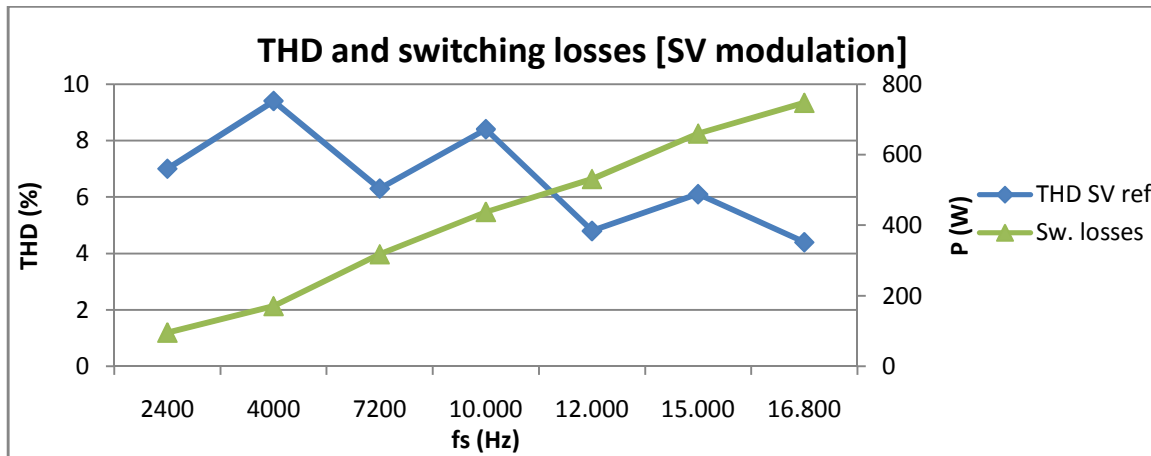


Figure 5.12: Simulation results for SVC modulation

As already shown in figure 5.7 and figure 5.8, the THD of the space vector modulation does not result in substantial differences compared to the carrier base modulator with third harmonic injection shown in figure 5.9. Therefore the same conclusions hold for the space vector modulation method. The properties show also similarities:

- Digital implementation required
- Fixed switching frequency
- Losses and THD are directly related to the switching frequency
- $\alpha\beta$ reference is directly transformed to a PWM pattern

5.4. Selective harmonic elimination (SHE)

Selective harmonic elimination is a PWM method which is based on a combination of square wave switching and PWM to control the fundamental output voltage. Several notches are introduced in a normal square wave to eliminate predefined harmonics shown in figure 5.13. The angles of these notches depends on the harmonics to eliminate, mostly lower order harmonics are eliminated since it is easier to filter higher frequencies. The calculated waveform has to be odd half-wave symmetrical and therefore only odd harmonics will be present. Since the third harmonic and its multiples do not appear in three phase systems, these harmonics are not required to be filtered out by SHE.

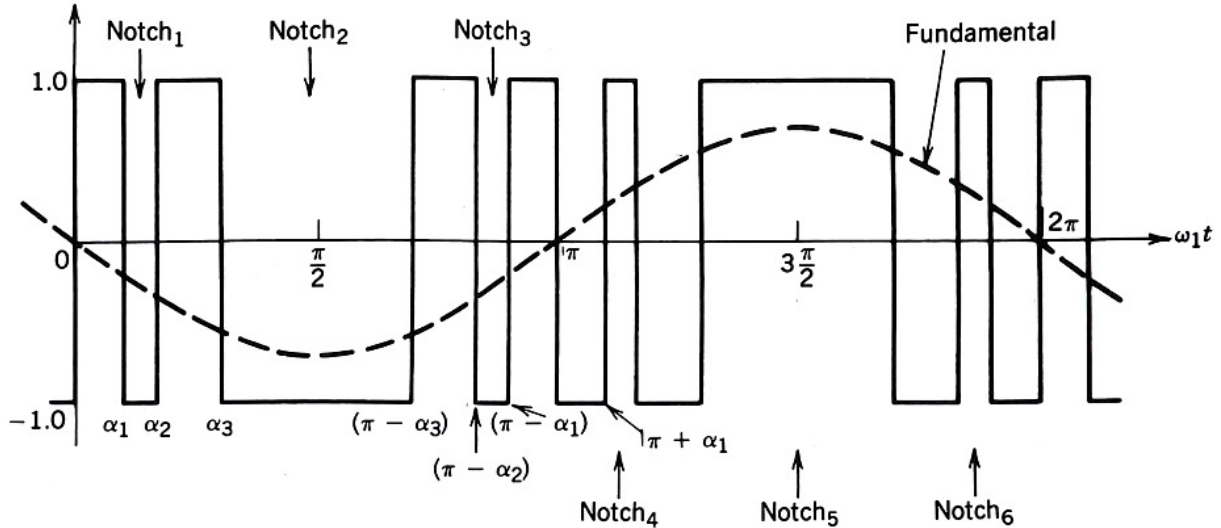


Figure 5.13: Notches and angles in SHE [26]

The theory seems to be straightforward, but the calculation of the switching angles is a complex problem. Newton's iteration method must be used to calculate the angles, but the solution depends on the initial estimate of the angles. A wrong estimate will result in a converging solution so many attempts have to be done to achieve the correct switching angles. Therefore the harmonic elimination involves extensive offline computing to determine the switching angles. Once the switching angles are calculated, they are stored into the microcontroller in the form of a lookup table. Consequently, a large number of LUTs are required to reproduce the complete range of switching angle characteristics and a certain level of interpolation is required to provide continuous voltage control [34].

Therefore the harmonic elimination is not discussed any further in this thesis.

5.5. Control Methods

The previous paragraphs described different ways to create PWM patterns for the six switches of the full bridge converter. All the proposed PWM methods generate these patterns based on an external reference signal. This signal is created by the controller depending on the required torque, speed, voltage, current or power. A simple overview is presented in figure 5.14.

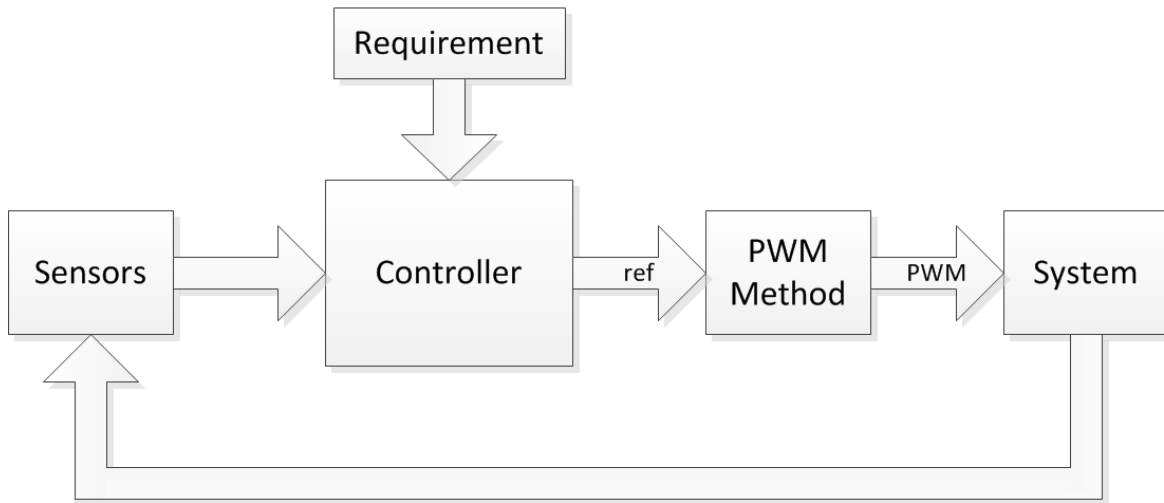


Figure 5.14: Simple overview control loop

The output of the controller needs to be compatible with the input reference of the PWM generation block. Therefore not every PWM method can be combined with every control method. The two most popular and robust motor control principles are shortly discussed in the next subparagraphs. There are many more control methods, but they rely often on the next proposed principles.

5.5.1. Direct Torque Control (DTC)

Direct torque control is used to directly control the torque (and thus also the input/output power) of AC electric motors by controlling the phase current. DTC involves calculation and estimation of the motor's magnetic flux and torque based on measured voltage and currents. With a permanent magnet synchronous machine, the torque can be calculated by measuring the phase currents. The calculated torque based on the measured current will be compared to the required reference torque. If the calculated torque deviates too much ($>\Delta h$) from the reference, the switches will be switched in such a way that the torque will return in the tolerance band. DTC therefore equals the hysteresis modulation PWM method and has the same characteristics [31]:

- Simple implementation
- Switching frequency depends on load and hysteresis margin
- No defined switching frequency, but can be limited by hysteresis band
- High quality current measurement required, high sampling rate
- Noise or EMI can disturb measurements and cause incorrect gate signals
- Torque can be changed very fast by changing the reference value
- Step response has no overshoot
- No PI current controllers required
- Synchronization straightforward due to the fast control

5.5.2. Field Oriented Control (FOC)

Field oriented control is used to control the torque (and thus also the input/output power) of AC electric motors by controlling the phase current. The measured phase current is converted into a complex space vector in the $\alpha\beta$ domain by using the Clarke transformation. This current vector is then transformed into the rotating coordinate system (dq domain) by using the position sensor located at the machine. The output of the Park transformation is a flux vector (d) and a torque vector (q), which can be controlled separately. When using a permanent magnet synchronous machine, the flux vector can be controlled at zero, since the permanent magnets provide the flux. So the torque of the range extender can be controlled by only controlling the current vector i_q . In order to control the speed of the synchronous machine, two PI controllers can be cascaded, one to control the torque vector and the other to control the reference of the torque vector. After this the current references are transformed back to the stationary coordinate system ($\alpha\beta$ domain) and this signal can be applied directly into PWM modulator. Figure 5.15 shows the complete process of FOC.

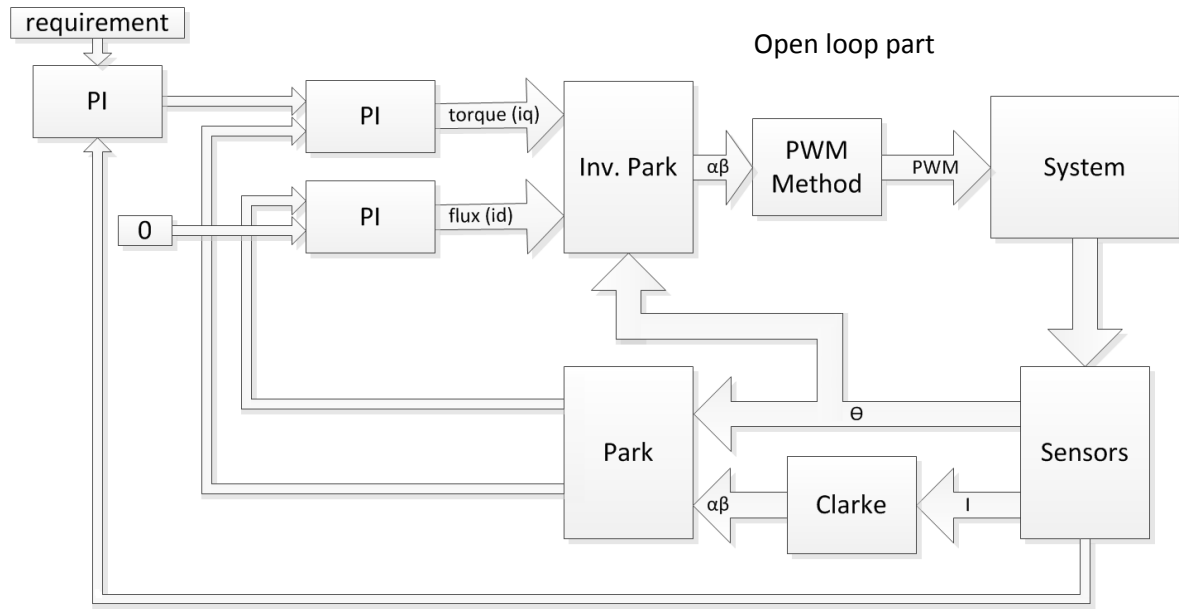


Figure 5.15: FOC loop

In contrast to direct torque control, field oriented control can be used with different PWM modulators. Two of the proposed PWM methods can be applied: carrier modulation and space vector modulation. With space vector modulation, the reference value from the inverse Park transformation is directly used to generate a PWM signal, since the space vector modulator requires a reference value in $\alpha\beta$ domain. Carrier based modulation can also be used, therefore the $\alpha\beta$ reference signal is transformed to a three phase reference value which is compared to a saw-tooth carrier. The choice of PWM method depends on performance and implementation requirements and its application. The properties of the chosen PWM method will be combined with the typical properties of field oriented control [32]:

- Speed sensor required
- Torque can be changed reasonably fast by changing the reference
- PI will cause overshoot in step response
- Fixed switching frequency
- Slower torque dynamic response compared to DTC
- Less accurate sensors and lower sampling rate required compared to DTC

5.6. Chosen PWM and control method

The previous paragraphs discussed different control and PWM methods with a focus on switching losses and harmonic distortion. Simulations were performed to prove that the literature study is applicable on the electronics in the range extender. As stated in chapter 1.2, the optimization should be done for the complete system and not only for the power electronics. Therefore an optimum has to be found for the losses in the machine and the losses in the converter. Since there is no model available for the losses in the machine produced by current harmonics, an optimum has to be found between THD and switching losses. Additionally, DSP implementation, robustness and costs have to be taken into account looking at the best control and PWM solution for the range extender.

Looking at the THD and switching losses, hysteresis modulation performs a little bit better than carrier based and space vector modulation. Hysteresis modulation produces around 5% harmonic distortion and 285W losses at a switching frequency of 7200Hz. Carrier and space vector modulation produce 6% harmonics and are dissipating 300W at 7200Hz. However, when looking to the robustness the hysteresis modulation performs worse compared to the other proposed PWM methods. The fixed switching frequency and lower current measurement requirements of the carrier and space vector modulators are providing a more robust solution. The cost and DSP implementation are expected to be equal for all the proposed PWM modulation methods.

Since the hysteresis modulation is directly related to the direct torque control it can be concluded that field oriented control is the best control method. The reference value of the field oriented controller can be directly imported into the space vector modulator. Moreover, the space vector modulator can be simply implemented in the chosen DSP by using the motor control blocks from Texas Instruments. Therefore the space vector modulator combined with field oriented control is the best solution to control the power electronics in the range extender.

The next chapter shows an implementation and measurements on the test setup with results of the chosen PWM and control method. These results are compared to the literature and simulations from this chapter.

Chapter 6: Implementation and measurements

In the previous chapters a complete design for the power electronic converter is discussed. Chapter 4 proposed the hardware part of the power electronic converter and chapter 5 shows the best PWM and control method for the power electronic converter in the range extender. The decisions in these chapters were based on literature study and some application specific simulations. This chapter will discuss the implementation and measurements of the proposed system. Measurements are done on voltage and current waveforms, harmonic distortion, switching performance and losses.

Measurements are carried out on the test setup discussed in 4.5. Due to limited hardware in the test facility the measurements are carried out under the following conditions:

- DC bus voltage of 150V
- Maximum frequency 200Hz
- Open loop control, because of difficulties with the DSP

An overview of the test setup is shown in appendix D.

6.1. Switching performance

In order to verify the data from the datasheet and the expectations on switching speed and losses the switching performance of the IGBTs is tested. This is done with an external inductor connected parallel to the upper IGBT. The upper IGBT is disabled and the lower IGBT is used to increase the current through the inductor L. The test setup is shown in figure 6.1:

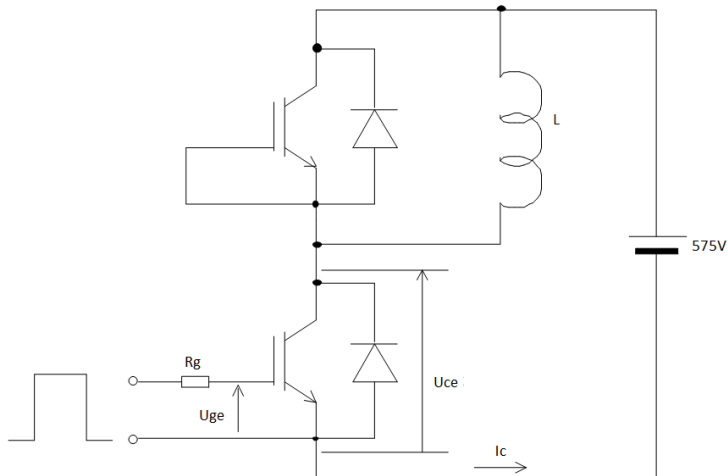


Figure 6.1: Test setup switching performance

By varying the on time of the lower IGBT, the amount of current to switch off can be controlled. When the IGBT is turned off, the current will flow through the upper diode and next the lower IGBT is turned on again. In this way, the switching performance at different current levels can be investigated. Due to the limitations of the current probes, a maximum current of 30A is tested. The results are shown in table 6.1.

Current [A]	Turn on time [ns]	Turn off time [ns]	Irr peak [A]	Dissipation on [mJ]	Dissipation off [mJ]
5	110	1000	60	0.9	1.82
10	110	600	80	1.19	2.40
15	110	500	100	1.45	3.03
20	130	450	111	1.65	3.33
25	150	350	126	1.83	3.73
30	150	300	138	2.08	4.16

Table 6.1: Switching time and losses at 0 - 30A @ 25°C

It is remarkable that the turn off time decreases when the current increased, this is caused by the tail current which was already noticed in paragraph 4.3. When the current is higher, the electrons are removed faster from their holes compared to a lower current (figure 6.2).

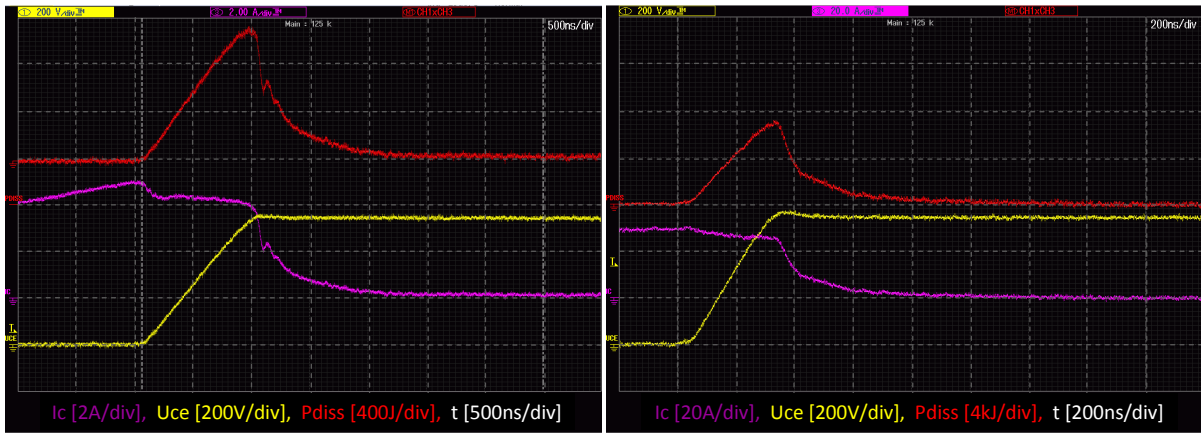


Figure 6.2: (a) Turn off at 5A,

Yellow=Uce, Purple=Ic, Red=Pdiss

(b) Turn off at 30A

The dissipation peak at turn on is significantly higher due to the reverse recovery current of the diode, but also much shorter. A turn on waveform is shown in figure 6.3.

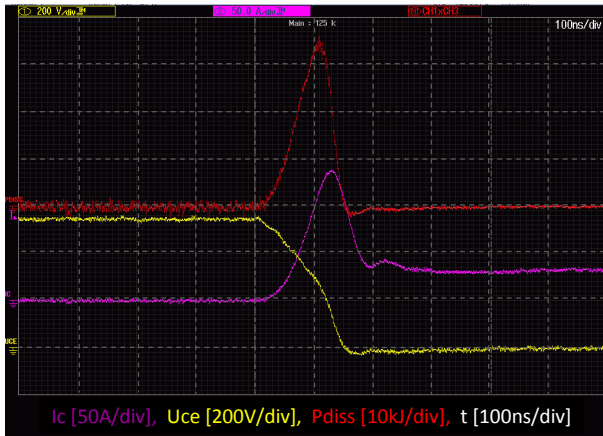


Figure 6.3: Turn on at 30A

The switching graphs are the same as expected in paragraph 4.3 and figure 4.3. If the turn on and off dissipation peaks are compared with “dissipation graph” in the datasheet (appendix c) it can be concluded that the measurements correspond with the values in the datasheet. Therefore the dissipation equations in paragraph 4.3 are a realistic approximation of the practical situation.

The conduction losses are investigated with a high current DC voltage source connected to the IGBT module. A certain amount of current is flowing through the IGBT or diode and the voltage across the IGBT or diode is measured. Results are presented in table 6.2.

Current [A]	Uce [V]	Uak [V]	Current [A]	Uce [V]	Uak [V]
5	0,82	0,79	55	1,32	1,20
10	0,98	0,86	60	1,35	1,22
15	1,05	0,92	65	1,38	1,24
20	1,11	0,98	70	1,42	1,26
25	1,14	1,01	75	1,45	1,29
30	1,18	1,04	80	1,47	1,31
35	1,21	1,09	85	1,50	1,33
40	1,25	1,12	90	1,52	1,35
45	1,26	1,14	95	1,55	1,37
50	1,30	1,17	100	1,57	1,40

Table 6.2: Conduction voltage drop for IGBT and diode at 0 – 100A (25°C)

The measured values correspond with the graphs at 25°C in the datasheet (appendix c) thus the calculations made in paragraph 4.3 are a realistic approximation for the practical situation. Based on these values and equation (4.12) and (4.13) a graph can be plotted with the conduction losses compared to the amplitude of the current.

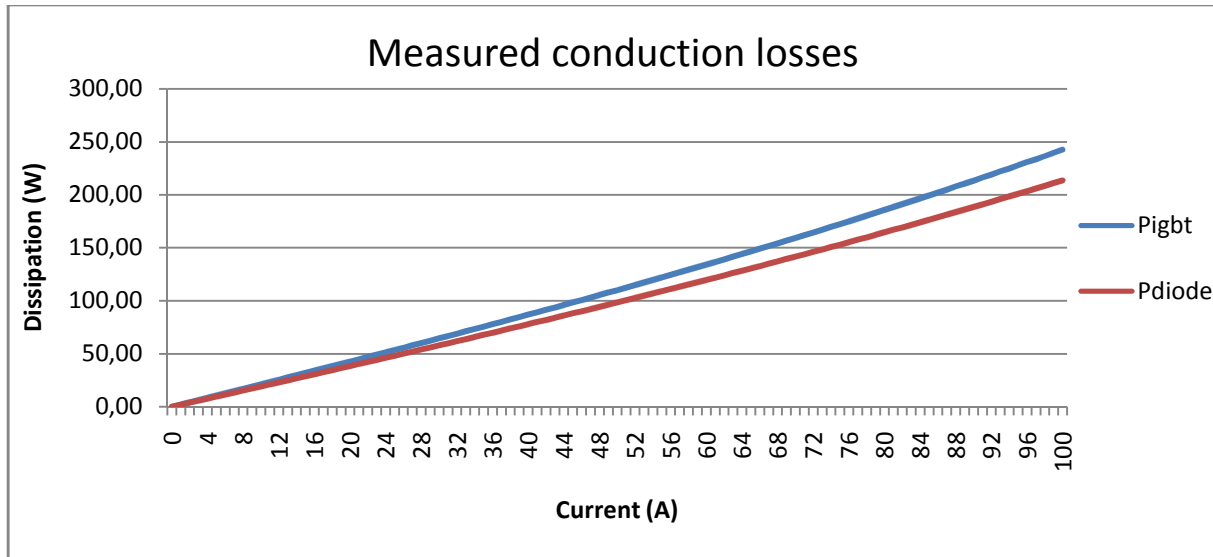


Figure 6.4: Approximated conduction losses for diode and IGBT

6.2. The Software DSP

The power electronic convert will be controlled by the DSP mentioned in subparagraph 4.2.6. The DSP can be programmed from MATLAB Simulink and a motor control library is provided by the manufacturer Texas Instruments. The library consists of mathematical functions, Park and Clark transformations and ramp control blocks. There have been a lot of difficulties to get the DSP running and therefore only open loop control is proposed in this chapter. A block diagram of the implemented open loop software in the DSP is shown in figure 6.5.

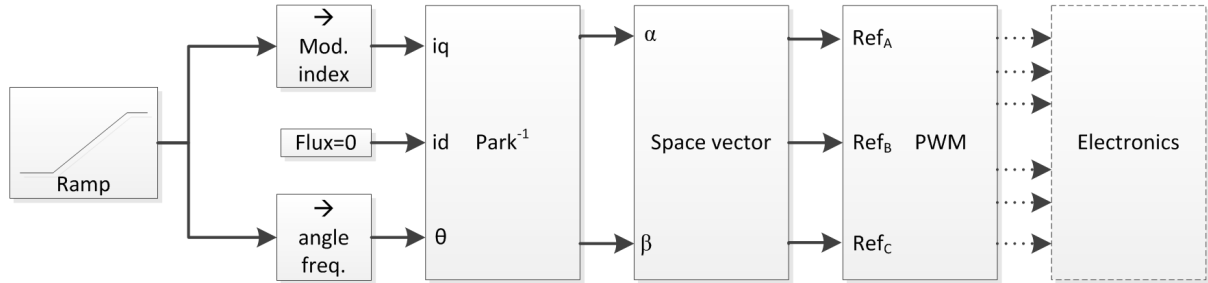


Figure 6.5: Block diagram implemented software

The closed loop control shown in figure 5.15 is able to control the speed and output power of the system by using the feedback signals. Based on the length of the torque (i_q) and flux (i_d) vectors from the sensors, the PI controllers generate an output to achieve the required torque and flux values. Together with the mechanical phase angle θ , the inverse park transformation is carried out which leads to a PWM pattern. However, in the open loop control shown in figure 6.5, there are no sensors to provide the mechanical phase angle θ and current vectors. Therefore the torque vector, flux vector and mechanical phase angle θ are set to a predefined value.

The output voltage of the converter is determined by the modulation index and the frequency of the fundamental output voltage is equal to the frequency of the mechanical phase angle θ . As already mentioned in paragraph 5.5.2, the length of the flux vector (i_d) is set to zero, but without feedback and closed loop control, the actual value of the flux vector cannot be verified and guaranteed during open loop control.

The electronics block shown in figure 6.5 is discussed in detail in chapter 4.5, a simple circuit is presented in figure 6.6.

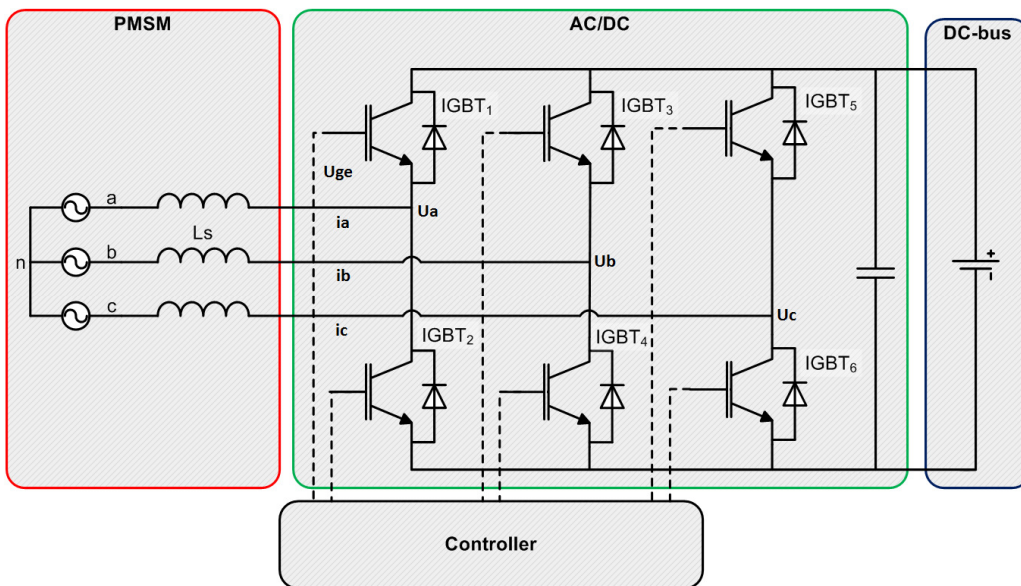


Figure 6.6: Hardware system

In order to start the machine, the frequency and modulation index are increased linearly while the flux vector (id) is kept zero (see also paragraph 5.5.2). The modulation index must be increased together with the frequency to ensure that the terminal voltage is higher than the induced voltage in the machine. Next the dq vectors and mechanical phase angle (θ) are transformed to a α and β vector. The space vector block generates three reference waveforms which are compared to a triangular carrier in the PWM block. Depending on these modulation results, the six output pins of the DSP are switched ON or OFF by the PWM block. A MATLAB Simulink model of the open loop software is shown in figure 6.7.

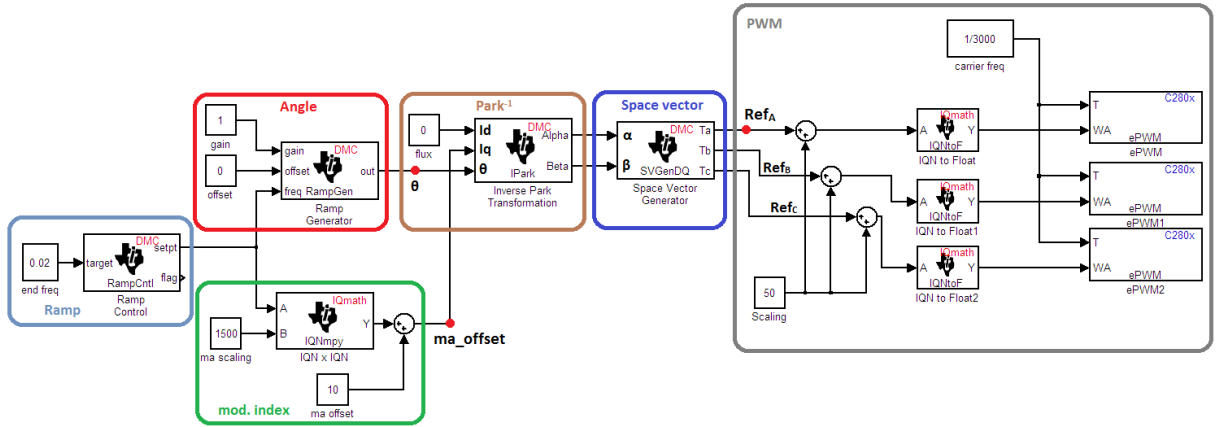


Figure 6.7: Simulink model

Since the chosen DSP is a fixed point type, all the TI blocks require a signed 32-bit fixed-point number with a Q value between 1 and 32. Depending on the required accuracy the Q value can be changed, a Q value of 16 is used in the proposed Simulink model.

The ramp control block provides an increasing ramp from zero to a determined final value. All the measurements are done with a final value of 0.02 which equals a fundamental frequency of 200Hz. The ramp control output is used to increase the modulation index of the output voltage and the frequency of the phase angle (θ). The ramp generator block generates a phase angle (θ) with a certain frequency (depending on ramp control block) which is used to perform the inverse park transformation.

A modulation index of 80% and a DC bus voltage of 150V will result in an output phase-to-phase voltage of:

$$\frac{Udc}{2} \sqrt{3} \cdot ma = \frac{150}{2} \sqrt{3} \cdot 0.8 = 104V \quad (6.1)$$

The induced voltage in the generator will be 88V at 200Hz (appendix A), therefore the voltage difference between the induced voltage and the terminal voltage will be 16 volts.

In order to start the machine, a starting torque is required to overcome the friction in the test setup. When the modulation index starts increasing from zero, the voltage difference across the inductance is too low and therefore the current and the produced torque are not high enough. To overcome this problem, an offset is given to the modulation index which results in a startup voltage of:

$$\frac{Udc}{2} \sqrt{3} \cdot ma = \frac{150}{2} \sqrt{3} \cdot 0.2 = 26V \quad (6.2)$$

This voltage results in a startup current and a magnetomotive force which is high enough to overcome the startup friction of the machine.

The modulation index ramp and offset is shown figure 6.8 (a) and phase angle for the inverse park transformation is shown in figure 6.8 (b).

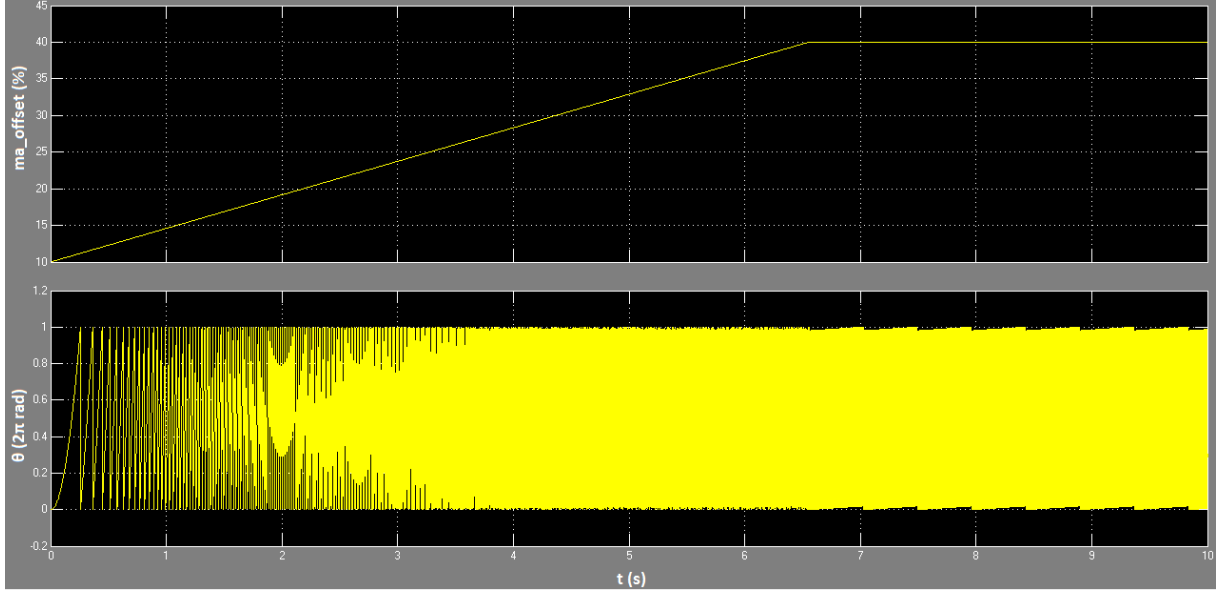


Figure 6.8: ma_offset (top) and mechanical phase angle θ (bottom)

As expected the modulation index offset ends at 40, which equals a modulation index of 80% (see next page). The phase angle starts with a long period but the period time is decreasing linearly according the output of the ramp control block and ends with a period of $1/200 = 5\text{ms}$.

Based on these signals, three reference waveforms are generated by the space vector generator block. These signals have an amplitude equal to the modulation index value given at the inverse park transformation block. Figure 6.9 shows the reference waveform of one phase during startup of the machine.

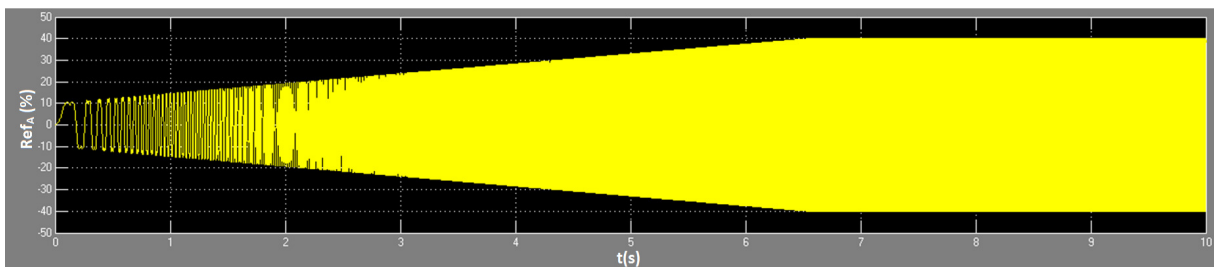


Figure 6.9: Space vector reference waveform during startup

The amplitude of the space vector reference waveform which will be compared to the triangular carrier is increasing since the modulation index increases linearly. The startup offset of the modulation index is clearly visible in figure 6.9. Also the frequency is increasing linearly together with the modulation index and ends at 200Hz in 6.5 seconds.

In steady state the space vector reference waveform looks very similar to the carrier waveform with third harmonic injection from figure 5.6:

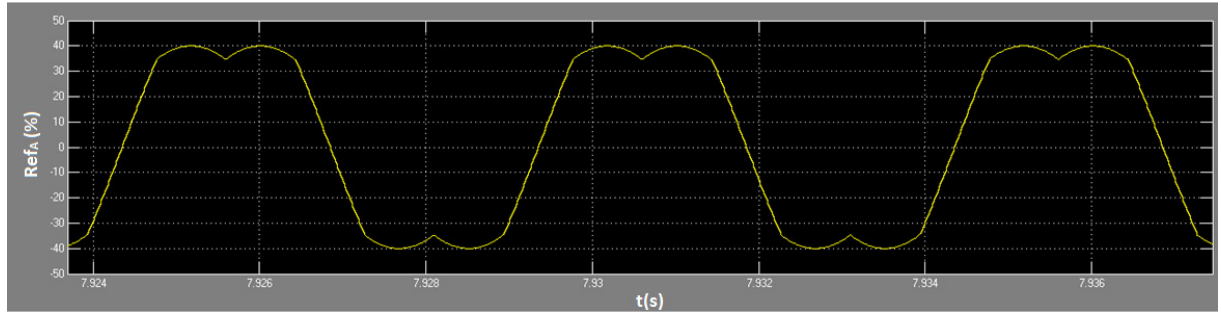


Figure 6.10: Space vector reference waveform in steady state

Since the value of the triangular carrier in the PWM block is between 0 and 100, an offset of 50 is given to the output of the space vector generator to center it around 50% (figure 6.7). Based on the space vector reference waveform, the PWM block will generate a gate pattern which result in a sinusoidal current and a chopped phase-to-phase voltage as shown in figure 6.11.



Figure 6.11: Green: Gate signal, yellow: phase current, purple: phase-to-phase voltage

6.3. Starting

As shown in the previous subparagraph, the frequency and modulation index will be increased linear during startup. It is important to increase the modulation index together with the frequency since the back EMF of the machine increases linear with the speed (appendix a). In order to keep control, the voltage on the terminals of the machine has to be higher than the back EMF (figure 6.12).

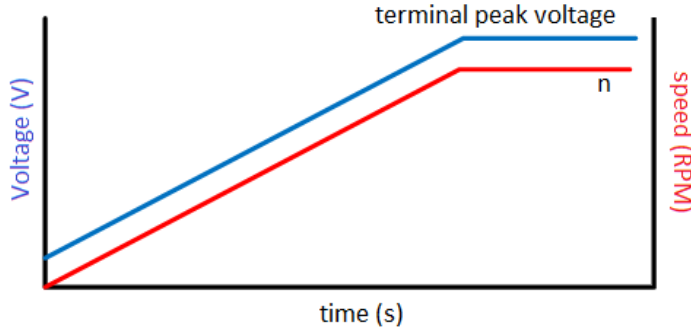


Figure 6.12: Terminal and induced voltage

Due to limitations of the ePWM block, the triangular carrier frequency could not be increased linear with the fundamental frequency. The fixed carrier frequency combined with a linear increment of the fundamental frequency will not always lead to an odd and multiple of 3 frequency modulation ratio. The voltage waveform is therefore not always symmetrical in time and in voltage with undesirable harmonics as result (subparagraph 5.2.1).

During startup these harmonics are in the system, but when the terminal voltage is increased together with the frequency, the voltage difference between the induced and terminal voltage is kept rather low (figure 6.12). Therefore the harmonic currents are also quite low and will have less impact on the startup behavior of the machine; they cause less powerful vibrations.

When the modulation ratio is fixed at a high value (e.g. 80%), the voltage difference during startup is much higher. Therefore the harmonic currents are higher and will cause heavy vibrations which can result in a situation where the rotor is lost by the field and stops rotating.

It is also important that the frequency modulation ratio at nominal operation is odd and a multiple of 3, otherwise undesirable harmonic currents will keep flowing in the system and cause vibrations and pulsating currents as shown in figure 6.13.

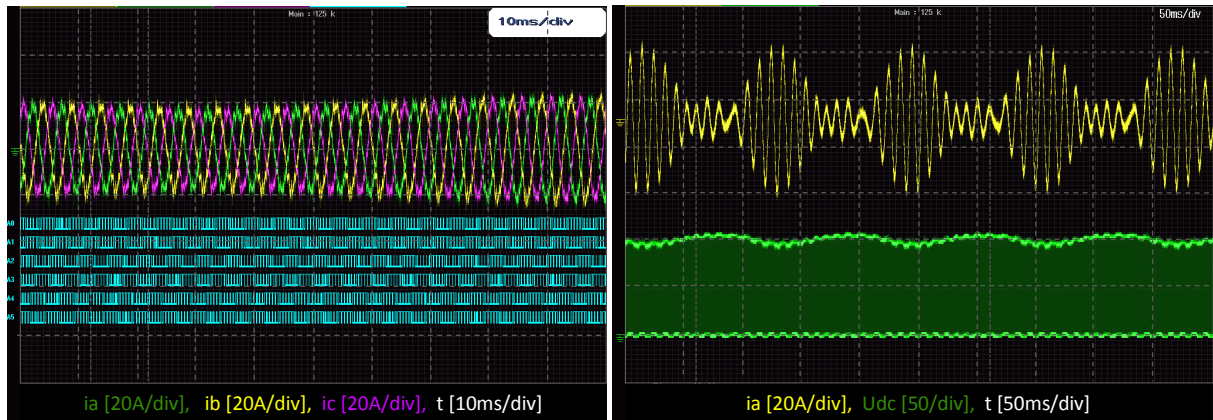


Figure 6.13: Left: three phase current and PWM signals

Right: single phase current and DC bus voltage

An incorrect modulation ratio doesn't lead only to higher harmonic distortion, but can also lead to saturation of the machine. Machine saturation can occur when the average of the PWM voltage waveform is not zero. An imbalance in the PWM pattern can result in a DC component in the voltage which can cause saturation in the machine. When saturating, the current in the machine will increase rapidly since the induction becomes very low. The current will be limited by the resistance of the machine, but the machine temperature will increase with risk of melted isolation.

A short time DC voltage offset can also cause problems, for example during startup. An imbalance during startup can lead to a DC current offset in nominal operation. This DC current leads to more harmonic distortion and losses in the system.

The startup current of the machine with the software discussed in paragraph 6.2 is shown in figure 6.14.

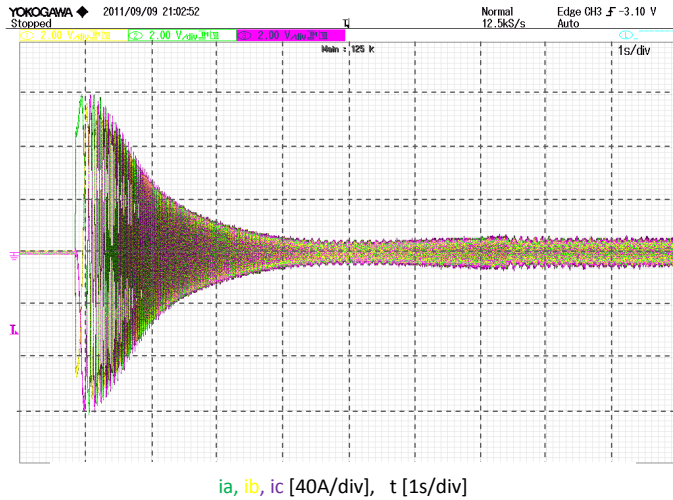


Figure 6.14: Three phase startup current

During start up the back EMF of the machine is limited and therefore the voltage across the self inductance is equal to the voltage on the terminals of the machine. The startup current is limited by the low modulation index as stated above. Once the machine is speeding up, the back EMF increases and the current will decrease until the steady state reached.

6.4. THD and efficiency

Total harmonic distortion and converter losses were two important aspects in the decision of the PWM and control method. Based on these aspects, the space vector modulator combined with the field oriented control method is chosen.

The proposed solution is implemented (figure 6.7) and total harmonic distortion and efficiency are measured. The measurements are done under the following conditions:

- Fundamental frequency: 200Hz
- DC bus voltage: 155V
- Open loop control
- Inverter operation

The motor was connected with a shaft to a generator which was loaded with three resistors of 25Ω , appendix D shows the test setup.

Measurements are done at different frequency modulation ratios to investigate the harmonic distortion and switching losses. It is expected that the efficiency will decrease at higher modulation ratios. Additionally the harmonic distortion will decrease and show dips at odd modulation ratio and a multiple of 3 as shown in figure 5.9.

The values are measured with a power analyzer (Yokogawa PZ4000) placed between the converter and the motor, also the DC bus voltage and current are measured by the analyzer to calculate the total efficiency.

Measurements are done at modulation ratios of 9, 13, 15, 17 and 21, the results are shown in table 6.3.

mf	Output [W]	Input [W]	Total losses [W]	Efficiency [%]	THD (%)
9	669	704	35	95.09	45.48
13	793	867	74	91.18	51.72
15	628	721	93	87.11	39.29
17	630	746	116	84.35	39.95
21	582	693	111	83.98	26.18

Table 6.3: Harmonic distortion and efficiency at different modulation ratios

The total converter efficiency and THD are plotted in figure 6.15.

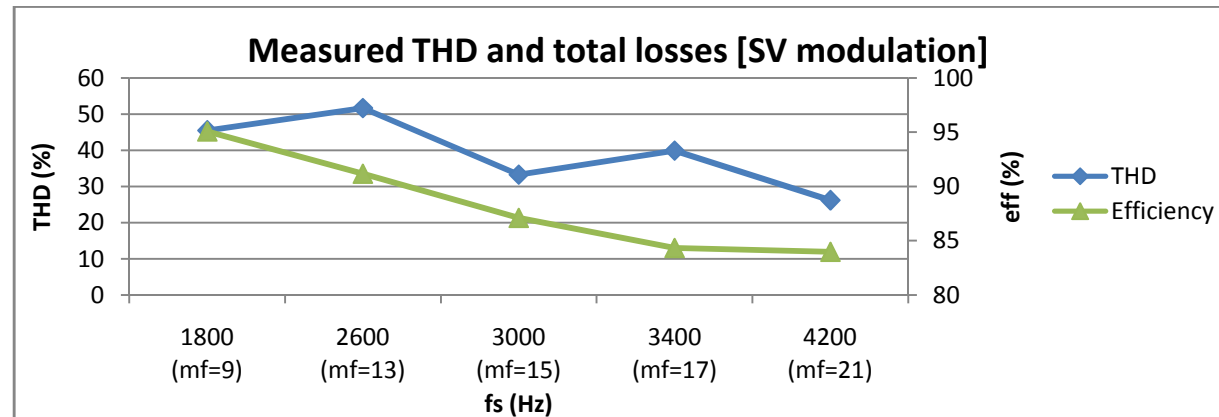


Figure 6.15: Measured THD and efficiency

As expected is the converter efficiency decreasing when higher switching frequencies are used and the dips in the THD are at odd frequency ratios with a multiple of 3. However, the losses are higher than expected and also the harmonic is much higher compared to the THD in figure 5.9. These differences can occur because of the following reasons:

- Unbalanced load
- Variations on the DC bus
- Current offset
- Incorrect PWM pattern

The DC bus voltage showed some voltage and current fluctuations, therefore the phase current waveforms can contain unexpected current peaks and a DC offset. The current in the DC bus is shown in figure 6.16.

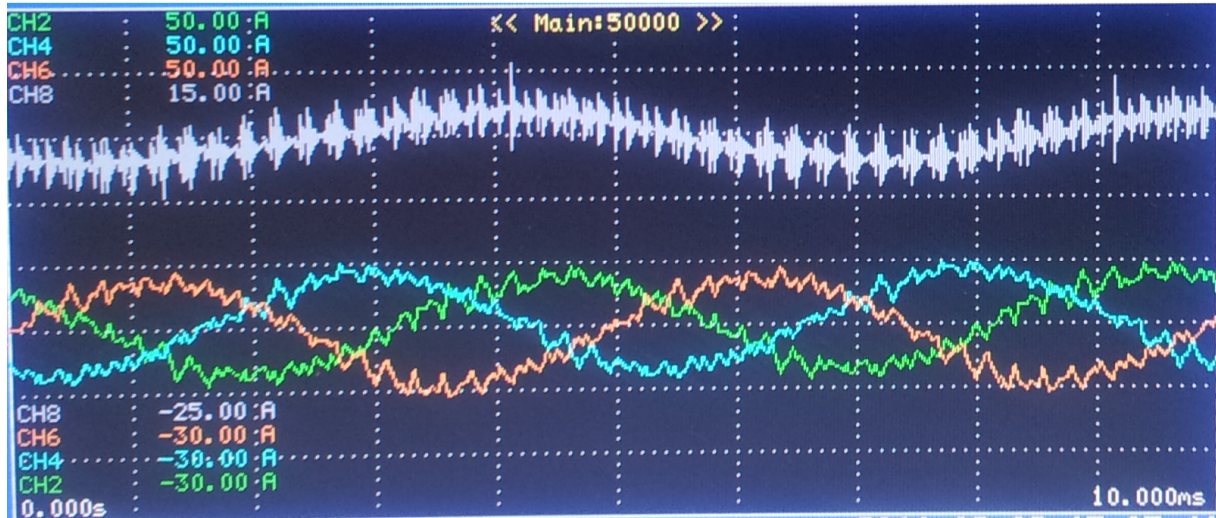


Figure 6.16: Three phase and DC current waveform

A DC current offset will result in a significant increase of the THD, also the switching and conduction losses will increase. A LC filter on the input of the DC bus can limit the fluctuations and improve the converter operation.

Chapter 7: Conclusion and future work

7.1. Contributions and conclusions

This thesis deals with the design and implementation of a bi-directional full bridge power electronic converter for range extender application. The converter is able to rectify the voltage in generator operation and act as inverter during starting operation. The discussed solution is optimized in cost, controllability, efficiency and weight.

The hardware design of the full bridge converter consists of different components which are optimized according operating characteristics, price, efficiency and robustness:

- IGBTs are used for the six switches in the design since they are available in the required high power ratings, provide relative low switching and conduction losses and support switching frequencies up to 200kHz.
- A fly-back converter is preferable to supply the gate drivers and other electronics. It provides multiple isolated outputs and is a cost efficient solution. However, for the test setup standard DC/DC converters are used, because of the lack of time to design a fly-back converter.
- Opto-couplers are the best solution to provide electrical isolation between the DSP and gate drivers since they are economic, compact and have a good performance. However, optical cables are used in the test setup because they are less sensitive for EMI compared to opto-couplers, but are also more expensive.
- Hall sensors are used to measure the current. They provide an efficient and accurate current measurement with high electrical isolation and bandwidth.

Since the range extender has to operate as efficient as possible, the losses in the electronics combined with the generator losses must be minimized. A high switching frequency will lead to lower harmonic losses but also increase the switching losses in the power electronic converter. Therefore a literature study is done about different PWM methods with harmonic distortion and switching losses as research goals. To verify the literature study, simulations are done on the range extender application. Hysteresis modulation, carrier based modulation, space vector modulation and harmonic elimination are investigated. From literature it appears that space vector and third harmonic injected carrier modulation performs equal and are preferable PWM modulation methods. They provide the best harmonic distortion and switching losses ratio. Additionally, they are robust and require a lower current measurement and sampling rate quality.

The space vector modulation and field oriented control is implemented in the DSP and measurements are done on switching characteristics, starting behavior, harmonics and efficiency.

Starting the synchronous machine requires a linear increment of frequency and modulation index. A low modulation index will limit the startup current which appears to be high since the back EFM of the machine is low due to the low rotational speed. An incorrect frequency modulation ratio can cause harmonics and vibrations in the system. During startup the impact of these harmonic currents must be limited by the modulation index otherwise they have a substantial impact and will cause vibrations which can result in a situation where the rotor is lost by the field and stops rotating.

Harmonics in a three phase converter can be significant when the currents have a small DC offset. This offset can be caused by a fluctuating DC bus voltage and therefore it is important to limit the fluctuations on the DC bus by using a filter.

7.2. Future work

A test setup is developed which can be used to measure the hardware performance, but it can also be used to test different software control loops. Since the converter is used in a commercial application some optimizations have to be done on hardware and software.

Software implementation

The implemented software is limited to open loop control. However, to control the power electronic converter, the proposed field oriented control loop needs to be implemented and tested. This consists of implementing the feedback signals in the DSP and finding the right parameters for the PI controllers shown in figure 5.15. An important aspect is the transition from starting operation to generator operation, because it has to be synchronized before the combustion engine can deliver energy to the battery bus.

Research has to be done about the possibilities of vibration reduction by using the generator to anticipate on the compression and combustion cycle of the combustion engine as shown in figure 2.2. The synchronous machine can be used as generator and motor in one cycle, but the amount of required power, efficiency and control speed must be investigated.

Hardware implementation

A production version of the hardware has to be developed. Therefore different parts of the design have to be improved or redesigned. The DC/DC converters must be replaced by a fly-back converter because it is a more compact and economic solution. Measurements have to be done on the current test setup to investigate the power consumption of the components in more detail. The fly-back converter has to be designed according the results of these measurements and other requirements.

Another aspect are the opto-couplers. They are more economic and compact compared to the optic fiber cables. The switching behavior and requirements of these opto-couplers have to be investigated and a redesign has to be made in order to achieve a compact and robust solution.

References

- [1] History of the electric vehicle, http://en.wikipedia.org/wiki/History_of_the_automobile, (Accessed 23 June 2011)
- [2] Transportation emission, http://www.eoearth.org/article/Carbon_footprint, (Accessed 23 June 2011)
- [3] Mission and Vision, <http://www.peec-power.com/index.php> (Accessed 14 Juli 2011)
- [4] Q. Huang, "HARMONIC REDUCTION IN A SINGLE-SWITCH THREE-PHASE BOOST RECTIFIER WITH HARMONIC-INJECTED PWM", MSc. Thesis, Blacksburg, VA, 1997
- [5] J. Dixon, "Three-Phase controlled rectifiers", Pontificia Universidad Católica de Chile, Chile
- [6] N. Mohan, T. M. Undeland, W. P. Robbins (2003). *Power Electronics*. 3rd ed. Hoboken: Wiley. Chapter 21, 23 and 24.
- [7] Why opt for IGBTs in SMPS Applications?,
http://powerelectronics.com/mag/power_why_opt_igbt/index.html, (Accessed 25 January 2011)
- [8] Silicon Carbide MOSFETs Challenge IGBTs,
http://powerelectronics.com/power_semiconductors/power_mosfets/silicon_carbide_mosfets_igbt-809/index.html (Accessed 25 January 2011)
- [9] Insulated-gate bipolar transistor, http://en.wikipedia.org/wiki/Insulated-gate_bipolar_transistor, (Accessed 25 January 2011)
- [10] C. Blake, C. Bull, International Rectifier, "IGBT or MOSFET: Choose Wisely",
<http://www.irf.com/technical-info/whitepaper/choosewisely.pdf>
- [11] Fuji Electric, "IGBT Module Selection and Application",
http://www.fujielectric.com/products/semiconductor/technical/application/pdf/REH984a/REH984a_03.pdf
- [12] Datasheet Microchip TC4451, ww1.microchip.com/downloads/en/devicedoc/21987a.pdf
- [13] IGBT gate drivers, Farnell, <http://nl.farnell.com/igbt-gate-drivers>
- [14] Datasheet Avago HFBR-x521Z
- [15] Datasheet LEM LA 125-P, www.lem.com/docs/products/la%20125-p%20sp4%20e.pdf
- [16] Datasheet LEM LV 25-P, www.lem.com/docs/products/lv%2025-p%20sp2%20e.pdf
- [17] Datasheet Bourns EMS22D51-B28-LS5 rotary encoder,
<http://www.bourns.com/data/global/pdfs/ems22D.pdf>
- [18] Datasheet Spectrum Digital eZdsp TMS320 F2808,
c2000.spectrumdigital.com/ezf2808/docs/2808_ezdspusb_techref_c.pdf
- [19] <http://www.eetimes.com/design/power-management-design/4012153/IGBT-tutorial--Part-1--Selection> (accessed 14 April, 2011)
- [20] J. Dixon, Pontificia Universidad Católica de Chile, "TREE-PHASE CONTROLLED RECTIFIERS"
- [21] K. Zhou, D. Wang, "Relationship between space-vector modulation and three-phase carrier-based PWM: A comprehensive analysis"
- [22] D. W. Chung, S-Ki. Sul, "Minimum-loss stragegy for three-phase PWM rectifier"
- [23] D. C. Rus, N. S. Preda, I. I. Incze, M. Imecs, Cs. Szabó, "Comparative Analysis of PWM Techniques: Simulation and DSP Implementation"
- [24] S. Fukuda, K. Suzuki, "Harmonnic evaluation of carrier-based PWM methods using harmonic distortion determing factor" IEEE PCC, pp. 259-264, 1997
- [25] Space vector modulation,
https://secure.wikimedia.org/wikipedia/en/wiki/Space_vector_modulation
- [26] N. Mohan, T. M. Undeland, W. P. Robbins (2003). *Power Electronics*. 3rd ed. Hoboken: Wiley. p240.
- [27] Farnell, <http://www.farnell.com>

- [28] CASPOC simulation software, <http://www.caspoc.com>
- [29] N. Mohan, T. M. Undeland, W. P. Robbins (2003). *Power Electronics*. 3rd ed. Hoboken: Wiley. p205 - p206.
- [30] N. Mohan, T. M. Undeland, W. P. Robbins (2003). *Power Electronics*. 3rd ed. Hoboken: Wiley. P225.
- [31] Direct torque control, https://secure.wikimedia.org/wikipedia/en/wiki/Direct_Torque_Control
(Accessed 1 September 2011)
- [32] Vector control, https://secure.wikimedia.org/wikipedia/en/wiki/Vector_control_%28motor%29
(Accessed 1 September 2011)
- [33] S. Fukada, Y. iwaji, "Introduction of the harmonic distortion determining factor and its application to evaluating real time PWM inverters"
- [34] S. R. Bowes, D. Holliday, "Optimal Regular-Sampled PWM Inverter Control Techniques"

Appendix A: Datasheet 48T SMPM generator set

- Generator nominal operating conditions:

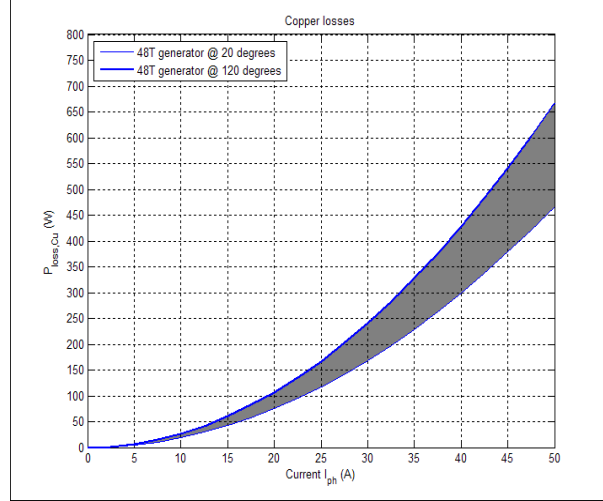
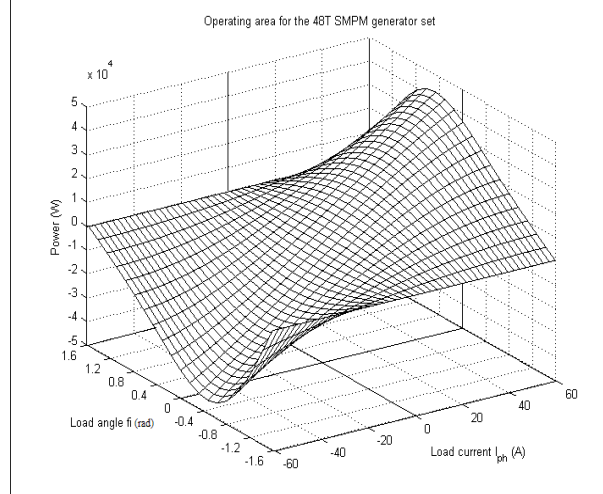
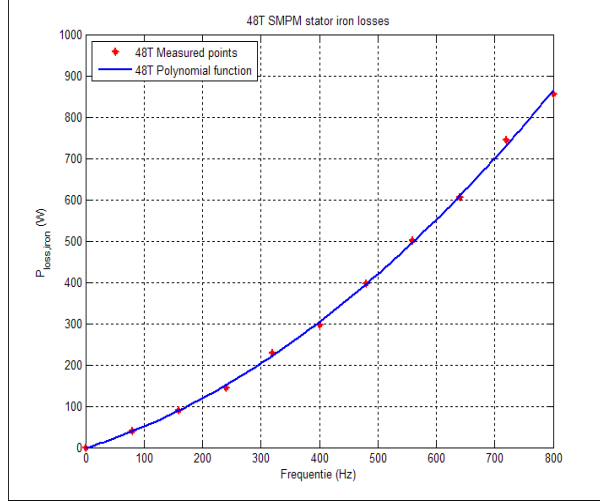
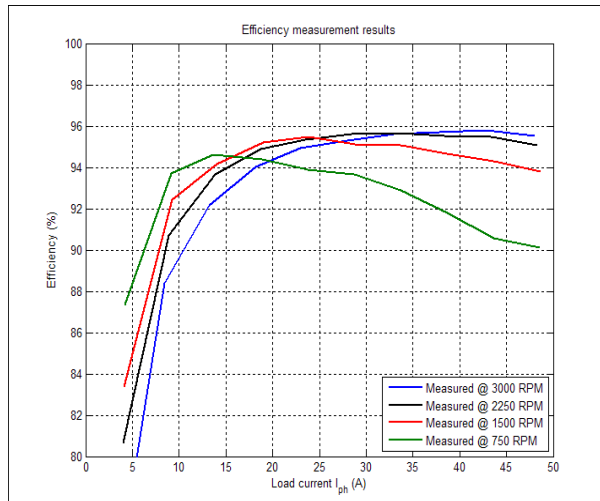
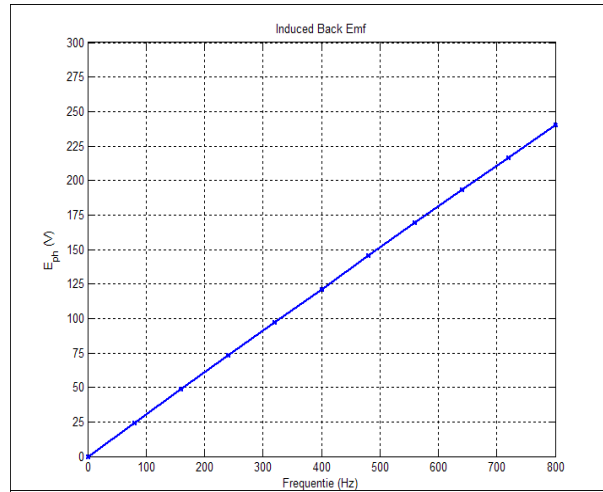
P	30.8	kW	U _t	251	V
n _m	3000	RPM	I _{ph}	45	A
f _e	800	Hz	Cos φ	0.91	
p	16		η	95.8	%

- Generator parameters:

Induced voltage : E_{ph} = 241 V
: C_T = 0.1 %/°C

Phase resistance : R_{ph} = 63 mΩ
: C_T = 0.43 %/°C

Phase inductance : L_{ph} = 410 μH



Appendix B: Hardware cost price calculation of proposed designs

This appendix contains confidential information and is therefore not included in the public version of the master thesis.

Appendix C: Datahseet Fuji 2MBI200U4B-120-50

SPECIFICATION

Device Name : IGBT MODULE

(RoHS compliant product)

Type Name : 2MBI200U4B-120-50

Spec. No. : MS5F6577

This material and the information herein is the property of Fuji Electric Device Technology Co.,Ltd. They shall be neither reproduced, copied, lent, or disclosed in any way whatsoever for the use of any third party nor used for the manufacturing purposes without the express written consent of Fuji Electric Device Technology Co.,Ltd.

DATE	NAME	APPROVED	Fuji Electric Device Technology Co.,Ltd.
DRAWN May. - 11 -'06	K.Muramatsu	T.Miyasaka	
CHECKED May. - 11 -'06	M.Watanabe		DWG.NO. 1 / 14 a
CHECKED - -	K.Yamada		MS5F6577

Revised Records

This material and the information herein is the property of Fuji Electric Power Device Technology Co.,Ltd. They shall be neither reproduced, copied, lent, nor disclosed in any way whatsoever for the use of any third party nor used for the manufacturing purposes without the express written consent of Fuji Electric Power Device Technology Co.,Ltd.

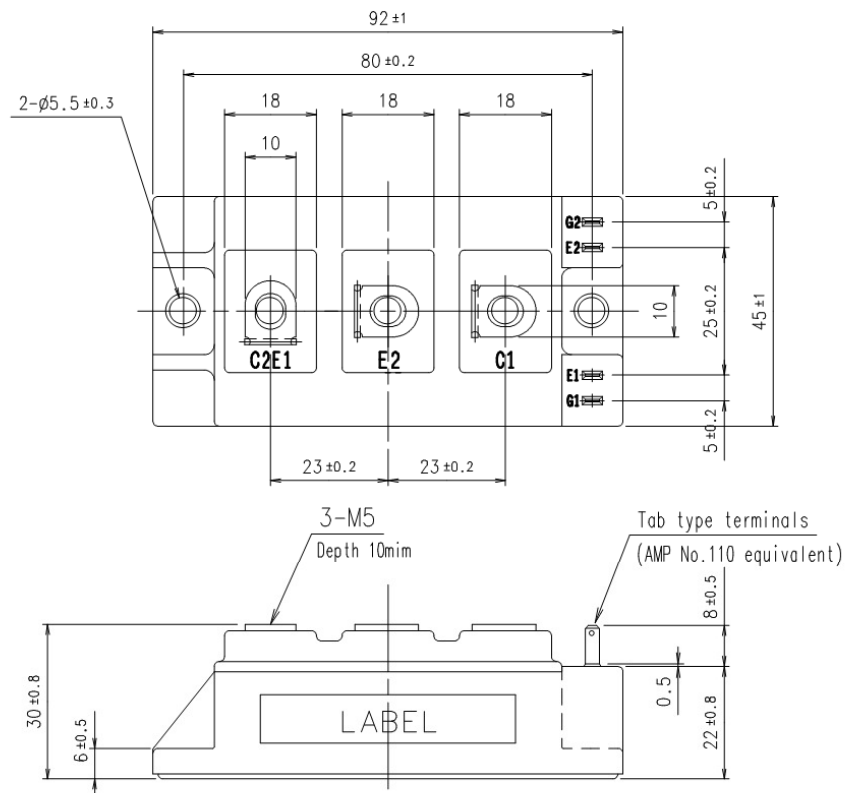
Fuji Electric Device Technology Co.,Ltd.

MS5F6577

2 / 14

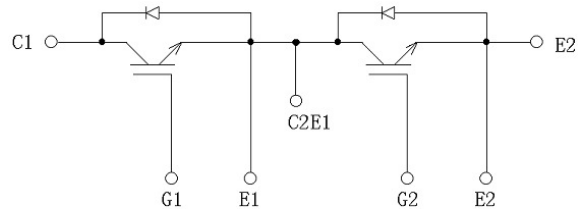
2MBI200U4B-120-50 (RoHS compliant product)

1. Outline Drawing (Unit : mm)



This material and the information herein is the property of Fuji Electric Device Technology Co.,Ltd. They shall be neither reproduced, copied, lent, or disclosed in any way whatsoever for the use of any third party nor used for the manufacturing purposes without the express written consent of Fuji Electric Device Technology Co.,Ltd.

2. Equivalent circuit



Fuji Electric Device Technology Co.,Ltd.

DWG.NO.

MS5F6577

3 / 14

a		

3. Absolute Maximum Ratings (at $T_c = 25^\circ C$ unless otherwise specified)

Items	Symbols	Conditions		Maximum Ratings	Units
Collector-Emitter voltage	VCES			1200	V
Gate-Emitter voltage	VGES			± 20	V
Collector current	Ic	Continuous	$T_c = 25^\circ C$	300	A
			$T_c = 80^\circ C$	200	
	Icp	1ms	$T_c = 25^\circ C$	600	
			$T_c = 80^\circ C$	400	
	-Ic			200	
	-Ic pulse	1ms		400	
Collector Power Dissipation	Pc	1 device		1040	W
Junction temperature	Tj			$+150$	$^\circ C$
Storage temperature	Tstg			-40 to +125	
Isolation voltage	between terminal and copper base (*1)		Viso	AC : 1min.	2500 VAC
Screw Mounting (*2)					
Torque Terminals (*2)	-			3.5	N m

(*1) All terminals should be connected together when isolation test will be done.

(*2) Recommendable Value : 2.5 to 3.5 Nm (M5)

4. Electrical characteristics (at $T_i = 25^\circ C$ unless otherwise specified)

Items	Symbols	Conditions	Characteristics			Units
			min.	typ.	max.	
Zero gate voltage collector current	ICES	VCE=1200V VGE=0V	-	-	2.0	mA
Gate-Emitter leakage current	IGES	VCE=0V VGE= $\pm 20V$	-	-	400	nA
Gate-Emitter threshold voltage	VGE(th)	VCE=20V Ic=200mA	4.5	6.5	8.5	V
Collector-Emitter saturation voltage (terminal)	VCE(sat) (terminal)	Ic=200A VGE=15V	Ti=25°C Ti=125°C	- - - -	2.10 2.30 1.90 2.10	V
Collector-Emitter saturation voltage (chip)	VCE(sat) (chip)		Ti=25°C Ti=125°C	- -	2.05 -	
Input capacitance	Cies	VCE=10V,VGE=0V,f=1MHz	-	22	-	nF
Turn-on time	ton	Vcc=600V	-	0.32	1.20	us
	tr	Ic=200A	-	0.10	0.60	
	tr(i)	VGE= $\pm 15V$	-	0.03	-	
Turn-off time	toff	RG=3.0Ω	-	0.41	1.00	
	tf		-	0.07	0.30	
Forward on voltage (terminal)	VF (terminal)	IF=200A	Ti=25°C Ti=125°C	- - - -	1.85 1.95 1.65 1.75	V
Forward on voltage (chip)	VF (chip)	VGE=0V	Ti=25°C Ti=125°C	- -	1.80 -	
Reverse recovery time	trr	IF=200A	-	-	0.35	us
Lead resistance, terminal-chip (*3)	R lead		-	0.97	-	mΩ

(*3) Biggest internal terminal resistance among arm.

This material and the information herein is the property of Fuji Electric Device Technology Co.,Ltd. They shall be neither reproduced, copied, lent, or disclosed in any way whatsoever for the use of any third party nor used for the manufacturing purposes without the express written consent of Fuji Electric Device Technology Co.,Ltd.

Fuji Electric Device Technology Co.,Ltd.

DWG NO.

MS5F6577

4 / 14

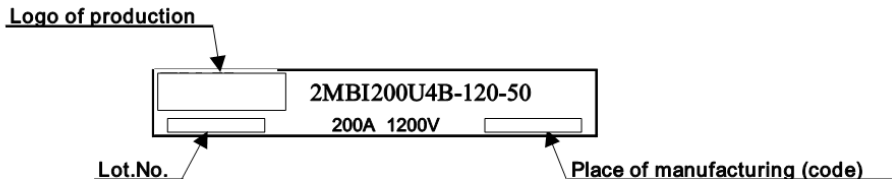
a

5. Thermal resistance characteristics

Items	Symbols	Conditions	Characteristics			Units
			min.	typ.	max.	
Thermal resistance(1device)	Rth(j-c)	IGBT	-	-	0.12	°C/W
Contact Thermal resistance (1 device) (*4)	Rth(c-f)	FWD with Thermal Compound	-	0.025	-	

(*4) This is the value which is defined mounting on the additional cooling fin with thermal compound.

6. Indication on module



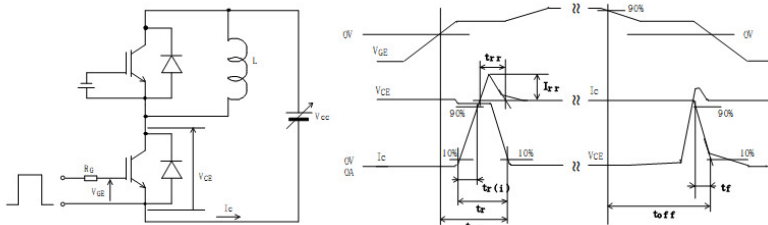
7. Applicable category

This specification is applied to IGBT-Module named 2MBI200U4B-120-50.

8. Storage and transportation notes

- The module should be stored at a standard temperature of 5 to 35°C and humidity of 45 to 75% .
- Store modules in a place with few temperature changes in order to avoid condensation on the module surface.
- Avoid exposure to corrosive gases and dust.
- Avoid excessive external force on the module.
- Store modules with unprocessed terminals.
- Do not drop or otherwise shock the modules when transporting.

9. Definitions of switching time

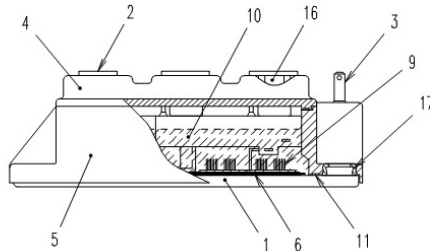


10. Packing and Labeling

- Display on the packing box
- Logo of production
 - Type name
 - Lot No.
 - Products quantity in a packing box

This material and the information herein is the property of Fuji Electric Device Technology Co.,Ltd. They shall be neither reproduced, copied, lent, or disclosed in any way whatsoever for the use of any third party nor used for the manufacturing purposes without the express written consent of Fuji Electric Device Technology Co.,Ltd.

11. List of material (材料リスト)



(Total weight of soldering material(typ) : 6.3 g)

No.	Parts	Material (main)	Ref.
1	Base Plate	Cu	Ni plating
2	Main terminal	Cu	Ni plating
3	Sub terminal	Cu or Brass	Ni plating
4	Cover	PPS resin	UL 94V-0
5	Case	PPS resin	UL 94V-0
6	Isolation substrate	Al ₂ O ₃ + Cu	
7	IGBT chip	Silicon	(Not drawn in above)
8	FWD chip	Silicon	(Not drawn in above)
9	Wiring	Aluminum	
10	Silicone Gel	Silicone resin	
11	Adhesive	Silicone resin	
12	Solder (Under chip)	Sn/Ag base	(Not drawn in above)
13	Solder (Under Isolation substrate)	Sn/Ag base	(Not drawn in above)
14	Solder (Between terminal and Isolation substrate)	Sn/Ag base	(Not drawn in above)
15	Label	Paper	(Not drawn in above)
16	Nut	Fe	Trivalent Chromate treatment
17	Ring	Brass	

This material and the information herein is the property of Fuji Electric Device Technology Co.,Ltd. They shall be neither reproduced, copied, lent, or disclosed in any way whatsoever for the use of any third party nor used for the manufacturing purposes without the express written consent of Fuji Electric Device Technology Co.,Ltd.

12. RoHS Directive Compliance (RoHS 指令適用について)

本IGBTモジュールは富士電機デバイステクノロジーが発行しているRoHSに関する資料MS5F6209を適用する。日本語版(MS5F6212)は参考資料とする。

The document (MS5F6209) about RoHS that Fuji Electric Device Technology issued is applied to this IGBT Module. The Japanese Edition(MS5F6212) is made into a reference grade.

Fuji Electric Device Technology Co.,Ltd.

DWG No.

MS5F6577

6 / 14

a	

13. Reliability test results

Reliability Test Items

Test categories	Test items	Test methods and conditions	Reference norms EIAJ ED-4701 (Aug.-2001 edition)	Number of sample	Acceptance number
Mechanical Tests	1 Terminal Strength (Pull test)	Pull force : 40N Test time : 10±1 sec.	Test Method 401 Method I	5	(0 : 1)
	2 Mounting Strength	Screw torque : 2.5 ~ 3.5 N·m (M5) Test time : 10±1 sec.	Test Method 402 method II	5	(0 : 1)
	3 Vibration	Range of frequency : 10 ~ 500Hz Sweeping time : 15 min. Acceleration : 100m/s ² Sweeping direction : Each X,Y,Z axis Test time : 6 hr. (2hr./direction)	Test Method 403 Reference 1 Condition code B	5	(0 : 1)
	4 Shock	Maximum acceleration : 5000m/s ² Pulse width : 1.0msec. Direction : Each X,Y,Z axis Test time : 3 times/direction	Test Method 404 Condition code B	5	(0 : 1)
Environment Tests	1 High Temperature Storage	Storage temp. : 125±5 °C Test duration : 1000hr.	Test Method 201	5	(0 : 1)
	2 Low Temperature Storage	Storage temp. : -40±5 °C Test duration : 1000hr.	Test Method 202	5	(0 : 1)
	3 Temperature Humidity Storage	Storage temp. : 85±2 °C Relative humidity : 85±5% Test duration : 1000hr.	Test Method 103 Test code C	5	(0 : 1)
	4 Unsaturated Pressurized Vapor	Test temp. : 120±2 °C Test humidity : 85±5% Test duration : 96hr.	Test Method 103 Test code E	5	(0 : 1)
	5 Temperature Cycle	Test temp. : Low temp. -40±5 °C High temp. 125 ±5 °C RT 5 ~ 35 °C Dwell time : High ~ RT ~ Low ~ RT 1hr. 0.5hr. 1hr. 0.5hr. Number of cycles : 100 cycles	Test Method 105	5	(0 : 1)
	6 Thermal Shock	Test temp. : High temp. 100 +5 °C Low temp. 0 -5 °C Used liquid : Water with ice and boiling water Dipping time : 5 min. per each temp. Transfer time : 10 sec. Number of cycles : 10 cycles	Test Method 307 method I Condition code A	5	(0 : 1)

This material and the information herein is the property of Fuji Electric Device Technology Co., Ltd. They shall be neither reproduced, copied, lent, or disclosed in any way whatsoever for the use of any third party nor used for the manufacturing purposes without the express written consent of Fuji Electric Device Technology Co., Ltd.

Fuji Electric Device Technology Co., Ltd.

DWG NO.

MS5F6577

7 / 14

a	

Reliability Test Items

Test categories	Test items	Test methods and conditions	Reference norms EIAJ ED-4701 (Aug-2001 edition)	Number of sample	Acceptance number
Endurance Tests	1 High temperature Reverse Bias	Test temp. : $T_a = 125 \pm 5^\circ C$ Bias Voltage : $V_C = 0.8 \times V_{CES}$ Bias Method : Applied DC voltage to C-E $V_{GE} = 0V$ Test duration : 1000hr.	Test Method 101	5	(0 : 1)
	2 High temperature Bias (for gate)	Test temp. : $T_a = 125 \pm 5^\circ C$ ($T_j \leq 150^\circ C$) Bias Voltage : $V_C = V_{GE} = +20V$ or $-20V$ Bias Method : Applied DC voltage to G-E $V_{CE} = 0V$ Test duration : 1000hr.	Test Method 101	5	(0 : 1)
	3 Temperature Humidity Bias	Test temp. : $85 \pm 2^\circ C$ Relative humidity : $85 \pm 5\%$ Bias Voltage : $V_C = 0.8 \times V_{CES}$ Bias Method : Applied DC voltage to C-E $V_{GE} = 0V$ Test duration : 1000hr.	Test Method 102 Condition code C	5	(0 : 1)
	4 Intermittent Operating Life (Power cycle) (for IGBT)	ON time : 2 sec. OFF time : 18 sec. Test temp. : $\Delta T_j = 100 \pm 5^\circ C$ $T_j \leq 150^\circ C$, $T_a = 25 \pm 5^\circ C$ Number of cycles : 15000 cycles	Test Method 106	5	(0 : 1)

Failure Criteria

Item	Characteristic	Symbol	Failure criteria		Unit	Note	
			Lower limit	Upper limit			
Electrical characteristic	Leakage current		ICES	-	USL×2	mA	
			\pm IGES	-	USL×2	μA	
	Gate threshold voltage		$V_{GE(th)}$	$LSL \times 0.8$	$USL \times 1.2$	mA	
	Saturation voltage		$V_{CE(sat)}$	-	$USL \times 1.2$	V	
	Forward voltage		VF	-	$USL \times 1.2$	V	
	Thermal resistance	IGBT	ΔV_{GE} or ΔV_{CE}	-	$USL \times 1.2$	mV	
Visual inspection	FWD		ΔVF	-	$USL \times 1.2$	mV	
	Isolation voltage		$Viso$	Broken insulation		-	

LSL : Lower specified limit.

USL : Upper specified limit.

Note : Each parameter measurement read-outs shall be made after stabilizing the components at room ambient for 2 hours minimum, 24 hours maximum after removal from the tests.
And in case of the wetting tests, for example, moisture resistance tests, each component shall be made wipe or dry completely before the measurement.

Fuji Electric Device Technology Co., Ltd.

DWG NO.

MS5F6577

8 / 14

a

Reliability Test Results

Test categories	Test items	Reference norms EIAJ ED-4701 (Aug.-2001 edition)	Number of test sample	Number of failure sample
Mechanical Tests	1 Terminal Strength (Pull test)	Test Method 401 Method I	5	0
	2 Mounting Strength	Test Method 402 method II	5	0
	3 Vibration	Test Method 403 Condition code B	5	0
	4 Shock	Test Method 404 Condition code B	5	0
Environment Tests	1 High Temperature Storage	Test Method 201	5	0
	2 Low Temperature Storage	Test Method 202	5	0
	3 Temperature Humidity Storage	Test Method 103 Test code C	5	0
	4 Unsaturated Pressurized Vapor	Test Method 103 Test code E	5	0
	5 Temperature Cycle	Test Method 105	5	^a 0
	6 Thermal Shock	Test Method 307 method I Condition code A	5	0
Endurance Tests	1 High temperature Reverse Bias	Test Method 101	5	0
	2 High temperature Bias (for gate)	Test Method 101	5	0
	3 Temperature Humidity Bias	Test Method 102 Condition code C	5	0
	4 Intermittent Operating Life (Power cycling) (for IGBT)	Test Method 106	5	0

This material and the information herein is the property of Fuji Electric Device Technology Co., Ltd. They shall be neither reproduced, copied, lent, or disclosed in any way whatsoever for the use of any third party nor used for the manufacturing purposes without the express written consent of Fuji Electric Device Technology Co., Ltd.

Fuji Electric Device Technology Co., Ltd.

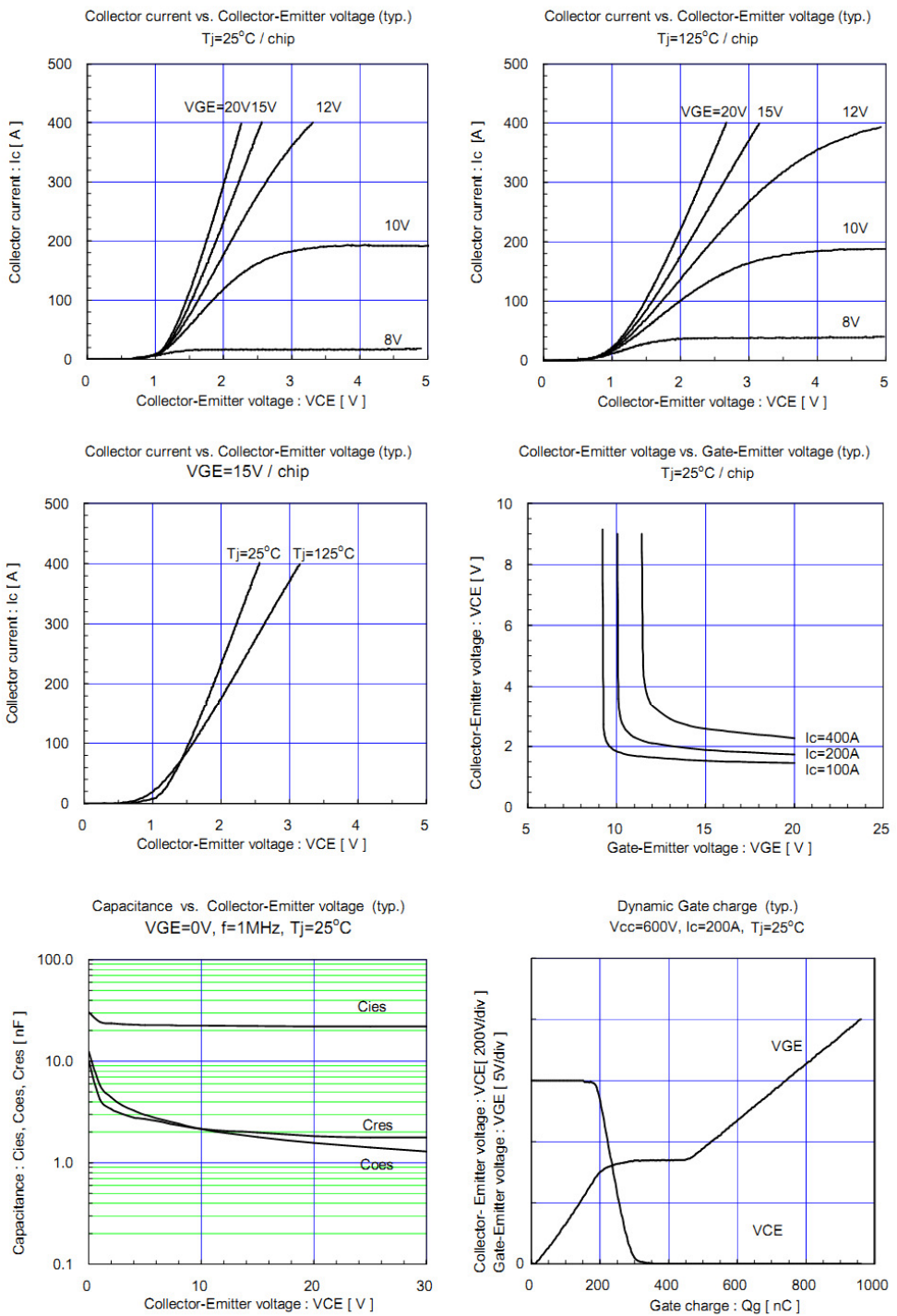
DWG NO.

MS5F6577

9 / 14



This material and the information herein is the property of Fuji Electric Device Technology Co., Ltd. They shall be neither reproduced, copied, lent, or disclosed in any way whatsoever for the use of any third party nor used for the manufacturing purposes without the express written consent of Fuji Electric Device Technology Co., Ltd.



Fuji Electric Device Technology Co., Ltd.

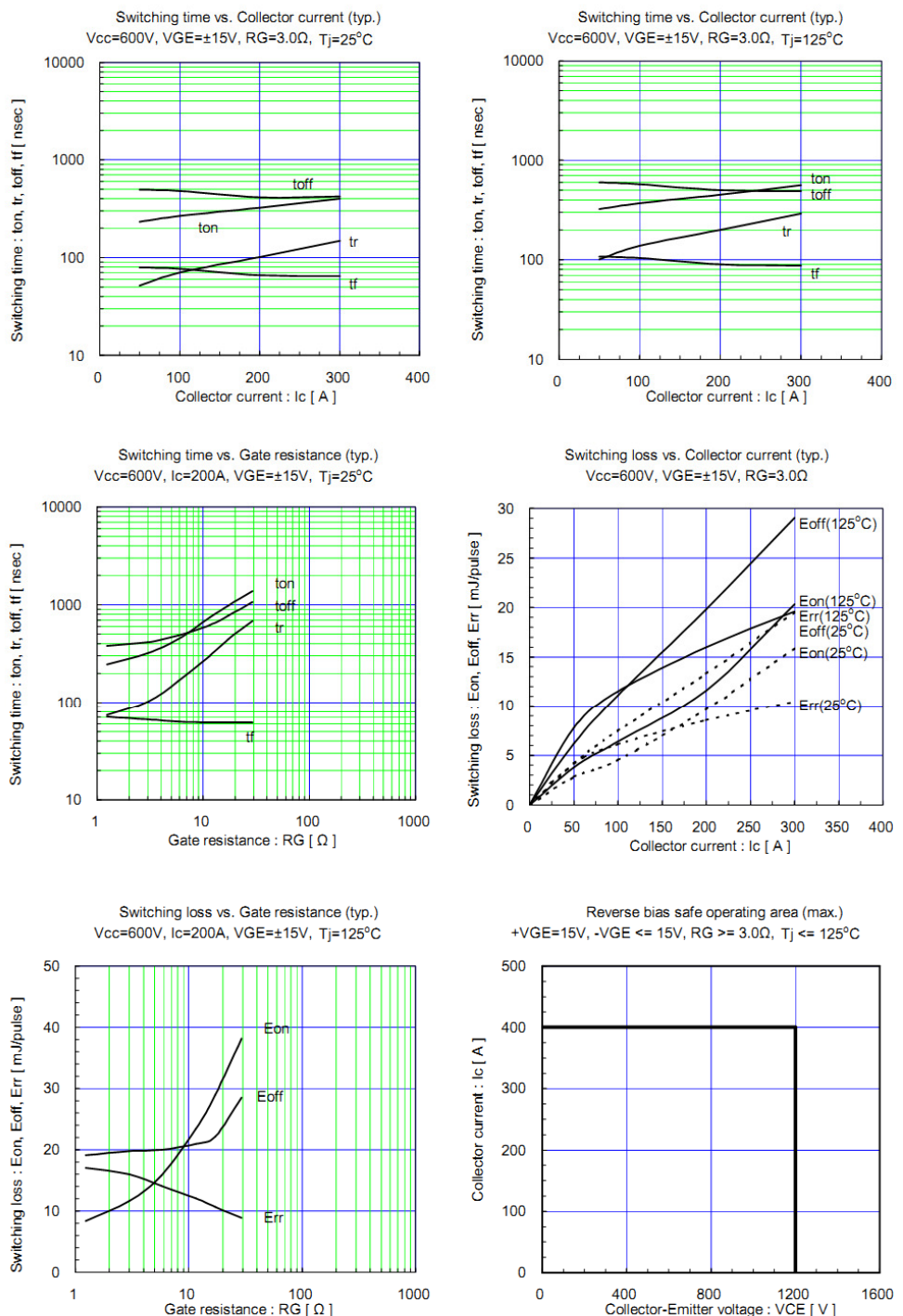
DWG.NO.

MS5F6577

10 / 14



This material and the information herein is the property of Fuji Electric Device Technology Co., Ltd. They shall be neither reproduced, copied, lent, or disclosed in any way whatsoever for the use of any third party nor used for the manufacturing purposes without the express written consent of Fuji Electric Device Technology Co., Ltd.



Fuji Electric Device Technology Co., Ltd.

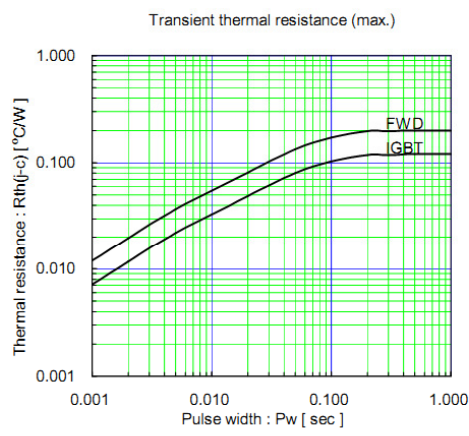
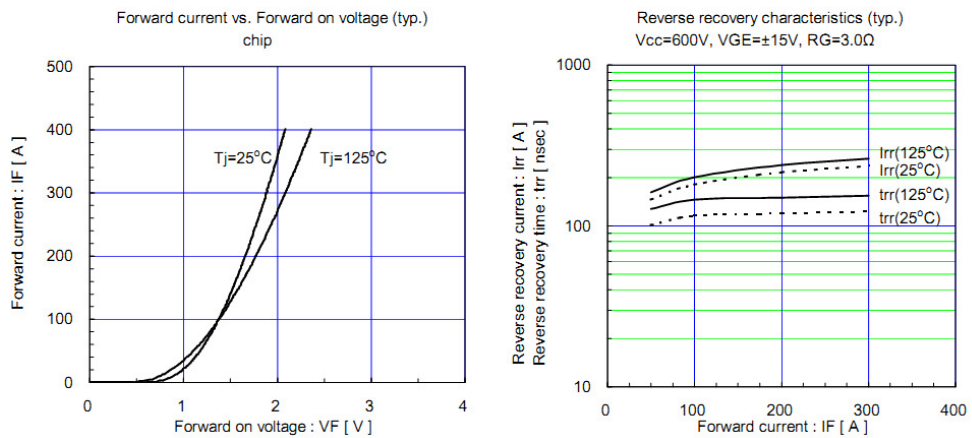
DWG.NO.

MS5F6577

11 / 14

a
b
c
d
e

This material and the information herein is the property of Fuji Electric Device Technology Co., Ltd. They shall be neither reproduced, copied, lent, or disclosed in any way whatsoever for the use of any third party nor used for the manufacturing purposes without the express written consent of Fuji Electric Device Technology Co., Ltd.



Fuji Electric Device Technology Co., Ltd.

DWG NO.

MS5F6577

12 / 14

a

Warnings

- This product shall be used within its absolute maximum rating (voltage, current, and temperature). This product may be broken in case of using beyond the ratings.
製品の絶対最大定格(電圧、電流、温度等)の範囲内で御使用下さい。絶対最大定格を超えて使用すると、素子が破壊する場合があります。
- Connect adequate fuse or protector of circuit between three-phase line and this product to prevent the equipment from causing secondary destruction, such as fire, its spreading, or explosion.
万一の不慮の事故で素子が破壊した場合を考慮し、商用電源と本製品の間に適切な容量のヒューズ又はブレーカーを必ず付けて火災、爆発、延焼等の2次破壊を防いでください。
- Use this product after realizing enough working on environment and considering of product's reliability life.
This product may be broken before target life of the system in case of using beyond the product's reliability life.
製品の使用環境を十分に把握し、製品の信頼性寿命が満足できるか検討の上、本製品を適用して下さい。製品の信頼性寿命を超えて使用した場合、装置の目標寿命より前に素子が破壊する場合があります。
- If the product had been used in the environment with acid, organic matter, and corrosive gas (hydrogen sulfide, sulfurous acid gas), the product's performance and appearance can not be ensured easily.
酸・有機物・腐食性ガス(硫化水素、亜硫酸ガス等)を含む環境下で使用された場合、製品機能・外観等の保証はできません。
- Use this product within the power cycle curve (Technical Rep.No.: MT5F12959). Power cycle capability is classified to delta-T_j mode which is stated as above and delta-T_c mode. Delta-T_c mode is due to rise and down of case temperature (T_c), and depends on cooling design of equipment which use this product. In application which has such frequent rise and down of T_c, well consideration of product life time is necessary.
本製品は、パワーサイクル寿命カーブ以下で使用下さい(技術資料No.: MT5F12959)。パワーサイクル耐量にはこの△T_jによる場合の他に、△T_cによる場合があります。これはケース温度(T_c)の上昇下降による熱ストレスであり、本製品をご使用する際の放熱設計に依存します。ケース温度の上昇下降が頻繁に起こる場合は、製品寿命に十分留意してご使用下さい。
- Never add mechanical stress to deform the main or control terminal. The deformed terminal may cause poor contact problem.
主端子及び制御端子に応力を与えて変形させないで下さい。端子の変形により、接触不良などを引き起こす場合があります。
- Use this product with keeping the cooling fin's flatness between screw holes within 100um at 100mm and the roughness within 10um. Also keep the tightening torque within the limits of this specification. Too large convex of cooling fin may cause isolation breakdown and this may lead to a critical accident. On the other hand, too large concave of cooling fin makes gap between this product and the fin bigger, then, thermal conductivity will be worse and over heat destruction may occur.
冷却フィンはネジ取り付け位置間で平坦度を100mmで100um以下、表面の粗さは10um以下にして下さい。過大な凸反りがあったりすると本製品が絶縁破壊を起こし、重大事故に発展する場合があります。また、過大な凹反りやゆがみ等があると、本製品と冷却フィンの間に空隙が生じて放熱が悪くなり、熱破壊に繋がることがあります。
- In case of mounting this product on cooling fin, use thermal compound to secure thermal conductivity. If the thermal compound amount was not enough or its applying method was not suitable, its spreading will not be enough, then, thermal conductivity will be worse and thermal run away destruction may occur.
Confirm spreading state of the thermal compound when its applying to this product.
(Spreading state of the thermal compound can be confirmed by removing this product after mounting.)
素子を冷却フィンに取り付ける際には、熱伝導を確保するためのコンパウンド等をご使用ください。又、塗布量が不足したり、塗布方法が不適だったりすると、コンパウンドが十分に素子全体に広がらず、放熱悪化による熱破壊に繋がる事があります。コンパウンドを塗布する際には、製品全面にコンパウンドが広がっている事を確認してください。
(実装した後に素子を取りはずすとコンパウンドの広がり具合を確認する事が出来ます。)
- It shall be confirmed that IGBT's operating locus of the turn-off voltage and current are within the RBSOA specification. This product may be broken if the locus is out of the RBSOA.
ターンオフ電圧・電流の動作軌跡がRBSOA仕様内にあることを確認して下さい。RBSOAの範囲を超えて使用すると素子が破壊する可能性があります。
- If excessive static electricity is applied to the control terminals, the devices may be broken. Implement some countermeasures against static electricity.
制御端子に過大な静電気が印加された場合、素子が破壊する場合があります。取り扱い時は静電気対策を実施して下さい。

This material and the information herein is the property of Fuji Electric Device Technology Co., Ltd. They shall be neither reproduced, copied, lent, or disclosed in any way whatsoever for the use of any third party nor used for the manufacturing purposes without the express written consent of Fuji Electric Device Technology Co., Ltd.

Fuji Electric Device Technology Co., Ltd.

DWG NO.

MS5F6577

13 / 14

a

Warnings

- Never add the excessive mechanical stress to the main or control terminals when the product is applied to equipments. The module structure may be broken.
素子を装置に実装する際に、主端子や制御端子に過大な応力を与えないで下さい。端子構造が破壊する可能性があります。
- In case of insufficient -VGE, erroneous turn-on of IGBT may occur. -VGE shall be set enough value to prevent this malfunction. (Recommended value : -VGE = -15V)
逆バイアスゲート電圧-VGEが不足しますと誤点弧を起こす可能性があります。誤点弧を起さない為に-VGEは十分な値で設定して下さい。（推奨値：-VGE = -15V）
- In case of higher turn-on dv/dt of IGBT, erroneous turn-on of opposite arm IGBT may occur. Use this product in the most suitable drive conditions, such as +VGE, -VGE, RG to prevent the malfunction.
ターンオン dv/dt が高いと対抗アームのIGBTが誤点弧を起こす可能性があります。誤点弧を起さない為の最適なドライブ条件(+VGE, -VGE, RG等)でご使用下さい。
- This product may be broken by avalanche in case of VCE beyond maximum rating VCES is applied between C-E terminals. Use this product within its absolute maximum voltage.
VCESを超えた電圧が印加された場合、アバランシェを起こして素子破壊する場合があります。VCEは必ず絶対定格の範囲内でご使用下さい。

This material and the information herein is the property of Fuji Electric Device Technology Co.,Ltd. They shall be neither reproduced, copied, lent, or disclosed in any way whatsoever for the use of any third party nor used for the manufacturing purposes without the express written consent of Fuji Electric Device Technology Co.,Ltd.

Cautions

- Fuji Electric Device Technology is constantly making every endeavor to improve the product quality and reliability. However, semiconductor products may rarely happen to fail or malfunction. To prevent accidents causing injury or death, damage to property like by fire, and other social damage resulted from a failure or malfunction of the Fuji Electric Device Technology semiconductor products, take some measures to keep safety such as redundant design, spread-fire-preventive design, and malfunction-protective design.
富士電機デバイステクノロジーは絶えず製品の品質と信頼性の向上に努めています。しかし、半導体製品は故障が発生したり、誤動作する場合があります。富士電機デバイステクノロジー製半導体製品の故障または誤動作が、結果として人身事故・火災等による財産に対する損害や社会的な損害を起さないように冗長設計・延焼防止設計・誤動作防止設計など安全確保のための手段を講じて下さい。
- The application examples described in this specification only explain typical ones that used the Fuji Electric Device Technology products. This specification never ensure to enforce the industrial property and other rights, nor license the enforcement rights.
本仕様書に記載してある応用例は、富士電機デバイステクノロジー製品を使用した代表的な応用例を説明するものであり、本仕様書によって工業所有権、その他権利の実施に対する保障または実施権の許諾を行うものではありません。
- The product described in this specification is not designed nor made for being applied to the equipment or systems used under life-threatening situations. When you consider applying the product of this specification to particular used, such as vehicle-mounted units, shipboard equipment, aerospace equipment, medical devices, atomic control systems and submarine relaying equipment or systems, please apply after confirmation of this product to be satisfied about system construction and required reliability.
本仕様書に記載された製品は、人命にかかるような状況下で使用される機器あるいはシステムに用いられることを目的として設計・製造されたものではありません。本仕様書の製品を車両機器、船舶、航空宇宙、医療機器、原子力制御、海底中継機器あるいはシステムなど、特殊用途へのご利用をご検討の際は、システム構成及び要求品質に満足することをご確認の上、ご利用下さい。

If there is any unclear matter in this specification, please contact Fuji Electric Device Technology Co.,Ltd.

Fuji Electric Device Technology Co.,Ltd.

DWG NO.

MS5F6577

14 / 14

a

Appendix D: Test setup

